STUDY OF SECULAR AND SEISMIC STRAINS

OBSERVED BY EXTENSOMETERS AT ERIMO

BY

Minoru KASAHARA

A Thesis Submitted to Hokkaido University

for the Degree of

Doctor of Science

1982

ABSTRACT

Since 1971, continuous observation of crustal strain variation by three components of fused-quartz extensometer of 30 m long has been conducted in the vault of the Erimo Geophysical Observatory (EGO). The purpose of this study is to demonstrate the availability of the extensometer in geophysical interest on the basis of the data obtained at EGO with an improvement of extensometer system.

Secular strain accumulation obtained by the extensometric observation in the vault and by the repeated measurements for the long-base line network around EGO during the period from 1971 to 1980 show that the principal strains were $+5.9 \times 10^{-6}$ with a N5°E and -1.6×10^{-6} with a N85°W from the former, and $+4.5 \times 10^{-6}$ with a N22°W and -2.0×10^{-6} with a N68°E from the latter, extension reckoned positive. The both results are tolerably consistent in both orientation and amount with one another. It was confirmed that the extensometric observation in the vault of EGO could well follow the wide-areal crustal movement progressing around the Erimo region.

The abnormal strain changes related to the 1973 Earthquake off the Nemuro Peninsula (Ms=7.7) were quantitatively revealed with consideration of precipitation around EGO and discharge water from the vault. Pre-seismic strain change which is contrary to co-seismic strain step seemed to begin more than 40 days and less than 100 days before the event. Post-seismic strain change indicated the same manner as the co-seismic one and continued about 15 days after the event. The amount of the pre- and post-seismic strain changes did not

exceed that of the co-seismic one.

The extensometer observed distinct strain steps associated with 44 earthquakes with magnitudes ranging from 4.7 to 7.7. The observed strain steps were consistent in both polarity and amplitude with the theoretical ones for six earthquakes of which source parameters were obtained by conventional seismological method. The observed strain step is proportional to seismic moment and to inverse of cube of hypocentral distance as being predicted by simple dislocation model. Neither mechanical problem nor serious site effects for the extensometer installed at the vault of EGO were found. Therefore, seismic moment of an earthquake can be estimated from the observed strain step and the hypocentral distance within an accuracy of a factor of 2 to 3.

Body wave analyses of the strain seismograms recorded by newly improved digital system were carried out for 55 earthquakes with magnitudes ranging from 3.3 to 7.7 in comparison with the synthetic strain seismogram generated by a point shear dislocation in an infinite homogeneous medium. The waveform and amplitude of the observed strain seismogram could be well explained by the synthetic one with source parameters obtained by other method. It is also shown that seismic moment and source process time of an earthquake could be estimated from amplitude and period of the observed S-wave alone within a factor of 2. Source process time ranging from 0.3 to 60 secconds and seismic moment ranging from 10^{20} to 10^{27} dyne·cm were obtained from the analyses of the observed strain seismograms for 55 earthquakes. The relationship between both parameters was consistent with that predicted by earthquake model.

Finally, usefulness of the extensometer as a seismometer was

demonstrated by an example of source process analysis of the Kunashiri Strait Earthquake with magnitude of 7.7. Body wave analysis suggested that the main rupture with low rupture velocity propagated uni-laterally for 60 seconds and 18 secondary ruptures were successively triggered during the main rupture process. The observed strain steps were also consistent with this sequence. The improved recording system could demonstrate that the strain step is directly connected with the bodily deformation caused by faulting at the source.

It has been confirmed throughout this study that the extensometer with a solid length standard 30 m long can satisfactorily respond to crustal strain changes ranging frequency from 3 Hz to DC generated by earthquakes as well as to secular strain accumulation progressing around the observatory.

TABLE OF CONTENTS

CHAPTER 1

INTRODUCTION

Crustal movements have a large variety of ground motion; movements of the earth's surface due to motions of seismic vibration as a short-lived or transient term up to ones of secular variation caused by tectonogenesis as a very long term are all included in the crustal movement. These movements, however, cannot directly be measured in a space coordinate system. One should recognize the movements either as relative motions of a pendulum or as variations in the distance adjacent two points of the ground. The observable longest period of the movement is limited by the natural period of the pendulum for relative motions, practically being less than several hundred seconds. The longer periodic or non-vibratory movements are observable when the distance variation is measured; the movements are measured as strain or tilt variation of the ground.

If an extensometer is used for the measurement, the observation of crustal movement may have the following two merits: One is that it is possible to observe a ground motion of such continuous and precise crustal movement near the observatory that we cannot observe by geodetic surveys with intermittent operations. Practically, this observation

has been adopted as one of the most important subjects to be studied in the earthquake prediction research, because it may probably reveal premonitory phenomena of earthquakes (Tsuboi et al.,1962).

Another is that the extensometer can be used as a seismometer. The extensometer may uniformly respond to crustal strains with periods ranging from several Hz to DC. Recently, much attention has given for slow earthquakes generated by rupture process with a long time constant (Kanamori,1972; Fukao and Furumoto,1975; Sasatani and Kasahara,1978; Sacks et al.,1978; Kanamori and Stewart, 1979; Tocher,1960; Aoki,1975; Kanamori and Cipar,1974; Fujii,1976; Chung and Kanamori,1978). For these earthquakes, usual seismometers have provided no records or incomplete records, but the extensometer could record the whole deformation caused by the rupture process; other side of source process behind our knowledge of earthquake mechanism could successfully be revealed by the extensometer.

For development of the extensometer a brief history will be reviewed.

Crude but essential design of the extensometer was made by John Milne who had conducted it on the ground surface at a place in Tokyo, Japan in 1884 to 1885. The extensometer was to measure "the relative motions of neighboring points of ground" (Milne,1888). Later, a work of the measurement was carried out in Italy by Odden (1900) who had submitted the manuscript titled "study of the strainmeter as a seismometer without pendulum". Although their primitive

works had achieved no fruitful results because of the substantial deficiency of sensitivity of their systems, they have been honored as pioneers.

As a properly conceived geophysical technique, strain measurement originated with Hugo Benioff in 1935 working in California (Benioff,1935). He initially used a steel tube length standard 20 meters coupled to an electro-magnetic velocity transducer and place it underground for thermal stability. This system gave his instrument a frequency response similar to a pendulum-type displacement seismometer. He called it a strain seismograph. But it did not allow him to record tidal and secular strains. He later adopted a quartz rod length standard in stead of a steel tube to deduce thermal coefficients and used both optical and electronic displacement transducer in place of his original velocity transducer (Benioff,1959). This extended the frequency response of his instrument down to DC component and therefore he changes its name to an extensometer. By this improvement, his instrument could assist in identification of free modes of oscillation of the Earth (Benioff et al.,1961; Alsop et al.,1961). It is one of the most notable achievements of extensometers.

On the other hand, in Japan, Ryutaro Takahashi developed a new extensometer with a quartz tube length standard 25 meters long coupled to an etalon as a displacement transducer in 1934, in which no attention was paid to Benioff's work, for measuring crustal deformations in

relation to earthquake prediction (Takahashi,1934,1939). After the intermittence due to the World War II, some newly designed extensometers were operated in tunnels by two groups for the purpose of measuring secular and tidal strains but seismic one (Hagiwara et al.,1948,1949; Sassa et al.,1949,1952). Therefore, Japanese groups could not record free modes of oscillation of the Earth at the time of the 1960 gigantic Chilean Earthquake.

Press (1965) demonstrated that the residual strain field at large distance from major earthquakes are large enough to be detected by modern extensometers on the basis of the computation of its field due to the dislocation theory representation of faulting of earthquake and that the strain steps were recorded by Benioff's extensometers actually . He proposed to view the observation and interpretation of static fields as "zero frequency seismology" and highlighted the attractive possibility of the extensometer. In fact, in this discipline the instrument like an extensometer is useful as mentioned above. That is, the most important characteristics of the extensometer is to be able to respond to any crustal movements ranging from short period seismic motion to permanent deformation.

However, with an increase in sensitivity of instrument it was found that considerable variations due to a meteorologically induced effect are commonly observed and they severely affect the recognition of an anomalous

earthquake precursor from the observed data. Furthermore, the observed strain steps at several places did not always show good agreement with the theoretical ones. Therefore, it was pointed out that siting or mounting problems as well as an instrumental one are important for the systematic interpretation of extensometer records (King,1971; King and Bilham,1973; Harison,1976). Due to a variety of site effects the measured strain field seems to differ from the strain field of geophysical interest, e.g. confusion in the case of the observed strain steps (Aki and Richards,1980; Okada,1980b).

However, to understand the mechanisms and the characteristics of tectonic movements including the premonitory movements of an earthquake it is still important and indispensable to watch continuous crustal movement. For this observation, the extensometer is excellent as a practical tool. In order to study the exact source process including an earthquake having an abnormal long time constant, it is important to observe the whole movements caused by the earthquake. This observation can be realized only by the extensometer. Therefore, we need to verify the reliability of the extensometric observations at each station including the site effects by comparison of the data obtained by the extensometer with those by other methods. For the purpose analysis of seismic strain, especially body waves which have not received much attention are relevant to the calibration for the extensometer system

including the site problems (Benioff,1963; Kanamori and Cipar,1974; Okada,1975a; Sasatani and Kasahara,1978; Okada, 1980a). The following problems are concretely pointed out in relation to the reliability of the extensometric observation.

One of them, concerning the secular movements, is whether the results based on the short base line-length at most several ten meters can represent wide-areal crustal movements or not. Another, concerning seismic movements, is whether the mechanical part of extensometer can stably respond to them having rather large acceleration or not. Although these two problems are extremely different in the frequency of the movements, the behavior of the extensometer to both are quite the same in principle. Therefore, if either condition is not satisfied, the reliability for the other result will decrease. After the verification of the reliability for both problems it is truly said that the extensometer can observe the various crustal movements widely ranging in time. Under this verification it will be possible to discuss the extraordinary crustal movement in relation to the earthquake precursor based on the observed data. Until now, inquiries into two problems have not been made sufficiently at each station because the geodetic data around the station are deficient for the former problem, and useful data are scarce and interpretation methods are not far advanced for the latter.

The purpose of this study is to show the availability of the use of extensometer in geophysical interest by solving two problems. The data used are obtained by three components of quartz-tube extensometer with a length of 30 meters installed in a newly constructed vault at Erimo, Hokkaido during the period from the beginning of observation in August 1971 to March 1981.

Chapter 2 consists of the descriptions about the instrumental features of the extensometer used and the physical environment of the station as well as the improvement of the recording system possible to provide useful data for analyzing strain seismograms.

Chapter 3 being concerned with secular strain variations is divided into two sections. In the first section the results obtained by extensometric observation are compared with those by the repeated length measurements of the long base-line network located around the observatory by means of an electro-optical distance-measuring instrument (EDM). In the second section abnormal strain changes before and after the 1973 Earthquake off the Nemuro Peninsula are examined in detail with considering a meteorologically induced effect.

Chapter 4 being related to seismic strains is composed of three sections. In the first section the observed strain steps associated with 44 earthquakes during about 10 years' observation are examined in terms of the static source parameter of the earthquake. In the following

section the synthetic strain seismograms due to a point shear dislocation in an infinite, homogeneous medium are derived and are compared with the observed ones effectively provided through the improved recording system. This comparison is made to reveal the dynamic source parameters of the event as well as the mechanical stability of the extensometer. In the last section the source characteristics of the 1978 Kunashiri Strait Earthquake with magnitude of 7.7, which is an example of slow earthquakes , are deduced from the observed strain seismograms in order to demonstrate the excellent availability of the extensometer as a seismometer.

CHAPTER 2

OBSERVATIONAL SYSTEM AND DATA

Principle of extensometer and installation at the Erimo Geophysical Observatory

Extensometers are operated by the principle shown in Fig.1. Two piers A and B separated by a distance, l , are coupled to the rock. One end of the rod R as a length standard is rigidly fastened to the pier B and another end extends to within a short distance of pier A. Owing to several ten meters of the solid length standard, the rod should be supported by some instruments which effectively constrain the rod so that it can move only in the longitudinal direction. Changes in their separation of the longitudinal direction, dl , are detected by a displacement transducer with an appropriate sensitivity. One can determine the linear strain of this direction to divide the separation change, dl , by the distance of two points, l , i.e. $\varepsilon = dl/l$.

Instead of the rod as a length standard, one can, of cource, use a thin invar wire (Sassa et al.,1951, King et al.,1969; Sydenham,1969,1972) or a laser interferometer system (e.g. van Veen et al,1966; van Veen,1970; King and

Gerard,1969; Berger and Lovberg,1970).

Due to economical reasons and the stability in operation the following rod system extensometer was selected in the Erimo Geophysical Observatory (EGO). Schematic representation of the main parts of the extensometer at EGO is shown in Fig.2. It was intended to make simple constitution of mechanical design as a whole. The fused-quartz tube length standard is 30 meters long and is made up of 2 meter sections of milky quartz tubing 2.6 cm in outside diameter by 0.25 cm wall thickness. The sections are connected end to end by welding. The standard is fixed by fasthening mechanism using a tapered iron pipe with a narrow gap. The quartz tube is supported at one meter intervals by supporting structure, which was the inverted pendulum type at first as shown in Fig.2 (A) (Blayney and Gilman,1965; Okada et al.,1975) and is now the hanging system by double slings of stainless-steel wire 0.1 mm in diameter as shown in Fig.2 (B) from the end of 1979. The latter is a slight modified form of the Benioff's design (Benioff,1959). The standard is covered with 5 cm thickness poly-styrene in order to deduce thermal effects resulting by short term disturbances. Differential transformer has been used as a displacement detector. Magnesensor is also added at the time when the sensitivity of the system is increased. Sensitivity calibration of each displacement detector is carried out by the comparison between the output voltage of the transducer and the

displacement given to it by shortening mechanism and read out by a micrometer.

Physical environment of the station

The upper part of Fig.3 shows a geological sketch map around EGO (Funahashi and Hashimoto,1951). An observational vault was dug in 1970 to 1971 at the foot of a hill with a relative altitude of about 130 meters which consists of entirely the triassic slate. The northern part of the line A-A' as shown in this figure, which is called Horoizumi (old name of Erimo) Sheared Zone, is occupied by complex metamorphic rock. On the other hand, the southern part of this line including the vault shows uniform geological structure. A cross section along the longest direction of the vault and the ground plane of the vault are shown in the middle and lower parts in this figure. Three components of the extensometer installed in the vault named as E-AB (NW-SE direction), E-CD (NE-SW direction), and E-EF (E-W direction) components are shown in the ground plane, where the fixed ends of the components are B, D, and E, respectively. More detailed description about EGO has presented in the previous paper (Kasahara et al.,1972)

Observed data and influence factors

Figure 4 shows a schematic representation about the relation between the signal flow and influence factors through the crustal movement observation in the vault (after Shichi and Okada,1979 with a slight simplification). The data that can be obtained by the extensometer in the vault may be distorted by the effects of miscellaneous factors, which are called site effects, and may be superimposed with the noises of various sort as shown in this figure.

Therefore, it is important to observe other factors simultaneously in order to elucidate their induced mechanisms. In addition, for the verification of the data observed at the vault it is very useful to observe crustal movements by other methods and to derived those from the theory.

The wide-areal crustal movement around the station should be measured on the basis of a geodetic method. By the comparison of the secular variations observed in wide-areal network and at the vault one can examine a long term stability of the extensometer. The movements associated with earthquakes which are recorded as strain seismograms including strain steps can provide another useful data. By the comparison of the observed strain seismograms with the synthetic ones due to a relevant source model, one can investigate the total response of the extensometer in relation to its mechanical stability as well as site effects.

Instrumental stability test

Mechanical stability of the extensometer is closely related with its design. Frictional resistance force due to a supporting system and optical magnification mechanics for the displacement transducer may affect the stability (Balavadze et al.,1962; Takemoto,1975). Although such instrumental instability was carefully avoided when the extensometer was designed, it is still useful to check the mechanical stability of our system experimentally. The method used is that the response is checked by the longitudinal pulsive loading to the fixed end point (Balavadze et al.,1962; Yamauchi et al.,1974).

Figure 5 shows the records of three components for the loading experiment. An arrow with the mark '*m*' in this figure denotes the strain change of the ground by the load of two persons near the fixed end. The disturbance denoted by an arrow with the mark '*w*' in the E-EF component is generated by collision between the quartz tube and the poly-styrene cover. In the records the variation with amplitudes of 5 to 10 part in 10^{10} at periods of several to several ten seconds corresponds to microseism. The monotonous contractive variations, which are deceptive ones due to thermal expansion of the quartz tube by persons and electric lights during the experiment, are clearly shown in all the components. Solid and open triangles show the beginning and the finish of the loading test. Considering

these noises we could not find any abnormal step-like differences on the records before and after the loading test.

Magnitude of the load applied to the fixed end is measured by a spring balance and the resultant displacement at the free end is determined from the record trace. The stress-strain relation of each component obtained by this experiment is shown in Fig.6. Precision of the load measurement is about 0.5 kg in this procedure. The good linearity can be seen in the variation less than 1 part in 10^9 for each component. Thus it may be concluded that the extensometers installed at EGO have no hysterisis.

The experiment shown in Fig.5 was carried out for the suspension system of the supporting mechanism. An inverted pendulum system was also tested by this loading experiment and adjusted to keep the non-hysterisis condition. Resultant deformation with amplitudes of about 2 part in 10^9 is arised because of the load of one person at the end point as shown in Fig.5. When a person stands at the end point to make a manual observation for the water-tube tiltmeters which are set parallel to the extensometers, the load deformation always occurs and is recorded on the routine record trace of the extensometers. From these records, one can continuously check the hysterisis of the extensometers.

Observational system

Figure 7 shows a block diagram of the system for observation and recording used in the present study. The observation which started in August, 1971 was made by only recording the output voltage from differential transformer of each component individually to increase the detectability for the strain step. The sensitivity and the chart speed of the recording system have been kept in 1.8×10^{-9}/mm and 25 mm/h, respectively from the beginning of the observation. The records by this recording system is called the routine records, from which hourly values are read. The records provide the fundamental data for studying the crustal movements longer than a day. This recording system is not suitable for obtaining a good time resolution on the movements shorter than five minutes.

When one attempts to record seismic strain with a favorable response up to DC component by analog mode, records are obtained frequently out of scale on the chart due to the tidal and secular strain variation. This verifys that the extensometer can respond to DC. Therefore, it is usually carried out in the observation to cut off the variations longer than a period 53 minutes which corresponds to approximately the longest period that the modes in the free oscillation of the Earth have. Moreover, the limitation of chart speed due to economical reasons requires an appropriate high cut filter, by which a good record is

obtained so that the total system of extensometer as a seismometer may also show a function as band pass filter (Benioff,1963; Major et al.,1964; Kishimoto et al.,1968; Oike et al.,1969; Okada,1980a). These recording system cannot make a good use of the frequency-independent characteristics which is a notable feature of the extensometer.

In order to analyze the observed strain seismograms as well as to study the source process of earthquakes, the direct records of the extensometer with a good time resolution without any low-cut filter are required. For the reason, a digital recording system possible to maintain a wide dynamic range is the best one for the extensometric observation (Berger and Wyatt,1973). On the telemeterization in July, 1976 for the seismic and geodetic observation network of Hokkaido University, the digital system as shown in Fig.7 was introduced (Kasahara,1976; Maeda et al.,1978). Sampling rate for data by the extensometer is determined as twice of an available shortest frequency by the quartz tube extensometer of 30 meters long. The upper limit of the observable frequency possible to measure a relative displacement between two points with a distortion less than 1 % is about 3.5 Hz for the extensometer used (Benioff, 1935). Therefore, sampling frequency for the extensometer as a strain seismometer is provided with 6.15 Hz. The data are sampled in 10 bits linear quantization mode and are transformed with non-linear quantization in 8 bits mode

for transmitting and recording the data. All the data are continuously recorded on a magnetic tape through the High Density Data Recorder.

During the period from July, 1976 to November, 1977 the data through the high-cut filter with a short-period cut-off at 1 Hz have been recorded with a sensitivity of 0.785×10^{-9}/bit. The sensitivity and the cut-off frequency of the high-cut filter have been varied to 1.36×10^{-9}/bit and to 0.5 Hz, respectively from March of 1978. From these conditions we could obtain the strain seismograms enough to analyze the earthquakes with magnitudes of about 5 or less and with an epicentral distance of about 100 km. In addition to these channels, a high gain channel which consists of the band-pass filtered data between 3 Hz and 0.01 Hz with a sensitivity of 1.13×10^{-10}/bit has been provided for the purpose of analyzing smaller earthquakes and checking the availability of the extensometer up to their limited period.

CHAPTER 3

SECULAR STRAIN VARIATIONS

One of the most important purpose of the continuous crustal strain observation in the vault is to elucidate the progress of its accumulation that cannot be observed by the geodetic surveys. However, this opinion is true on the assumption that the observed result in the vault represents the wide-areal crustal movment. Only after the establishment of this assumption at each station one can discuss problems concerning the progress of crustal strain accumulation as well as the extraordinary phenomena associated with earthquakes based on the data obtained by the continuous observation in the vault.

A long base-line network was constructed around EGO in 1972 to examine this assumption because there had been no precise triangulation network around the Erimo region conducted by Geographical Survey Institute of Japan. A measurement of length of each base line has been carried out every year by the use of EDM. Secular strain becomes large enough to compare with both results after nine years' accumulations of the data due to the relation between the precision of the EDM and the accumulation rate of crustal strain in the Erimo region. Both results are in fairly good agreement. Hence, it can be said that the data

observed by the extensometers in the vault can be of the representation of the wide-areal crustal strain accumulation. This result will be described in section 3.1.

The data obtained by continuous observation can be positively examined in relation to premonitory phenomena of earthquakes. Actually, abnormal strain changes have been observed just before and after the 1973 Earthquake off the Nemuro Peninsula which is the largest event during the last ten years' observation. Raw data obtained contain deceptive variation by external origins described in the previous section. The crustal strain in the vault of EGO is severely affected by precipitation. Pore pressure change due to groundwater table variation, which is, of course, brought about by precipitation, may be the cause of serious variation of crustal strain. The observed abnormal strain changes associated with this event are qualitatively revealed with considering water-discharge from the vault as an indicator of groundwater table. This result will be described in section 3.2.

3.1 COMPARISON OF THE SECULAR STRAINS OBTAINED BY EXTENSOMETER AND BY LONG BASE-LINE NETWORK

Extensometer data

Figure 8 shows daily variations of crustal strain obtained by three components of extensometers during the period from the beginning of observation in August 1971 to March, 1981. Daily variations of precipitation and water discharge from the vault are also shown. Short period variations of crustal strains appear to be mainly due to the change of water discharge caused by precipitation as clearly shown in this figure in each of three components. Considerable variations with a sense of monotonous contraction in E-AB and E-CD components are shown in early stage of the observation. These variations are well represented by exponential decay functions and are, therefore, probably caused by the construction of the new vault. The results subtracting these effects are shown in Fig.9. The secular variations longer than 1 year and 4 years which are obtained by digital filtering (Shichi,1972.1973) are also shown in this figure. These results are regarded as the secular variations accumulated during the last decade that the extensometers could observed in the vault. Accumulation rate of crustal strain obtained by the extensometers is

about 2 to 3 part in 10^7 per year. This rate accords with the stationary strain accumulation rate revealed by triangulation surveys over the whole Japan (Nakane,1973a, 1973b).

Long base-line strain data

Figure 10 shows an arrangement of long base-lines constructed around EGO. The network started with eight base-lines in 1972 and has lasted with fifteen base-lines from 1974 to the present. The 6-A type of Geodimeter was used until 1974 and the 6-BL has been used from 1975 as an EDM. The base-line length is determined with the atmospheric refraction correction by use of air temperatures and barometric pressures observed at both end points. Special pier with a bolt anchored was constructed to avoid a setting error in each measurement at all the points except E and S points utilizing the third order triangulation points.

Figure 11 shows the observational results of repeated length measurements for fifteen base-lines. Assuming linear strain accumulation for all the base-lines, their annual rates of lengthening are determined by a least squares fit to those measurements over the nine intervals. In this procedure the data shown by open circles were excluded because their measurements were carried out under

rather different atmospheric conditions from those of other measurements. The result by the least squares fit to the fifteen base-lines are summarized in Table 1.

The standard deviation of prediction errors of fifteen base-lines is shown as a function of line length in Fig.12. It can be seen that the relative precision of about 1 ppm of line length is maintained as a whole. The accumulated strain amount for the fifteen base-lines for ten years is shown as a function of azimuth of the base-line in Fig.13. The vertical bar of each plot denotes the standard deviation of strain amount as deduced from the least squares fit to each of fifteen base-lines. The results obtained by three components of extensometer in the vault are also plotted by open squares in this figure.

The linear strain in a horizontal direction with angle θ is given by

$$e_\theta = e_{xx} \cos^2\theta + e_{yy} \sin^2\theta + e_{xy} \sin 2\theta$$

where e_{xx} , e_{yy} , and e_{xy} are the three components of plane strain. They are calculated by a least squares fit to the results of twelve base-lines except three base-lines shown by open circles in Fig.13 for a coordinate system in which the x axis is directed to the east and the y axis to the north. The best fit curve has also been plotted in the figure. We have no answer why three base-lines differ from the strain field as a whole. However, it can be considered

that this result represents the horizontal crustal strain accumulation around the Erimo region during the last decade, judging from the extent covered with twelve base-lines. The results of secular strain accumualtions obtained by geodetic measurements around EGO and by the extensometric observation in the vault are summarized in Table 2.

Comparison of both results and concluding remarks

Figure 14 shows the principal strains of the accumulated strains for ten years obtained by both measurements. Although there is a slight difference in orientation of principal strain axes, the tendency of the compressional strain field with azimuth of almost east to west and their accumulated strain amounts are in good agreement. The east to west compressional strain field obtained by geodetic measurement is consistent with the results by the analyses of fault plane solutions of earthquakes which occurred around the southern part of Hokkaido (Takanami,1978; Suzuki, personal communicatio,1981). The earthquakes occurring in the sea region and in the deeper part around southern part of the Hidaka range show the fault plane solutions with P-axis of NW-SE direction parallel to the slip vector of Pacific plate motion. On the contrary, the shallower earthquakes occurring in the western part of the Hidaka range including the Erimo region indicate P-axis of E-W

direction,

From these observations, it is concluded that the strain accumulation with a rate of about 2 to 3 part in 10^7 per year and with the east-west compressional strain field has progressed around the Erimo region for the last ten years and the extensometers in the vault have responded nearly to this movement. Therefore, the availability of the extensometer in the vault at EGO for detecting regional crustal movement was confirmed.

3.2 ABNORMAL CRUSTAL STRAIN CHANGES BEFORE AND AFTER THE 1973 EARTHQUAKE OFF THE NEMURO PENINSULA

Description about the event

At the time when the continuous observation of crustal movement started at EGO, the occurrence of an earthquake with a magnitude of about 8 had been forecasted off the Nemuro Peninsula in the near furture on the basis of the seismicity gap conception by Utsu (1972). On June 17, 1973 the earthquake (Ms=7.7, NOAA) occurred just in the predicted area about two years after the beginning of the observation at EGO. Just after the event, there was discussion about the possibility whether a large earthquake would occur again around there or not because the magnitude of the event was smaller than that expected (Abe and Yokoyama, 1974; Hatori,1975; Abe,1977; Utsu et al.,1977). Until now, another earthquake in question has not occurred in the area. The 1973 earthquake was the largest one observed at Erimo during the observation period from 1971 to 1981.

Figure 15 shows the location of EGO and the aftershock area of this event determined by Japan Meteorological Agency (JMA). The source parameters of this earthquake have been obtained by Shimazaki (1974) and Tada (1974) on the basis of the seismological data and the geodetic ones,

respectively. According to their results, the event was characterized as a typical low dip angle reverse faulting which occurred normally along the island arc with a fault area of 100x(60-100) km^2, an average dislocation of 1-1.6 meter, and a seismic moment of $6.7x10^{27}$ dyne·cm. The epicentral distance to EGO is about 250 km.

Observed data and results of analyses

According to the observed data by the extensometers for about ten years shown in Fig.9 in the previous section, abnormal change of crustal strain is recognized only before and after this event of which occurrence time is denoted by an arrow in each component. The anomalous extension, which is clearly shown in the E-EF component before the event, is considered as the abnormal change related to this earthquake.

The detailed variations during the period from 1972 to 1974 are shown in Fig.16. The co-seismic strain steps were also observed distinctly. They are shown by dotted lines in the figure. The observed strain steps agree with the theoretical ones based on the fault parameters as will be described in the following section. The water-discharge from the vault have been measured together with the precipitation at EGO from the beginning of observation.

These results are also shown at the lower part of this figure. As can be seen in the figure the short period variation of crustal strain clearly corresponds to that of water-discharge which is caused by precipitation. The extension of crustal strain in the E-AB and E-CD components corresponds to the increase of water-discharge and the contraction to the decrease of water-discharge. The opposite correspondence appears in the E-EF component.

While the water-discharge had gradually decreased from the beginning of May, 1973 to the earthquake occurrence time, the rate of contraction for the E-AB and E-CD components had become smaller and that of extension for the E-EF component had reached three times as large as the normal rate. Such unusual strain changes had appeared only at this period during the last about 10 years observation.

In all the components, a good linear relation between the variation of crustal strain and the logarithm of water-discharge continues during the decreasing stage of water-discharge. The variations under tha similar condition of water-discharge as shown in Fig.16 were compared with each other to demonstrate the abnormal variation of this period. Figure 17 shows the relation of logarithm of water-discharge to strain, which are shown by solid circles, open circles and cross marks for the relation in 1972, 1973, and 1974, respectively. The relations in 1972 and 1974 are very similar to each other in all the

components except for the increasing stage of water-discharge in the middle of 1974. The relation before and after the earthquake of 1973 is distinctly different from these relations, but about 15 days after the event it recovered to the normal relation in all the components.

To represent only the abnormal portion appearing in the relations, the correction of the strain change due to the water-discharge was made for the variations in 1973. As the corrected value the mean value of variations of each component in 1972 and 1974 was taken.

Figure 18 shows the residual strain change subtracting the effect of water-discharge. If the abnormal change did not occur, the variation of strain should be zero and the plot of it should be flat in Fig.18. Therefore, the changes except those between two horizontal lines after the event in the figure may be concluded to be the abnormal changes associated with this large earthquake observed at EGO.

Before the event the abnormal change was characterized by extension in all the components. Unfortunately, it is difficult to determine the exact time of the beginning of this phenomenon because the phenomenon probably began in the increasing stage of water-discharge. However, the duration of the phenomenon may be more than 40 days from Fig.18 but less than 100 days estimated by the seismic activity around the source region (Kasahara,1976). After the event the crustal strain in each component behaved as continuation of the co-seismic one for about 15 days.

Some constants of the crustal strain changes associated with the event are summarized in Table 3.

Concluding remarks

The abnormal changes of crustal strain were clearly observed at EGO before and after the 1973 Earthquake off the Nemuro Peninsula and could be demonstrated by considering the meteorologically induced effects on the basis of simultaneous observations of their factors.

Pre-seismic strain change was characterized by the increase of areal dilatation which is contrary to the co-seismic strain step and seems to begin more than 40 days and less than 100 days before the event. On the other hand, post-seismic strain change was the same as the co-seismic one and continued about 15 days after the event. The amounts of the pre- and post-seismic abnormal strain changes did not exceed that of the co-seismic one.

From these results, it may be concluded that the maximum amount of precursory crustal movement which will be expected from an earthquake at a station should be less than the amount of the co-seismic movement observed at the same station.

CHAPTER 4

SEISMIC STRAINS

A pronounced availability of the extensometer as a seismometer is that it can uniformly respond to crustal movements in the frequency range from several Hz to DC without such transient characteristics as a pendulum-type seismometer has.

A notable demonstration for this availability may be shown by the evidence that the permanent strain field change associated with earthquakes, which is the called strain step, can be detected by the extensometer. After the theoretical representation of strain step was developed by Frank Press (1965), the observed strain steps have been examined in relation to static source parameters by many investigators (Wideman and Major,1967; Takemoto and Takada, 1969; Japanese Network of Crustal Movement Observatory,1970; Shichi et al.,1970; Mikumo,1973,1974; Kasahara,1973,1974; Okada,1975b,1978,1980b). In fact, a strain step can be determined even from the offset of a record trace following an earthquake obtained by a low-chart-speed record. According to these examinations, some stations have often experienced that polarities of observed strain steps are not in agreement with theoretical ones and also that

amplitudes of strain steps are larger than those expected in theory by one order or more. Such inconsistency may be attributed to the mechanical problem of instruments installed or the site effects of stations placed (Shichi et al.,1970; Okada,1980).

Until now, strain seismograms of body waves have not received much attention because available data for analysis of strain seismograms have been scarce and the methods of interpretation have not been far advanced. The extensometer actually can record not only strain steps but also dynamic strain variations due to an earthquake. On the other hand, both the strain step and the dynamic strain variation can be calculated by applying the theory of elasticity. For the analysis of strain seismograms, therefore, the systematic comparison should be made on both the observed and calculated quantities of the strain step and dynamic strain variation. Of these quantities, the dynamic strain seismograms will give new information for the study of the source process of earthqaukes. More extensive analysis should be made on the dynamic strain seismograms. The comparison is also very useful for the calibration of the extensometer system; that is, the compared results may provide answers for the site effects and instrumental problems.

In the first section of this chapter, 44 strain steps observed at EGO during the period of the last decade will be investigated in relation to the static source parameters

of earthquakes. This investigation will also contribute to check reliability of the extensometers for the response to seismic strains.

In the following section, the exact solution of the strain fields excited by a double-couple point source model in an infinite, homogeneous medium will be derived. After that, mainly for dynamic strains associated with earthquakes, synthetic strain seismograms will be compared with the observed strain seismograms that the improved observational system could record.

Since distinction between dynamic and static monitoring is, in a sense, an artificial one, the extensometer can fully record strain step and dynamic strain due to an earthquake; therefore, it can provide complete data for the study of earthquake source mechanism. In the last section, the analysis of strain seismogram will reveal the source characteristics of the 1978 Kunashiri Strait Earthquake. The result to be obtained from the analysis will throughly prove the highly excellent availability of the extensometer.

4.1 STRAIN STEPS ASSOCIATED WITH EARTHQUAKES

Data

Extensometers of EGO have registered distinct strain steps associated with 44 earthquakes with magnitudes ranging from 4.7 to 7.7 in JMA scale during the period from August, 1971 to January, 1980. The range of epicentral distances of these events is 13 kilometers to 1,300 kilometers. The strain step observed was defined as the offset of a record trace before and after the event on the routine record.

Figure 19 shows the epicenter distribution of the 44 earthquakes accompanied with the strain steps at EGO. Figure 20 shows seven examples of the strain steps registered on the routine records. The strain steps with amplitudes greater than 1 part in 10^8 could easily be measured as shown in Fig.20 (a) to (d). The minimum amplitude available depends on both the ground noise level at the time and the appearance of coda wave of the earthquake. Under the good condition, the strain step with amplitudes of 1 to 2 part in 10^9 can be recognized as shown in Fig.20 (e) to (g).

The hypocenters and the magnitudes determined by JMA, the epicentral distances to EGO, the amplitudes of strain steps observed by three components, and the seismic moments estimated from both magnitudes and observed strain steps

are listed in Table 4 for all the earthquakes.

Comparison of observed strain steps with theoretical ones

To check the reliability of the observed strain step, comparison was made between the observed strain step and the theoretical one. The theoretical strain step was calculated using the analytical solution derived by Okada (1975), which was obtained for the surface static strain field due to a double-couple point source model in a semi-infinite, homogeneous medium. In the following calculation, the source parameters, the fault plane solutions and the seismic moments obtained by conventional seismological methods are used, where rigidity was assumed to be 3.3×10^{11} dyne/cm^2. For the purpose six earthquakes are available : No.1 (Kasahara,1973), No.9 and No.10 (Shimazaki,1974), No.18 (Sasatani,1980), No.37 (Seno et al.,1980) and No.40 (Sudo and Sasatani,1979) in Table 4.

Figure 21 shows the relation between the observed and theoretical strain steps obtained for these earthquakes. The amplitudes in the range from 1 part in 10^9 to 5 part in 10^7 as well as the polarities excluding a case of the E-AB component for the No.18 earthquake are well harmonized with one another within a factor of 2 to 3. Scatter of the amplitude correlation may be partly attributed to a simple model employed.

Since the extensometer gave the records with a wide coverage for the amplitude of the observed strain step, it may be concluded that the strain steps observed at EGO are not suffered from the serious site effect and also from the instrumental effect. This means that the strain steps observed at EGO can be directly connected to the source parameters.

It is known that the amplitude of observed strain step is more sensitive to the seismic moment than the fault geometry of the earthquake. The amplitudes of the observed strain steps remaining unexplained will be discussed in relation to the seismic moment alone on the basis of an empirical relation between magnitudes and seismic moments of earthquakes.

Relationship between observed strain steps and seismic moments

Figure 22 shows the maximum strain step in three components for an earthquake plotted as a function of hypocentral distance and earthquake magnitude. Let us assume the following relation between the magnitude of earthquake, M_{JMA} , and the maximum strain step, e_{step} in 1 part in 10^9, observed at the hypocentral distance , R . in kilometers :

$$M_{JMA} = a_0 + a_1 \cdot \log(e_{step}) + a_2 \cdot \log(R) \quad , \qquad (1)$$

where a_0 , a_1 , and a_2 are constants.

The coefficient in equation (1) were determined by a least squares fit to the data for 42 events excluding No.20 and No.32 which are deep focus earthquakes. The result is as follows :

$$M_{JMA} = 1.35 + 0.67 \cdot \log(e_{step}) + 2.0 \cdot \log(R) . \qquad (2)$$

Here, the standard deviation of prediction error of M_{JMA} is 0.21. From this empirical formula, the contours are shown in Fig.22 which indicate the epicentral distances at which strain steps of 1 part in 10^5 to 1 part in 10^{10} are expected after the occurrence of earthquakes with various magnitudes. It is more favorable to substitute the seismic moment instead of the magnitude in equation (2) for comparison between this observational result and the relation expected by the theory of earthquake model.

The following relation between the seismic moment, Mo, and the moment magnitude scale, $\overline{M}$, has been shown by Hanks and Kanamori (1979),

$$\log(Mo) = 1.5 \cdot \overline{M} + 16.05 \qquad (3)$$

This formula is uniformly valid for $3 \leq M_L \leq 7$ and $5 \leq M_S \leq 7.5$ instead of $\overline{M}$.

It is well known that the magnitude determined by JMA, M_{JMA}, used in this study, is approximately equivalent to M_L for $4 \leqslant M_{JMA} \leqslant 6$ (Katsumata and Kashiwabara,1977) and to M_s for $6 \leqslant M_{JMA} \leqslant 7.5$ (Noguchi,1979). Therefore, the equation (3) is also valid for $4 \leqslant M_{JMA} \leqslant 7.5$ instead of $\bar{M}$. When we substitute the right-hand side of equation (2) into equation (3), we obtain

$$\log(Mo) = 18.1 + 1.0 \cdot \log(e_{step}) + 3.0 \cdot \log(R) \qquad (4)$$

where Mo is in dyne·cm, e_{step} is in 1 part in 10^9 and R is in kilometers. We change the above equation into the following form :

$$e_{step} = \frac{1}{1.3 \times 10^{18}} \frac{Mo}{R^3} \quad . \qquad (5)$$

That is, the strain step amplitude observed at EGO is proportional to the seismic moment and to the inverse of the cube of the distance. This equation accords well with the following theoretical representation of the surface strain field due to a double-couple point source in a semi-infinite elastic medium obtained by Okada (1975).

$$e_{step} = \frac{Rc}{2\pi\mu} \frac{Mo}{R^3} \quad , \qquad (6) \quad .$$

where Rc is the constant relating to the geometry of the

source and the instrumental orientation and μ is the rigidity of medium. We choose the maximum strain step in three components as a strain step in equation (5). We must, therefore, take a little larger value than the average one of Rc in equation (6) to compare equations (6) with (5). Assuming that Rc is about 1 and the rigidity of medium is 3.3×10^{11} dyne/cm^2 in equation (6), we obtain

$$e_{step} = \frac{1}{2 \times 10^{18}} \frac{Mo}{R^3} \quad . \qquad (7)$$

The proportional constant is also in agreement between the observational result and the theoretical one within the bounds of data and theory used here. That is, the strain steps observed at EGO accord with the expected ones from the theory of elasticity assuming a rigidity of about 3.3×10^{11} dyne/cm^2.

Concluding remarks

The three extensometers installed in the vault of EGO can well registered the strain steps ranging from 1 part in 10^9 to 1 part in 10^6 in amplitude associated with earthquakes without any instrumental problems. The seismic moment of the event can be estimated within a factor of

2 to 3 from the observed strain step and the hypocentral distance, even if the fault plane solution and any site effects are not taken into account.

4.2 ANALYSES OF STRAIN SEISMOGRAMS

Theoretical strain seismogram

In order to interpret the observed strain seismograms we will consider synthetic strain seismograms for an earthquake model and match them with the observed records to obtain appropriate source parameters. As source model we will take a double-couple point source in an infinite homogeneous medium for the first approximation. It is well known that this approximation provides good comparison of wave forms so far as the early part of P- and S-waves prior to the arrival of surface waves is taken.

Let us take the Cartesian co-ordinates (x,y,z) in an infinite medium and put a double-couple point source with the moment rate function, $M(t)$, parallel to the plane (x,y) on the origin as shown in Fig.23. This point source is equivalent to the shear faulting (Maruyama,1963). Dynamic displacements (U_x,U_y,U_z) at a point (x,y,z) are given (Honda,1962) by

$$U_x = - \frac{Mo}{4\pi\rho} \{ 2 \frac{\partial^3}{\partial x^2 \partial y} (\Phi - \Psi) + \frac{\partial}{\partial y} \nabla^2 \Psi \}$$

$$U_y = -\frac{Mo}{4\pi\rho}\left\{ 2\frac{\partial^3}{\partial x \partial y^2}(\Phi - \Psi) + \frac{\partial}{\partial x}\nabla^2\Phi \right\} \qquad (8)$$

$$U_z = -\frac{Mo}{4\pi\rho}\left\{ 2\frac{\partial^3}{\partial x \partial y \partial z}(\Phi - \Psi) \right\}$$

where, $\Phi = \frac{1}{r} F(t-t_\alpha)$, $\Psi = \frac{1}{r} F(t-t_\beta)$,

$r = (x^2 + y^2 + z^2)^{1/2}$, $t_\alpha = \frac{r}{\alpha}$, $t_\beta = \frac{r}{\beta}$,

$$F(t) = \int_0^{t'}\int_0^{t''} F''(t'')dt''dt' \quad , \quad F''(t) = \frac{1}{Mo} M(t) \ ,$$

ρ is the density of the medium, α and β are the velocities of P- and S-waves and Mo is the final seismic moment. The spatial differentiation of these displacement fields may give the dynamic strain fields, ε_{ij}.

$$\varepsilon_{ij} = \frac{1}{2}\left(U_{i,j} + U_{j,i} \right)$$

$$U_{i,j} = -\frac{Mo}{4\pi\rho r^5}\left[\frac{1}{r^3} \cdot C^1_{ij}\, G(r,t) \right.$$

$$+ \frac{1}{r^2}\left\{ \frac{C^{2p}_{ij}}{\alpha^2} F''(t-t_\alpha) + \frac{C^{2s}_{ij}}{\beta^2} F''(t-t_\beta) \right\}$$

$$+ \frac{1}{r}\left\{ \frac{C^{3p}_{ij}}{\alpha^3} F'''(t-t_\alpha) + \frac{C^{3s}_{ij}}{\beta^3} F'''(t-t_\beta) \right\}$$

$$\left. + \left\{ \frac{C^{4p}_{ij}}{\alpha^4} F''''(t-t_\alpha) + \frac{C^{4s}_{ij}}{\beta^4} F''''(t-t_\beta) \right\} \right] \qquad (9)$$

where, $G(r,t) = \frac{1}{r}\{F(t-t_\alpha)-F(t-t_\beta)\} + \frac{1}{\alpha}F'(t-t_\alpha) - \frac{1}{\beta}F'(t-t_\beta)$.

$U_{i,j}$ denotes the differentiation of U_i component with repect to j axis and the suffix of i and j takes all of x, y, and z. Coefficient of C_{ij}^{l} to C_{ij}^{4s} are summarized in Table 5. A parabolic ramp function was assumed as a moment rate function (Okada,1975; Sasatani and Kasahara,1978). The moment rate function, M(t) , is given by

$$M(t)/Mo = \frac{2}{\tau_e^2}\cdot t^2 \qquad \text{for } 0 \leq t \leq \tau_{e/2}$$

$$= 1 - \frac{2}{\tau_e^2}\cdot(\tau_e - t)^2 \qquad \text{for } \tau_{e/2} \leq t \leq \tau_e$$

$$= 1 \qquad \text{for } t \geq \tau_e$$

as shown in Fig.24. The rise time, τ_e , is approximately equivalent to the total duration of faulting for an earthquake (Kanamori and Anderson,1975) and is, therefore, called "source process time" hereafter.

To evaluate the synthetic strain seismograms the following procedure are taken. We assume an imaginary plane in an infinite medium so as to coincide with the ground surface. On the plane, a new co-ordinate system will be set up (see Fig.23). Hence, the old co-ordinate system may completely be described in the new one with the source depth and the dip and slip angles of fault plane. Using equation (9), synthetic strain seismograms at an arbitary point on the surface can be calculated with

parameters of the source location, the fault plane solution, the final seismic moment, and the source process time of an earthquake. In the calculation, P and S wave velocities which are calculated from the observed S-P time by assuming the poisson ratio of 0.25 for the medium are used. Finally, the synthetic strain seismograms are transformed into directions of actual extensometers installed (Jaeger and Cook,1965) for comparison of the observed strain seismograms and the synthetic strain seismograms. The free-surface effect is approximated by doubling the calculated amplitude. Okada (1980a) has represented the exact solution of the strain field in a semi-infinite medium, in which our approximation for the part of body waves is available. In the following analyses the initial part of body waves will mainly be investigated.

Data and method of analysis

Figure 25 shows the first one of the strain seismograms observed by the newly improved recording system. The seismogram shows simple features so that there seems to be no problem in the dynamic characteristic of the extensometer. In this section, the observed strain seismogram is referred to until synthetic strain seismograms calculated for different source parameters give a close agreement with the observed one. Through the procedure, the source

parameters giving such agreement will be taken as ones of the earthquake observed.

Synthetic strain seismograms can be computed if the location, the fault plane solution, the source process time, and the seismic moment are given for the event. In the computation, the location and the fault plane solution accurately determined by the data from short period seismic observation networks were used. From several calculations and careful comparison of waveform between the observed and the synthetic strain seismograms, the optimal source process time was determined. In addition, the seismic moment was obtained with good agreement between the amplitudes of both seismograms.

Among the strain seismograms observed from the beginning of July, 1976, with which the new system started, to January, 1979, those for 14 earthquakes were taken for the analysis. Figure 26 shows the epicenters and the fault plane solutions of these earthquakes. Their hypocentral parameters, magnitudes, and epicentral distances to EGO are presented in Table 6. The number of the events in Table 6 will be refer to in the later figures.

The fault plane solutions for the eight earthquakes from No.4 to No.11 were newly determined in this study on the basis of the P-wave first-motion data obtained by the micro-earthquake observation networks of Hokkaido University, Tohoku University, and Hirosaki University together with JMA network. The P-wave first-motion data on an equal area

projection of the upper focal hemisphere for the eight earthquakes are shown in Fig.27, in which the nodal planes are also shown. Fault plane solutions for three earthquakes from No.1 to No.3 given by Sasatani and Kasahara (1978) were used. Those for three large earthquakes from No.12 to No.14 given by Sudo and Ishibashi (1978) and Seno et al. (1980), and Sudo and Sasatani (1979) were referred to.

Comparison of observed and synthetic strain seismograms

Figure 28 shows the observed strain seismograms for the 1976 Hidaka Mountains earthquake and the optimal synthetic ones. Waveform showing a one-directional drift from P and S wave arrivals, which could not possibly be recorded by pendulum type seismometers, may be explained by a near field term in equation (9). As shown in the figure, agreement is quite good between the observed and synthetic waveforms including the one-directional drift. This agreement suggests that the extensometer with a solid length standard 30 meters long can satisfactorily respond to a short-period crustal strain change up to an amplitude of 1 part in 10^9.

Figure 29 shows an example of the strain seismograms for the shallow event (No.11) with an epicentral distance of 222 kilometers. The seismograms show that a remarkable phases arrived between the arrivals of P- and S-waves.

This phase may correspond to an SP-wave, which expected from the calculation of travel time. For the event, synthetic strain seismograms were computed, which are also shown in Fig.29. Except the SP-wave which is not obtained in the synthetic strain seismograms because of the assumption of an infinite medium in computation, good agreement was obtained between the observed and synthetic records for both the P-wave and the initial part of S-wave. More quantitative comparison between the observed and synthetic seismograms provided that a source process time is 3.0 seconds.

Figure 30 shows a strain seismogram obtained for the deep-focus earthquake of March 7, 1978 in the South of Japan which is located at about 1,200 kilometers southwest of the station. The first one-cycle of S-wave in the seismogram seems to be simple in waveform. In the lower of the figure, the waves for about 25 seconds which include the S-wave are expanded in time, with which three synthetic strain seismograms are also shown. These synthetic strain seismograms were calculated for different source process times (τ_e) of 8, 6, and 4 seconds with a seismic moment of $1x10^{26}$ dyne.cm. From comparison of waveform and the amplitudes between the observed and synthetic seismograms, the source process time (τ_e) was obtained to be 6 sec and the seismic moment (Mo) $1.0x10^{26}$ dyne·cm.

The upper part of Fig.31 shows two components of the strain seismograms obtained for the shallow event which

occurred off Miyagi Prefecture on June 12, 1978 with a magnitude of 7.4. As shown in the figure, the seismograms record remarkably predominant surface waves immediately after the S-wave arrival, so that only the first half cycle of the S-wave could be taken for comparison with the synthetic seismograms.

Three examples of synthetic strain seismograms for the S-wave are shown in the lower part of the figure in comparison with the observed ones. Among these synthetic seismograms, the second ones are the most similar to the observed ones. Then, we estimated that the seismic moment (Mo) and the source process time (τ_e) are 3×10^{27} dyne·cm and 15 sec, respectively. Those values are nearly the same as those of Seno et al. (1980), in which the seismic moment is 3.1×10^{27} dyne·cm and the source process time is estimated as about 15 sec from their one segment model.

Figure 32 (a) and (b) show the strain seismograms for ten near earthquakes. For convenience of the later interpretation, these earthquakes were classified into two groups depending on their source regions. If the ratio of the focal depth to the epicentral distance is less than the critical value for the appearance of SP-wave, the observed strain seismograms are expected to show very simple features. Since the earthquakes occurring under the southern part of the Hidaka range have that ratio for EGO, fairly good agreement between the observed and the synthetic strain seismograms may be obtained as shown in Fig.32 (a).

On the other hand, the strain seismograms of the events which occurred off Urakawa and Kushiro are rather complicate. However, the observed and synthetic strain seismograms give fairly good agreement so long as S-waves only are taken for these earthquakes.

The seismic moments determined through these analyses are plotted in Fig.33 with respect to those obtained by other methods. Seismic moment shown by solid and open circles are estimated from conventional seismological method and from the empirical relation between magnitude and seismic moment that is described in the previous section. This figure shows that the seismic moment estimated from the strain seismogram is consistent with that from other methods within a factor of 2 except a few moderate earthqaukes. A little large difference for a few moderate events may be caused by complex waveform of the observed strain seismogram and also the simple model used in the analysis.

It can be said through the analyses that the first one cycle of the S-wave, which will be called the period of S-wave, is sensitive to the source process time; that is, the period of S-wave is proportional to the source process time.

Estimation of source parameters from S-wave of strain seismogram

Simple waveform allows us to apply the following analysis to the observed strain seismograms. The previous analysis shows that the period of S-wave corresponds to the source process time and the amplitude of the wave, to the seismic moment; therefore, quantitative investigation of S-wave form of the observed strain seismogram must provide the source parameters.

At a far field, a period of S-wave corresponds theoretically to the source process time τ_e, and the amplitude of S-wave $\bar{e}$ in an infinite medium is related to the last term in equation (9); that is,

$$\bar{e} = \frac{Mo}{\pi\rho r} \frac{Rc}{\beta^4} \frac{2}{\tau_e^2} \qquad (10)$$

where Rc is the constant due to the radiation pattern. The amplitude of S-wave e_s observed at the free surface is given by the equation, $e_s=2\bar{e}$. Then, the seismic moment Mo is obtained as

$$Mo = \frac{\pi\rho\beta^4}{4Rc} e_s r \tau_e^2 \qquad (11)$$

This equation suggests that the seismic moment can be estimated easily from the period and amplitude of the observed strain seismogram if the distance from the source to station is given.

Figure 34 shows logarithymic plots of the seismic moments obtained by the method described as a function of the product of the distance r, the amplitude e_s and the squares of the period τ_e of the observed strain seismograms. The amplitude and the period were obtained from the mean value for the three components of the seismograms. The distance was calculated by $(\Delta^2+H^2)^{1/2}$. From these plots the constant, $\pi\rho\beta^4/4Rc$, in equation (11) was determined to be 4.5×10^{19}. That is, the seismic moment Mo in dyne·cm can be obtained from the equation,

$$Mo = 4.5\times10^{19}\ e_s\ r\ \tau_e^2 \qquad (12)$$

where e_s is measured in 1 part in 10^9, r in kilometers and τ_e in seconds. A straight line in Fig.34 gives this relation. The figure shows that the seismic moment within a factor of 2 can be determined from the amplitude and period of S-wave of the observed strain seismogram and the hypocentral distance even if a fault plane solution of the event is not given.

Using equation (12), the seismic moments as well as the source process times of other 11 earthqaukes occurring from Feburary to November in 1979 have been estimated. These parameters obtained and the amplitude and period of the observed S-wave are summarized in Table 6.

Strain seismograms of small earthquakes

The waveform of the observed strain seismograms may directly reflect the source parameters as mentioned above. Referring to this favorable relation the extensometer has been improved to be more sensitive. This improvement is to confirm not only whether this relation extends to small earthquakes or not, but also whether the extensometer can record small earthquakes with shorter periods and smaller amplitudes than those of moderate earthquakes or not.

For the purpose, a new channel with a sensitivity of 1.13×10^{-10}/bit in the frequency range 0.01 Hz to 3 Hz was equipped and the observation has been carried out by the E-AB component from December, 1979. During the total 40 days till the end of February, 1980 (including no observation for 50 days due to failure of the system by thunder) 32 earthquakes including aftershocks were recorded.

Figure 35 shows spatial distribution of the epicenters of all the earthquakes, of which strain seismograms were analyzed in this study.

The middle part of Fig.36 shows the strain seismogram of the smallest earthquake with a magnitude of 3.3 among all of the observed earthquakes. Other seismograms observed by short-period horizontal seismometers (the natural period 1 Hz) which were applied to a low-pass filter with a short-period cut-off at 3 Hz are also shown in the upper and

lower parts in this figure. We cannot compare with each other in detail, because both instruments are installed in different directions. However, it can be seen that main features of both seismograms are very similar. A scale of 1 micron of ground displacements at 3 Hz is shown for comparison. As shown in the figure, the observed amplitudes are also in good agreement. Therefore, this figure indicates that the extensometer can sufficiently respond to short-period crustal strain variations up to 3 Hz. Figure 37 shows the strain seismograms for four small earthquakes. Seismic moments and source process times of these small earthquakes have also been determined from amplitudes and periods of the first S-waves by using equation (12). These quantities determined are also summarized in Table 6.

Relationship between seismic moments and source process times

Seismic moments Mo are plotted against source process time τ_e in Fig.38, in which solid marks are obtained in the present study and open ones obtained by conventional seismological method. All of the data obtained by the present study are listed in Table 6 and the others, which are referred from the source parameters summarized by Geller (1976) and the new ones obtained by Abe (1978), are listed in Table 7. In Fig.38 circle and triangle marks

correspond to uni-lateral and bi-lateral rupture modes, respectively. The results obtained by strain seismograms rae conistent with those by the other method over the wide range of seismic moment. This figure demonstrates that the source parameters of small earthquakes estimated from the observed strain seismograms are also reasonable and the extensometer with a solid length standard 30 meters long is extremely excellent as a seismometer because of capability to respond to crustal movement in frequency range from 3 Hz to DC. In addition to the capability, the observable magnitude range can be extended, if the extensometer is used.

Two lines in this figure show the theoretical relations obtained by assuming rectangular fault model and similarity conditions with an average rupture velocity of 2.5 km/sec and a stress drop of 30 bars for inter-plate earthquakes (after Abe,1975 and Geller,1976).

Concluding remarks

The results obtained by analyses of strain seismograms confirmed that the extensometer can satisfactorily respond to crustal strain variations in the frequency range from 3 Hz to DC component caused by earthquakes. The observed strain seismograms can be well explained by the theoretical ones based on the theory of elasticity. It has been shown that the seismic moment and source process time of the event

can be determined directly by the observed strain seismogram because the extensometer has no transient characteristics.

4.3 SOURCE CHARACTERISTICS OF THE KUNASHIRI STRAIT EARTHQUAKE DEDUCED FROM STRAIN SEISMOGRAMS

Earthquake data

A great intermediate-depth earthquake occurred on December 6, 1978 beneath the Kunashiri Strait in the southern part of the Kurile arc. The focal coordinates and the magnitude determined by International Seismological Center (ISC) are as follows : origin time 14h02m 04.5s GMT: epicenter 44.55°N, 146.67°E; depth 118 km; m_b=6.3 and M_s= 7.1. The magnitude has also estimated as 7.7 (JMA), 6.8 (NEIS), 7.3 (BRK), and 7.5 (PAS), respectively.

The epicenters of the mainshock and aftershocks determined by ISC are shown in Fig.39. This event is the largest one among the events with a depth greater than 100 kilometers which occurred in this region during the last 30 years. This earthquake accompanied a lot of aftershocks as a large shallow earthquake does (Suzuki, 1979). Figure 40 (a) shows the epicentral distribution of aftershocks with a magnitude greater than 4 determined by ISC. As shown in the figure these epicenters concentrate on a narrow region with a NE-SW direction, which is roughly perpendicular to the strike of the Kurile trench. Figure 40 (b) shows the hypocenters projected onto a cross section

along this direction. The focus of the mainshock is located roughly at the southeastern end and in the uppermost part of the aftershock area. This suggests that the rupture propagated unilaterally northwest in a downward direction. Sudo and Sasatani (1979) have shown the strong asymmetry of the radiation pattern of long-period Love waves generated by this event, indicating a rupture propagation toward the northwest. This direction of the rupture propagation is different from that for large shallow earthquakes in this region, which is almost parallel to the strike of the Kurile trench (Kanamori,1970; Abe,1973).

The fault plane solution determined from the P-wave first-motions and the radiation pattern of surface waves observed by WWSSN long-period seismometers is shown in Fig.41 (Sudo and Sasatani,1979). The nodal plane with a strike of 155° and a dip angle of 83° is chosen as a fault plane. A slip angle on this fault plane is 49°. The strike of the fault plane agrees well with the direction of the epicentral distribution of aftershocks. According to the aftershock area the fault has a extent of 100x20 km^2 and is inclined about 40°. This inclination and the hypocentral distribution of aftershocks coincide with the dip and the depth of the deep seismic zone in this region (Fedotov et al.,1971; Utsu,1976; Sasatani,1976). The slip vector of fault movement is approximately parallel to the down-dip direction of the deep seismic zone. This fault geometry means that the Kunashiri event represents a left-lateral

strike slip motion along a nearly vertical fault which is located at the upper-most part of the descending lithospere. The sense of the motion is quite different from that usually observed in this region (Isacks and Molnar,1971; Stauder and Maulchin,1976; Sasatani,1976).

Features of observed strain seismograms

Figure 42 (a) shows the records obtained by a low-chart-speed recorder used for the routine observation. Strain steps can be clearly seen on all the components in the figure. Figure 42 (b) and (c) show the original strain seismograms and the low-pass filtered ones passed through a filter with a short-period cut-off at 30 sec, respectively. The strain seismograms shown in Fig.42 (b) and (c) have the following two features :

(1) A sequence of pulses with a period about 5 sec follows the first P-wave arrival and lasted for about 60 sec after the first S-wave arrival with considerable amplitude, and

(2) Each component records a significant long-period wave just after the first P-wave arrival.

In order to show that these features are of uniqueness for the Kunashiri event, the strain seismograms of the Earthquake off Etorofu Island are shown in Fig.43 which

occurred on March 24, 1978 in roughly the same region, and has a comparable magnitude (m_b=6.4, ISC; 7.3, JMA; 7.6, Neis; 7.5, PAS) but a shallower focal depth. The strain seismograms of the earthquake show long-period surface waves predominantly as expected to shallower depth earthquakes. No sequence of pulse and no long-period phase were observed in the part of body waves.

Two features of the strain seismograms of the Kunashiri event cannot be due to propagation effect. It is also clear that the long-period wave in the strain seismogram is neither due to the mechanical fluctuation of the extensometer nor due to the other external origin such as sea waves, judging from the stability of the record before the event (see Fig.42 (a) and Fig.48).

Analyses of strain seismograms

Source process of the Kunashiri event that can explain two special features of the strain seismograms will be estimated by comparing the synthetic strain seismograms with the observed ones.

A sequence of pulses in the observed strain seismograms, which cannot be generated by propagation effect, may be considered to be a series of body waves which originated from the individual events of a complex multiple shock. Sudo and Sasatani (1979) also concluded from the complex

P and S waveforms of WWSSN long-period seismograms that this event was a multiple shock. A question to be solved here is what causes the long-period wave in the strain seismograms. The following two cases are considered as a possible interpretation of this question.

(A) It would be caused by a long sequence of multiple events, each of which originates only a short-period wave.

(B) It would be caused by another event having a substantially long source process time.

The synthetic strain seismograms were calculated for the two cases, (A) and (B), which are called Model A and Model B in the figure shown later.

Identification of an individual event from the observed strain seismogram was made as follows :

(i) The main pulses exist for about 60 seconds after the first S-wave arrival (see Fig.44) so that the 60 seconds is considered as the duration of the multiple shock sequence. This duration agrees with that of the wavelet with a large amplitude recorded by a strong motion sesimometer at Nemuro, which is the nearest station in Japan to the source.

(ii) A pair of pulses corresponding to P and S waves from one event was identified by the following way: A synthetic

strain seismogram with a short source process time was calculated using the same fault plane solution as that obtained from long-period body and surface waves, and the synthetic strain seismogram thus obtained was compared with all the pulses for 60 seconds after the first P-wave arrival recorded in the observed strain seismogram in order of occurrence.

Consequently, 18 events were identified. The estimated P times of the events are marked on the observed strain seismogram in Fig.44. Although this identification of the individual event, of course, may contain considerable uncertainty because of the extremely complex waveform recorded, the seismic moment and the source process time of each event can be determined by the amplitude and the period of each identified pulse on the basis of the empirical equation (12). The P-time, the source process time, and the seismic moment of each event are listed in Table 8. The total moment of the sequence was obtained to be 2.5×10^{27} dyne·cm.

The synthetic strain seismograms based on these parameters (Model A) are shown in Fig.45. The over-all features of the synthetic strain seismogram are similar to the observed one for all the components within the limit of the short-period pulse sequence. Although the long-period waves appear in the low-pass filtered synthetic strain seismograms, the amplitudes are only one third to one fourth as large as the observed ones. To explain the

observed strain seismograms in more detail an additional event having a substantially long source process time should be required.

As one of the solutions, the event which has a seismic moment of 4.5×10^{27} dyne·cm and a source process time of 60 seconds was obtained by the method of trial and error. The synthetic strain seismograms thus obtained (Model B) are shown in Fig.46. These can well explain the two features of the observed strain seismograms. Based on the seismograms the over-all seismic moment was estiamted to be about 7.0×10^{27} dyne·cm and the duration of the rupture was about 60 seconds.

Strain step

The over-all seismic moment and the long source process time estimated above are reexamined in relation to strain steps. First, as a check of the source process time, waveform of the observed strain seismograms and the synthetic ones for various values of source process time (40,50,60, and 70 seconds) were compared in ultra-low frequency domain. Figure 47 shows the observed and synthetic low-pass filtered seismograms with a short-period cut-off at 250 seconds. For the source process time of 60 seconds, agreement between both records is satisfactorily good.

Furthermore, it can be seen that the pattern of the

strain step may be controled by the source process time; that is , the actual movement of so called strain step is not the step-like change. The strain step may be formed during the period from the P-wave arrival to the lapse of source process time after the S-wave arrival. That may be understood in Fig.47 ; the strain step recorded may be related to a bodily deformation caused by a faulting at the source.

The amplitude of strain step must be proportional to the seismic moment of the event. The observed strain step amplitude was defined by the values at 3 minites after the P-wave arrival shown in Fig.47. The following seismic moments for each component are estimated from comparison between the observed and synthetic strain seismograms:

E-AB component	6×10^{27} dyne·cm
E-CD component	4×10^{27} dyne·cm
E-EF component	7×10^{27} dyne·cm
Average	5.7×10^{27} dyne·cm .

In this calculation, the free surface effect is approximated by doubling the amplitude. Okada (1975) represented the exact solution for static strain field at the surface in a semi-infinite homogeneous medium. Using his representation the following seismic moments are also estimated by assuming the rigidity of 7×10^{11} dyne/cm^2:

E-AB component	7 x 10^{27}	dyne.cm
E-CD component	5 x 10^{27}	dyne·cm
E-EF component	6 x 10^{27}	dyne·cm
Average	6.0 x 10^{27}	dyne·cm .

The estimated seismic moment, about 6×10^{27} dyne·cm, which can explain the observed strain steps agree well with the over-all seismic moment of the multiple shock sequence that can explain the dynamic strain seismograms.

Extensometer is also able to record aseismic movement as well as strain step. It is very interesting question whether aseismic movement before the Kunashiri event had occurred or not. Figure 48 shows the strain records for about 3 minutes before the P-wave arrival of the main event which were reproduced from the magnetic tape with the maximum gain. As can be seen in the figure, no significant signals are available. It, therefore, may be concluded that any aseismic movement had not occurred beyond the limits of observation.

Interpretation of source process of the Kunashiri event

The source process of the Kunashiri Earthquake is characterized by the complex multiple shock sequence not only with 18 short period events, but also with a long

period event. Differences of two series in the multiple shock sequence will be discussed on the basis of the earthquake fault model. The seismic moments of the events of the sequence are plotted against their source process times in Fig.49. If similarity condition exists within the source parameters determined for two series of events, the relation between the two parameters can be represented by a straight line with a slope of one third as being described in the previous section. The figure clearly shows that the relation for the long period event differs from that for the short period events. Source process time, τ_e , defined here is roughly equivalent to the term L/Vr, where L and Vr are the fault length and the rupture velocity, respectively. Assuming a rectangular fault with L=2.W, seismic moment is approximately given by

$$Mo = 1.45 \times 10^{20} \, Vr^3 \, \tau_e^3 \, \Delta\sigma \qquad (13)$$

where Mo is the seismic moment in dyne·cm, Vr the rupture velocity in km/sec, τ_e the source process time in seconds, and $\Delta\sigma$ the stress drop in bars (Geller,1976; Sasatani,1980). For the long period event a rupture velocity of 1.67 km/s was estimated from a fault length of 100 kilometers and a source process time of 60 seconds. A stress drop of about 30 bars was obtained by giving the rupture velocity and the seismic moment of the long-period event into equation (13). If this rupture velocity is also adopted for the

short-period events, their stress drops become about 3,000 bars as shown in Fig.49. This stress drop is abnormally large even for intermediate-depth earthquakes (Sasatani, 1980). If a rupture velocity is assumed alternatively to be 3.6 km/sec which corresponds to about 80 percent of the S-wave velocity at this depth, the stress drop is obtained as about 300 bars. This value would be in agreement with the averarge stress drop for the intermediate-depth and deep-focus earthquakes obtained by Sasatani (1980).

The long-period event may be explained to be a slow earthquake because the event has a slow rupture velocity. Since the main rupture would have been propagated along the fault plane, 18 small ruptures may be successively triggered by passing the main rupture. This source process is qualitatively explained by a faulting model with non-uniform distribution of the rupture strength on the fault plane (Das and Aki,1977; Mikumo and Miyatake,1978).

According to this model, the part with relatively high fracture strength on the fault is not broken at the initial passage of the crack tip of main fracture, but is eventually broken due to a subsequent increase of dynamic stress. This lapse rupture may correspond to the short-period event of the Kunashiri event. Such fault plane condition may be one of the reasons why the Kunashiri event is accompanied by a lot of aftershocks as an exception of deep-focus earthquake.

In addition, the source parameters deduced from the strain seismograms are listed in Table 9 with those obtained by conventional seismological analysis (Sudo and Sasatani,1979) for the sake of comparison.

Concluding remarks

Extensometers of EGO completely recorded the strain variations radiated from the Kunashiri event. The following complex multiple shock sequence was estimated from only the observed strain seismograms as a source characteristics of the event : The main rupture with a seismic moment of 4.5×10^{27} dyne·cm and a source process time of 60 seconds occurred and during the main rupture 18 additional short-period events were successively triggered. The main rupture was characterized by low rupture velocity and low stress drop. On the contrary the 18 additional events showed normal rupture velocity and a little high stress drop at their depth. The observed strain steps are well explained by this sequence. The improved recording system could demonstrate that the strain step is directly connected with the bodily deformation caused by the faulting at the source.

CHAPTER 5

SUMMARY AND CONCLUSIONS

1) Secular strain accumulations were obtained by the extensometric observation in the vault and by the repeated measurements for the long base-line network around the Erimo region during the period from 1971 to 1980. The secular strain accumulations are that the principal strains are $+5.9 \times 10^{-6}$ with a N5°E and -1.6×10^{-6} with a N85°W by the extensometric observation, and $+4.5 \times 10^{-6}$ with a N22°W and -2.0×10^{-6} with a N68°E by the measurements for the long base-line network, where positive sign means extension. Both the results are tolerably consistent both in orientation and in amount with one another. It is confirmed that the extensometric observation in the vault of the EGO can well follow the wide-areal crustal movement progressing around the Erimo region.

2) The abnormal strain changes related to the 1973 Earthquake off the Nemuro Peninsula were quantitatively revealed with consideration of the meteorologically induced effects. Pre-seismic strain change was characterized by the increase of areal dilatation which is contrary to co-seismic strain step. The beginning of this change was estimated to be more than 40 days and less than 100 days before the event.

On the other hand, post-seismic strain change occurred with the same manner of co-seismic strain change and continued about 15 days after the event. The amount of the pre- and post-seismic abnormal strain changes did not exceed that of the co-seismic strain step.

3) Extensometers of EGO had registered distinct strain steps associated with 44 earthquakes with magnitudes ranging from 4.7 to 7.7 in JMA scale between 1971 to 1980. The observed strain steps were consistent in both polarity and amplitude with the theoretical ones for five earthquakes of which the source parameters were obtained by conventional seismological methods. The following relation was obtained from the observed data : The observed strain step amplitude is proportional to seismic moment and to inverse of cube of hypocentral distance as being predicted by a simple dislocation model. Neither mechanical problem nor serious site effects were found for the extensometer system installed at the vault of EGO. Therefore, seismic moment of an earthquake can be estimated within a factor of 2 to 3 from the observed strain step alone.

4) The digital system newly improved for the extensometric observation observed strain seismograms of 55 earthquakes with magnitudes ranging from 3.3 to 7.7 to which body wave analyses were applied on the basis of the theoretical strain seismogram generated by a point shear dislocation

in an infinite homogeneous medium. The waveform and amplitude of the observed strain seismogram could be well explained by the synthetic strain seismogram with the source parameters, which were consistent with those obtained by conventional seismological methods within a factor of 2. Seismic moment and source process time of an earthquake could be estimated from amplitude and period of the observed S-wave alone because the extensometer system used here had no transient characteristics. Source process time ranging from 0.3 to 60 seconds and seismic moment ranging from 10^{20} to 10^{27} dyne·cm were obtained from the analyses of the observed strain seismograms for 55 earthquakes. The relation between both parameters was also consistent with that predicted by the earthquake dislocation model.

5) The source process of the Kunashiri Strait Earthquake with a magnitude of 7.7 was deduced from the strain seismogram analysis to demonstrate usefulness of extensometer as a seismometer. The following complex multiple shock sequence was estimated: The main rupture with a seismic moment of 4.5×10^{27} dyne.cm and a source process time of 60 seconds occurred and 18 secondary events with the total seismic moment of 2.5×10^{27} dyne.cm were successively triggered during the main rupture. The main rupture was characterized by low rupture velocity and low stress drop.

On the other hand, secondary events were characterized by normal rupture velocity and a little high stress drop at their focal depth. The observed strain steps are also consistent with this sequence. The improved recording system could demonstrate that the strain step is directly connected with the bodily deformation caused by faulting at the source.

Finally, this study confirmed throughout analyses and measurements that the extensometer with a solid length standard 30 meters long can satisfactorily respond not only to seismic strains in the frequency range from 3 Hz to DC component radiated from an earthquake source, but also to secular strain accumulation progressing around the station.

ACKNOWLEDGEMENTS

I would like to express my gratitude to Professor Izumi YOKOYAMA for giving the opportinuty of this study and for his continuous support and encouragement during the course of this study. I am also very grateful to Professor Hiroshi OKADA who made many valuable suggestions and kindly reviewed the manuscript and to Dr. Katsuyuki ABE for his useful discussion on source parameters and his encouragement. I would practically like to acknowledge the invaluable advice, assistance and encouragement given by Drs. Tsutomu SASATANI and Sadaomi SUZUKI throughout this study.

I am thankful to the members of the Research Center for Earthquake Prediction, Hokkaido University for helpful discussions and to the Seismological Observatories of Tohoku and Hirosaki Universities for providing the P-wave first-motion data. Thanks are also due to Mr. Yasumori TANAKA for his efforts to routine observation at the Erimo Geophysical Observatory and to Dr. Juhei YAMADA for his consulting to construction of the observatory. Messrs. Muneo OKAYAMA and Tomio OGAWA helped with the field work of the long base-line distance measuring. This work also greatly benefited from discussions with Dr. Ryuichi SHICHI of Nagoya University and Dr. Yoshimitsu OKADA of National Research Center for Disaster Prevention.

REFERENCES

Abe,K., 1973. Tsunami and mechanism of great earthquakes. Phys.Earth Planet.Interiors, 7: 143-153.

Abe,K., 1975. Reliable estimation of the seismic moment of large earthquakes. J.Phys.Earth, 23: 381-390.

Abe,K., 1977. Some problems in the prediction of the Nemuro-oki earthquake. J.Phys.Earth, 25: Suppl., S261 -S271.

Abe,K., 1978. Dislocations, source dimensions and stresses associated with earthquakes in the Izu Peninsula, Japan. J.Phys.Earth, 26: 253-274.

Abe,K. and Yokoyama,I., 1974. An expected major earthquake off the coast of eastern Hokkaido. Rep.Coord.Comm. Earthq.Pred., 11: 45-50 (in Japanese).

Aki,K. and Richards,P.G., 1980. Quntitative seismology; Theory and Methods. W.H.Freeman and company, San Francisco, 488-490 in 932pp.

Alsop,L.E., Sutton,G.H. and Ewing,M., 1961. Free Oscillations of the Earth observed on strain and pendulum seismographs. J.Geophys.Res., 66: 631-631.

Aoki,H., 1975. Sudden occurrence of ground subsidence at Yokkaichi. Rep.Coord.Comm.Earthq.Pred., 13: 82-85 (in Japanese).

Balavadze,B.K., Karmaleeva,R.M., Kartvelishvili,K.Z. and Latynina,L.K., 1965. Horizontal extensometer observa-

tions at Tbilisi on tidal deformations of the Earth. Izv.Earth Phys.Series, 1965 No.2: 75-79.

Benioff,H., 1935. A linear strain seismograph. Bull.Seism. Soc.Am., 25: 283-309.

Benioff,H., 1959. Fused-quartz extensometer for secular, tidal, and seismic strains. Bull.Geol.Soc.Am., 70: 1019-1032.

Benioff,H., 1963. Source wave form of three earthquakes. Bull.Seism.Soc.Am., 53: 883-903.

Benioff.H, Press,F. and Smith,S., 1961. Excitation of the free oscillation of the Earth by earthquakes. J. Geophys.Res., 66: 605-619.

Berger,J. and Lovberg,R.H., 1970. Earth strain measurements with a laser interferometer. Science, 170: 296-299.

Berger,J. and Wyatt,F., 1973. Some observations of Earth strain tides in California. Phil.Trans.R.Soc.London A, 274: 267-277.

Blayney,J.L. and Gilman,R., 1965. A portable strainmeter with continuous interferometric calibration. Bull. Seism.Soc.Am., 55: 955-970.

Chung,W.Y. and Kanamori,H., 1978. Subduction process of a fracture zone and aseismic ridges -- the focal mechanism and source characteristics of New Hebrides earthquake of 1969 January 19 and some related events. Geophys.J.R.astr.Soc., 54: 221-240.

Das,S. and Aki,K., 1977. Fault plane with barriers: A versatile earthquake model. J.Geophys.Res., 82: 5658-5670.

Fedotov,S.A., Bagdasarova,A.M., Kuzin,I.P. and Tarakanov, R.Z., 1971. Earthquakes and the deep structure of the south Kurile iland arc. Israel Program for Scientific Translation, Jerusalem, 1971, 135pp.

Fujii,Y., 1976. Pre-slip as forerunner of earthquake occurrence. In: Z.Suzuki and S.Omote (Editors) Symp. Earthq.Pred.Proc., 127-137 (in Japanese with English abstract).

Fukao,Y. and Furumoto,M., 1975. Mechanism of large earthquakes along the eastern margin of the Japan sea. Tectonophysics, 26: 247-266.

Funahashi,M. and Hashimoto,S., 1951. Geology of the Hidaka zone, Hokkaido. Monograph of the association for the geological collaboration, No.6, 38pp (in Japanese).

Geller,R.J., 1976. Scaling relations for earthquake source parameters and magnitudes. Bull.Seism.Soc.Am., 66: 1501-1523.

Hagiwara,T., Rikitake,T. and Yamada,J., 1948. Observations of the deformation of the Earth's surface at Aburatsubo, Miura Peninsula. Part I. Bull.Earthq.Res. Inst., 26: 23-27.

Hagiwara,T., Rikitake,T., Kasahara,K. and Yamada.J., 1949. Observations of the deformation of the Earth's surface at Aburatsubo, Miura Peninsula. Part II. Bull. Earthq.Res.Inst., 27: 35-38.

Hanks,T.C. and Kanamori,H., 1979. A moment magnitude scale. J.Geophys.Res., 84: 2348-2350.

Harrison,J.C., 1976. Cavity and topographic effects in tilt and strain measurements. J.Geophys.Res., 81: 319-328.

Hatori,T., 1975. Tsunami activity in eastern Hokkaido after the off Nemuro Peninsula Earthquake in 1973. Zisin (J.Seism.Soc.Jap.), Ser.II, 28: 461-471 (in Japanese with English abstract).

Hilde,T.W.C., Isezaki,N. and Wageman,J.M., 1976. Mesozoic sea-floor spreading in the North Pacific. In: G.H. Sutton, M.H.Manghani and R.Mberly (Editors), The Geophysics of the Pacific Ocean Basin and Its Margin. Geophysical Monograph, 19: 205-228.

Honda,H., 1962. Earthquake mechanism and seismic waves. J.Phys.Earth, 10: 1-97.

Isacks,B. and Molnar,P., 1971. Distribution of stresses in the descending lithosphere from a global survey of focal-mechanism solutions of mantle earthquakes. Rev.Geophys.Space Phys., 9: 103-174.

Jaeger,J.C. and Cook,N.G.W., 1969. Fundamentals of Rock Mechanics. Methuen, London. 515pp.

Japanese Network of Crustal Movement Observatory, 1970. Spatial distribution of strain-steps associated with the Earthquake of central part of Gifu Prefecture, September 9, 1969. Bull.Earthq.Res.Inst., 48: 1217-1233 (in Japanese with English abstract).

Kanamori,H., 1970. Synthesis of long-period surface waves and its application to earthquake source studies --

Kurile Island earthquake of October 13, 1963. J. Geophys.Res., 75: 5011-5027.

Kanamori,H., 1972. Mechanism of tsunami earthquakes. Phys. Earth Planet.Interiors, 6: 346-359.

Kanamori,H. and Cipar,J.J., 1974. Focal process of the great Chilean earthquake of May 22, 1960. Phys.Earth Planet.Interiors, 9: 128-136.

Kanamori,H. and Anderson,D.L., 1975. Theoretical basis of some empirical relations in seismology. Bull.Seism. Soc.Am., 65: 1073-1095.

Kanamori,H. and Stewart,G.S., 1979. A slow earthquake. Phys.Earth Planet.Interiors, 11: 312-332.

Kasahara,M., 1973. On the strain-steps associated with the Earthquake off Erimo Cape on August 2, 1971. Abstr.Annu.Meet.Seism.Soc.Jap., No.1: 123 (in Japanese).

Kasahara,M., 1974. Spatial distribution of strain steps associated with the Earthquake off the Nemuro Peninsula, June 17, 1973. In: Y.Sakai (editor) General Report on the Earthquake off the Nemuro Peninsula, June 17, 1973. 36-62 (in Japanese with English abstract).

Kasahara,M., 1976a. Premonitory crustal movement observed at Erimo before the Earthquake off the Nemuro Peninsula on June 17, 1973. In: Z.Suzuki and S.Omote (editors) Rep.Symp.Earthq.Pred.Res., 3-14 (in Japanese with English abstract).

Kasahara,M., 1976b. Seismic and geodetic observations through the digital PCM telemetering system in Hokkaido,

Japan. J.Geod.Soc.Jap., 22: 292-294.

Kasahara,M., Tanaka,Y. and Yokoyama,I., 1972. Observation of crustal deformation at Erimo in Hokkaido -1971-. Geophys.Bull.Hokkaido Univ., 28: 83-96 (in Japanese with English abstract).

Katsumata,M. and Kashiwabara,S., 1977. Note on JMA magnitude scale. Zisin (J.Seism.Soc.Jap.), Ser.II, 33: 511-513 (in Japanese).

King,G.C.P., 1971. The siting of strainmeters for teleseismic and tidal studies. Bull.R.Soc.New Zealand, 9: 239-247.

King,G.C.P. and Gerard,V.B., 1969. Earth tides recorded by the 55 m Cambridge interferometer. Geophy.J.R.astr. Soc., 18: 437-438.

King,G.C.P., Bilham,R.G., Gerard,V.B., Davies,D. and Sydemham,P.H., 1969. New strainmeters for geophysics. Nature, London, 223: 818-819.

King,G.C.P. and Bilham,R.G., 1973. Strain measurement instrumentation and technique. Phil.Trans.R.Soc.Lond. A, 274: 209-217.

Kishimoto,Y., Oike,K. and Tsushima,Y., 1968. On a linear strain seismograph of a variable capacitance type. Disaster Prev.Res.Inst.Kyoto Univ.Annuals, 11: 67-73 (in Japanese with English abstract).

Maeda,I., Motoya,Y. and Suzuki,S., 1978. On the telemetered data recording and processing system for earthquakes earthstrains at Hokkaido University. Zisin (J.Seism.

Soc.Jap.), Ser.II, 31: 401-413 (in Japanese with English abstract).

Major,M.W., Sutton,G.H., Oliver,J. and Metsger,R., 1964. On elastic strain of the earth in the period range 5 seconds to 100 hours. Bull.Seism.Soc.Am., 54: 295-346.

Maruyama,T., 1963. On the force equivalences of dynamical elastic dislocations with reference to the earthquake mechanism. Bull.Earthq.Res.Inst., 41: 467-486.

Mikumo,T., 1973. Faulting mechanism of the Gifu Earthquake of September 9, 1969, and some related problems. J. Phys.Earth, 21: 191-212.

Mikumo,T., 1974. Some considerations on the faulting mechanism of the southeastern Akita Earthquake of October 16, 1970. J.Phys.Earth, 22: 87-108.

Mikumo,T. and Miyatake,T., 1978. Dynamical rupture process on a three-dimensional fault with non-uniform frictions and near-field seismic waves. Geophys. J. R.astr.Soc., 54: 417-438.

Milne,J., 1888. The relative motion of neighboring points of ground. Trans.Seism.Soc.Jap., 12: 63-66.

Nakane,K., 1973a. Horizontal tectonic strain in Japan (I). J.Geod.Soc.Jap., 19: 190-199 (in Japanese with English abstract).

Nakane,K., 1973b. Horizontal tectonic strain in Japan (II). J.Geod.Soc.Jap., 19: 200-208 (in Japaneses with English abstract).

Noguchi,S., 1979. On the relation between surface-wave magnitude and JMA magnitude. J.Fac.Sci.Hokkaido Univ., Ser.VII (Geophysics), 6, No.1: 213-224.

Oddene,E., 1900. Ricerche strumentali in sismometria con apparati non pendulari. Boll.Soc.Sismologica Italiana, 11: 168-180 (in Italian).

Oike,K., Koizumi,M. and Hirano,N., 1969. Continuous observation by strain seismographs and tiltmeters of variable capacitance type. Disaster Prev.Res.Inst. Kyoto Univ.Annuals, 12: 145-154 (in Japanese with English abstract).

Okada,Y., 1975a. Theoretical strain seismogram (1). Abstr. Annu.Meet.Seism.Soc.Jap.,No.1: 240 (in Japanese).

Okada,Y., 1975b. Strain- and tilt-steps associated with the two earthquakes, which occurred in the east off Hachijojima, Japan, on Feburary 29 and December 4, 1972. Zisin (Bull.Seism.Soc.Jap.), Ser.II, 28: 387-413 (in Japanese with English abstract).

Okada,Y., 1978. Fault mechanism of the Izu-Oshima-Kinkai Earthquake of 1978, as inferred from crustal movement data. Bull.Earthq.Res.Inst., 53: 823-840 (in Japanese with English abstract).

Okada,Y., 1980a. Theoretical strain seismogram and its applications. Bull.Earthq.Res.Inst., 55: 169-182 (in Japanese with English abstract).

Okada,Y., 1980b. Strain- and tilt-steps associated with the Izu-Hanto-Oki Earthquake of 1974 and Izu-Oshima-

Kinkai Earthquake of 1978. Zisin (Bull.Seism.Soc.Jap.), Ser.II, 33: 525-539 (in Japanese with English abstract).

Okada,Y., Watanabe,S. and Kasahara,K., 1975. Observation of crustal deformation at the Fujigawa Observatory, central Honshu, Japan (1). J.Geod.Soc.Jap., 21: 179-190 (in Japanese with English abstract).

Press,F., 1965. Displacements, strains, and tilts at teleseismic distances. J.Geophys.Res., 70: 2395-2412.

Sacks,I.S., Suehiro,S., Linde,A.T. and Snoke,J.A., 1978. Slow earthquakes and stress redistribution. Nature, London, 275: 599-602.

Sasatani,T., 1976. Mechanism of mantle earthquakes near the junction of the Kurile and the northern Honshu arcs. J.Phys.Earth, 24: 341-354.

Sasatani,T., 1980. Source parameters and rupture mechanism of deep-focus earthquakes. J.Fac.Sci.Hokkaido Univ., Ser.VII (Geophysics), 6, No.2: 301-384.

Sasatani,T. and Kasahara,M., 1978. Analyses of strain seismograms from near earthquakes. Zisin (Bull.Seism. Soc.Jap.), Ser.II, 31: 11-23 (in Japanese with English abstract).

Sassa,K., Ozawa,I. and Yoshikawa,S., 1949. Observation of earth-tide by new horizontal extensometer. Bull. Disaster Prev.Res.Inst.Kyoto Univ., 2: 113-114.

Sassa,K., Ozawa,I. and Yoshikawa,S., 1951. Observation of tidal strain of the Earth. Intern.Assoc.Geod., Brussels Assembley, 1951.

Sassa,K., Ozawa,I. and Yoshikawa,S., 1952. Observation of tidal atrain of the earth. Bull.Disaster Prev.Res.Inst. Kyoto Univ., 3: 1-3.

Seno,T., Shimazaki,K., Somerville,P., Sudo. and Eguchi,T., 1980. Rupture process of the Miyagi-oki, Japan, Earthquake of June 12, 1978. Phys.Earth Planet.Interiors, 23: 39-61.

Shichi,R., 1972. An improvement of digital filter for the analysis of crustal deformation. J.Geod.Soc.Jap., 18: 72-77 (in Japanese with English abstract).

Shichi,R., 1973. Long period deformation -- separation of long period components and some consideration to the long period crustal deformation. J.Geod.Soc.Jap., 19: 213-234 (in Japanese with English abstract).

Shichi,R., Iida,K. and Yamauchi,T., 1970. Some considerations on the strain-step associated with the Earthquake of the central part of Gifu Prefecture, September 9, 1969. Bull.Earthq.Res.Inst., 48: 1241-1249 (in Japanese with English abstract).

Shichi,R. Okada,Y., 1979. Strain measurement in the vault. J.Geod.Soc.Jap., 25: 101-134 (in Japanese with English abstract).

Shimazaki,K., 1974. Nemuro-oki Earthquake of June 17, 1973; A lithosphere rebound at the upper half of the interface. Phys.Earth Planet.Interiors, 9: 314-327.

Stauder,W. and Mualchin,L., 1976. Fault motion in the larger earthquakes of the Kurile-Kamchatka arc and

of the Kurile-Hokkaido corner. J.Geophys.Res., 71: 2981-3006.

Sudo,K. and Ishibashi,K., 1978. Source process of the deep-focus earthquake of March 7, 1978 beneath the Ogasawara Islands. Abstr.Annu.Meet.Seism.Soc.Jap., No.1: 98 (in Japanese).

Sudo,K. and Sasatani,T., 1979. Source mechanism of the Earthquake of December 6, 1978 beneath Etorofu Island (M=7.7). Abstr.Annu.Meet.Seism.Soc.Jap., No.1: 31 (in Japanese).

Suzuki,S., 1979. A great intermediate-depth earthquake which occurred around the Kunashiri Strait on December 6, 1978 (M=7.7). Notes Res.Cent.Earthq.Pred. Hokkaido Univ., 5 40-44 (in Japanese).

Sydenham,P.H., A tensioned wire strainmeter. J.Sci.Instrum., Ser.2, 2: 1095-1097.

Sydenham,P.H., 1972. Progress in the design of tensioned-wire earth strainmeters. Geophys.J.R.astr.Soc., 29: 319-327.

Tada,T., 1974. Fault model and crustal movement of the 1973 Nemuro-oki Earthquake. Zisin (J.Seism.Soc.Jap.), Ser. II, 27: 120-128 (in Japanese with English abstract).

Takahashi,R., 1934. A new extensometer for measuring crustal deformation. Bull.Earthq.Res.Inst., 12: 760-775.

Takahashi,R., 1939. Results of continuous observations on the length of a base-line at Komaba, Tokyo. Bull. Earthq.Res.Inst., 17: 579-589 (in Japanese with English abstract).

Takanami,T., 1978. Earthquakes around the southern most tip of the Okhotsk Sea Plate and its tectonic implication. Abstr.Annu.Meet.Seism.Soc.Jap., No.2: 175 (in Japanese).

Takemoto,S., 1975. On calibration of " roller " extensometers with a laser interferometer. J.Geod.Soc.Jap., 21: 81-90 (in Japanese with English abstract).

Takemoto,S. and Takada,M., 1969. Study of strain steps associated with earthquakes. J.Geod.Soc.Jap., 15: 68-74 (in Japanese with English abstract).

Tocher,D., 1960. Creep rate measurements at Vineyard, California. Bull.Seism.Soc.Am., 50: 396-415.

Tsuboi,C., Wadati,K. and Hagiwara,T., 1962. Prediction of earthquake -- Progress to date and plans for further development. Rep.Earthq.Pred.Res.Group Japan, Earthq. Res.Inst.Univ.Tokyo, Tokyo, 21pp.

Utsu,T., 1972. Large earthquakes near Hokkaido and the expectancy of the occurrence of a large earthquake off Nemuro. Rep.Coord.Comm.Earthq.Pred., 7: 7-13 (in Japanese).

Utsu,T., 1974. Distribution of earthquake hypocenters in and around Japan. Kagaku (Science), Iwanami shoten, Tokyo, 44: 739-746 (in Japanese).

Utsu,T., Abe,K., Kasahara,K., Sekiya,H. and Fujii,Y., 1977. Some problems related to the earthquake prediction in the eastern part of Hokkaido. Rep.Regional Coord.Comm. Earthq.Pred., 1: 45-64 (in Japanese).

Van Veen,H.J., 1970. A laser strain seismometer. North-Holland Publishing Company, Amsterdam, 79pp.

Van Veen,H.J., Savino,J. and Alsop,L.E., 1966. An optical laser strainmeter. J.Geophys.Res., 71: 5478-5479.

Wideman,C.J. and Major,M.W., 1967. Strain steps associated with earthquakes. Bull.Seism.Soc.Am., 57: 533-579.

Yamauchi,T., Yamada,M. and Aoki,H., 1974. On the observation of crustal deformation at Toyohashi, central Japan (1st report). J.Geod.Soc.Jap., 20: 45-56 (in Japanese with English abstract).

Table 1. Results of a least squares linear fit to the data obtained by repeated length measurements of each base line

Line	Azimuth*	Length km	No.of obs.	Rate mm/yr	S.D.	S.D.of residual(mm)
N-S'	12.5°	5.333	5	-0.77	± 0.64	3.3
N-S	16	5.325	6	-1.11	± 1.74	11.4
R-H	54	4.589	9	0.03	± 0.46	3.7
H-E	83	8.189	5	1.10	± 1.03	7.2
H-E'	84	8.200	7	3.63	± 2.55	13.3
N-R	86.5	6.740	8	2.97	± 0.70	5.5
N-E	96.5	11.281	5	5.15	± 2.31	14.7
N-E'	97	11.292	6	6.87	± 1.95	10.3
R-E	111.5	4.809	7	-2.19	± 0.64	3.5
R-E'	112.5	4.798	7	-0.75	± 0.37	2.4
N-H	126.5	3.895	7	3.98	± 0.35	2.6
R-S'	130	7.320	5	2.71	± 0.53	2.8
R-S	132	7.181	7	2.83	± 0.69	5.4
F-S	142.5	5.465	8	2.26	± 0.29	2.3
F-S'	146	5.342	6	1.51	± 0.54	2.9

**Degrees counterclockwise from east.*

Table 2. Comparison of strain analyses for secular strain accumulations obtained by the extensometers in the vault and by the long base-line network around the EGO from 1971 to 1980

	Geodetic measurement		Continuous observation	
Period	1972 Oct. - 1980 Dec.		1971 Aug. - 1980 Aug.	
Result	e_{xx}	-1.21 ± 0.35	E-AB(135°)	1.41×10^{-6}
	e_{yy}	3.44 0.25	E-CD(45°)	2.81
	e_{xy}	-2.03 0.26	E-EF(0°)	-1.56
(Reduction to 9 years' accumulation)				
e_{xx}		-1.33×10^{-6}		-1.56×10^{-6}
e_{yy}		3.77		5.78
e_{xy}		-2.23		0.70
Dilatation		2.44		4.22
Maximum shear strain		6.48		7.47
Principal strains				
e_1 *(orientation)**		4.46*(112°)*		5.85*(85°)*
e_2		-2.02*(22°)*		-1.63*(- 5°)*

**Degrees counterclockwise from east.*

Table 3. Some constant of the strain changes observed at the EGO associated with the 1973 Earthquake off the Nemuro Peninsula

	Pre-seismic	Co-seismic		Post-seismic
Duration	at least 40 days			Ca 15 days
E-AB	+ 1.0 $\times 10^{-7}$	-2.7 $\times 10^{-7}$		-0.9 $\times 10^{-7}$
E-CD	+1.2	+0.8		+0.8
E-EF	+1.6	-3.3		-0.7
Dilatation	+2.2	-1.9		-0.1
Maximum shear strain	+1.0	+5.9		+2.1
Maximum principal strain (orientation)*	+1.6 (0°)	+2.0 (72°)	CAL. +1.2 (30°)	+1.0 (63°)
Minimum p.s.	+0.6	-3.9	-0.7	-1.1

Degrees counterclockwise from east.

Table 4. List of the earthquakes accompanied with strain steps at the EGO from August, 1971 to January, 1980

No	Date	Time	Lat.	Long.	Depth	Mag. JMA	Delta	Strain step amplitude (AB)	(CD)	(EF)	Seismic moment (M_{JMA})	(strain)
		h m	°N	°E	km		km		$\times 10^{-9}$		$\times 10^{25}$ dyne·cm	
1	02 Aug 71	16 25	41.23	143.70	60	7.0	98	-126.3	*	*	32	23
2	02 Aug 71	22 00	41.23	143.67	60	5.8	97	+2.6	*	*	0.50	0.46
3	04 Aug 71	09 28	41.22	143.70	40	5.6	100	+1.7	*	*	0.25	0.25
4	11 Nov 71	19 20	42.02	142.65	80	5.3	42	-2.0	-0.9	+0.9	0.089	0.18
5	23 Feb 72	05 00	41.77	142.90	50	5.1	35	+0.9	-2.7	+0.9	0.045	0.073
6	20 Mar 72	00 58	40.85	142.00	80	6.0	162	-0.9	-1.8	0	1.0	1.3
7	11 Apr 72	23 14	42.25	142.95	50	5.0	31	0	+0.9	0	0.032	0.022
8	11 May 72	09 45	42.60	144.93	60	5.8	160	-2.7	0	-2.7	0.50	1.6
9	17 June 73	12 55	42.97	145.95	40	7.7	253	-277.0	+77.0	-330.0	360	660
10	24 June 73	11 43	42.95	146.75	30	7.1	313	-14.4	+12.6	-7.2	45	54
11	25 Jan 74	04 15	41.83	144.27	40	6.0	94	-25.6	+12.8	-3.2	1.0	3.9
12	21 Apr 74	01 03	42.48	143.03	60	5.0	32	-1.4	+2.2	+0.9	0.032	0.082
13	09 June 74	05 37	41.78	143.15	40	4.9	26	+0.5	0	+0.9	0.022	0.012
14	27 Sept 74	14 47	42.75	146.67	30	6.6	300	-1.8	-0.5	-0.5	8.0	5.9
15	10 Oct 74	15 57	40.88	143.38	30	6.4	127	-0.9	+1.8	-2.7	4.0	0.72
16	12 Oct 74	15 15	40.48	143.87	40	6.2	180	-1.5	-1.5	0	2.0	1.1
17	14 Oct 74	23 12	40.60	143.85	40	5.9	167	+0.5	-0.9	-0.5	0.71	0.55
18	09 Nov 74	06 23	42.48	141.78	130	6.5	125	-5.8	+4.5	-5.4	5.6	4.1
19	17 Nov 74	22 19	41.62	142.80	50	5.0	53	-0.5	+0.9	+0.5	0.032	0.042
20	30 Nov 74	07 06	30.60	138.77	420	7.6	1326	0	-3.2	-2.7	251	1033

No	Date	Time	Lat.	Long.	Depth	Mag. JMA	Delta	Strain step amplitude (AB)	(CD)	(EF)	Seismic moment (M_{JMA})	(strain)
		h m	°N	°E	km		km		$\times 10^{-9}$		$\times 10^{25}$ dyne·cm	
21	09 Mar 75	22 34	42.07	143.02	30	4.5	13	-0.5	+0.9	0	0.0056	0.0038
22	26 Aug 75	14 11	40.93	143.20	40	5.4	120	+0.3	-0.3	*	0.13	0.073
23	09 Sept 75	14 56	41.60	142.77	40	4.7	56	-0.9	+0.5	*	0.011	0.036
24	20 Sept 75	02 54	41.77	142.83	50	5.9	39	-12.6	-10.8	*	0.71	0.38
25	30 Oct 75	10 41	41.95	142.83	60	6.0	32	+11.7	+ 9.9	-20.7	1.0	0.78
26	11 Nov 75	17 54	41.62	144.50	50	5.5	116	-0.5	0	+1.8	0.18	0.44
27	31 Dec 75	23 12	41.58	142.07	50	5.1	103	*	-0.4	-0.2	0.045	0.071
28	29 Mar 76	07 20	41.83	142.80	60	5.0	36	*	-1.8	*	0.032	0.074
29	31 Oct 76	21 30	42.25	143.03	70	5.0	28	+0.9	0	*	0.032	0.046
30	18 Feb 77	13 08	41.45	141.97	60	5.4	117	+0.9	-1.8	*	0.13	0.49
31	24 Feb 77	20 40	42.42	142.60	70	5.8	64	-1.8	+2.2	0	0.50	0.23
32	09 Mar 77	23 29	41.97	131.42	600	7.2	975	+0.5	-1.8	*	63	324
33	06 May 77	07 14	41.97	142.42	70	5.2	62	-0.9	+0.5	*	0.063	0.087
34	17 Nov 77	04 36	41.92	142.25	70	5.3	76	*	-0.4	*	0.089	0.053
35	20 Mar 78	16 19	42.35	142.77	80	5.5	49	0	0	-1.8	0.18	0.18
36	25 Mar 78	04 48	44.33	149.82	40	7.3	599	-3.2	+0.5	-9.0	89	234
37	12 June 78	17 14	38.15	142.17	40	7.4	437	-5.4	+0.9	-0.9	130	55
38	16 July 78	02 44	41.85	142.65	60	5.3	46	-0.5	-1.8	0	0.089	0.093
39	07 Nov 78	00 08	42.20	143.13	70	5.5	21	+0.4	+2.7	+0.4	0.18	0.13
40	06 Dec 78	23 00	44.73	146.97	100	7.7	432	+13.5	-23.4	-5.4	360	245
41	19 Jan 79	20 56	41.47	144.12	30	5.4	100	-1.8	+1.8	*	0.13	0.25
42	20 Feb 79	15 32	40.22	143.87	0	6.5	208	+1.8	-1.8	-0.9	5.6	2.0
43	30 Dec 79	00 06	42.23	143.03	70	5.7	26	+0.5	+2.7	+2.7	0.36	0.14
44	13 Jan 80	00 57	41.63	143.88	60	6.1	74	+9.0	-10.8	-4.5	1.4	1.1

+ and - signs correspond to extension and contraction, respectively.

* indicates no observation.

Table 5. A list of the coefficients needed in equation (9)

$U_{i,j}$	C^{1}_{ij}	C^{2P}_{ij}	C^{2S}_{ij}	C^{3P}_{ij}	C^{3S}_{ij}	C^{4P}_{ij}	C^{4S}_{ij}
Ux,x	$120x^3y-90xy^3$ $-90xyz^2$	$54x^3y-36xy^3$ $-36xyz^2$	$-51x^3y+39$ $xy^3+39xyz^2$	$14x^3y-6xy^3$ $-6xyz^2$	$-11x^3y+$ $9xy^3+9xyz^2$	$2x^3y$	$-x^3y+xy^3$ $+xyz^2$
Ux,y	$-24x^4+162x^2y^2$ $-18x^2z^2-24y^4$ $-18y^2z^2+6z^4$	$-10x^4+70x^2y^2$ $-8x^2z^2-10y^4$ $-8y^2z^2+2z^4$	$9x^4-69x^2y^2$ $+6x^2z^2+12y^4$ $+9y^2z^2-3z^4$	$-2x^4+16x^2y^2$ $-2x^2z^2-2y^4$ $-2y^2z^2$	$x^4-15x^2y^2$ $+4y^4+3y^2z^2$ $-z^4$	$2x^2y^2$	$-x^2y^2+y^4$ $+y^2z^2$
Ux,z	$180x^2yz-30y^3z$ $-30yz^3$	$78x^2yz-12y^3z$ $-12yz^3$	$-75x^2yz+15$ $y^3z-15yz^3$	$18x^2yz-2y^3z$ $-2yz^3$	$-15x^2yz+5$ y^3z+5yz^3	$2x^2yz$	$-x^2yz$ $+y^3z+yz^3$
Uy,x	$C^{1}_{xy}(x\leftrightarrow y)$	$C^{2P}_{xy}(x\leftrightarrow y)$	$C^{2S}_{xy}(x\leftrightarrow y)$	$C^{3P}_{xy}(x\leftrightarrow y)$	$C^{3S}_{xy}(x\leftrightarrow y)$	$C^{4P}_{xy}(x\leftrightarrow y)$	$C^{4S}_{xy}(x\leftrightarrow y)$
Uy,y	$C^{1}_{xx}(x\leftrightarrow y)$	$C^{2P}_{xx}(x\leftrightarrow y)$	$C^{2S}_{xx}(x\leftrightarrow y)$	$C^{3P}_{xx}(x\leftrightarrow y)$	$C^{3S}_{xx}(x\leftrightarrow y)$	$C^{4P}_{xx}(x\leftrightarrow y)$	$C^{4S}_{xx}(x\leftrightarrow y)$
Uy,z	$C^{1}_{xz}(x\leftrightarrow y)$	$C^{2P}_{xz}(x\leftrightarrow y)$	$C^{2S}_{xz}(x\leftrightarrow y)$	$C^{3P}_{xz}(x\leftrightarrow y)$	$C^{3S}_{xz}(x\leftrightarrow y)$	$C^{4P}_{xz}(x\leftrightarrow y)$	$C^{4S}_{xz}(x\leftrightarrow y)$
Uz,x	$180x^2yz-30y^3z$ $-30yz^3$	$78x^2yz-12y^3z$ $-12yz^3$	$-78x^2yz+12$ $y^3z+12yz^3$	$18x^2yz-2y^3z$ $-2yz^3$	$-18x^2yz+2$ y^3z+2yz^3	$2x^2yz$	$-2x^2yz$
Uz,y	$C^{1}_{zx}(x\leftrightarrow y)$	$C^{2P}_{zx}(x\leftrightarrow y)$	$C^{2S}_{zx}(x\leftrightarrow y)$	$C^{3P}_{zx}(x\leftrightarrow y)$	$C^{3S}_{zx}(x\leftrightarrow y)$	$C^{4P}_{zx}(x\leftrightarrow y)$	$C^{4S}_{zx}(x\leftrightarrow y)$
Uz,z	$C^{1}_{zx}(x\leftrightarrow z)$	$C^{2P}_{zx}(x\leftrightarrow z)$	$C^{2S}_{zx}(x\leftrightarrow z)$	$C^{3p}_{zx}(x\leftrightarrow z)$	$C^{3S}_{zx}(x\leftrightarrow z)$	$C^{4P}_{zx}(x\leftrightarrow z)$	$C^{4S}_{zx}(x\leftrightarrow z)$

$(\alpha\leftrightarrow\beta)$ indicates the interchange of α and β .

Table 6. List of earthquakes of which strain seismograms are analyzed in the Section 4.2

No.	Date			Time		Lat.	Long.	H.	Δ	M_{JMA}	e_{s-9}	τ_e	Moment
	y	m	d	h	m	°N	°E	km	km		10^{-9}	sec	dyne·cm
1	76	10	31	21	30	42.37	142.98	61	42	5.0	38	4.1	2.1×10^{24}
2		11	1	13	5	42.32	142.98	60	37	4.7	19	2.7	4.4×10^{23}
3	77	2	24	20	40	42.49	142.60	47	70	6.0	174	3.8	$9.5 \times z0^{24}$
4		5	6	7	14	41.97	142.45	75	59	5.2	18	1.9	2.7×10^{23}
5		11	17	4	36	41.97	142.34	78	68	5.3	16	1.8	2.4×10^{23}
6	78	3	20	16	19	42.42	142.78	77	55	5.5	85	2.8	2.8×10^{24}
7		4	6	17	39	41.39	142.68	51	80	5.1	9	2.9	3.2×10^{23}
8		7	16	2	44	41.79	142.67	67	47	5.3	210	2.1	3.4×10^{24}
9		10	29	7	46	42.59	144.30	80	115	5.3	18	2.6	7.7×10^{23}
10		11	7	0	8	42.31	143.08	61	34	5.5	148	1.9	1.7×10^{24}
11	79	1	19	20	56	41.47	144.12	39	222	5.4	222	3.6	1.2×10^{25}
12	78	3	7	11	48	31.90	137.77*	440	1200	6.9	59	7.6	2.0×10^{26}
13		6	12	17	14	38.15	142.17*	40	445	7.4	329	13.1	1.1×10^{27}
14		12	6	23	3	44.12	146.94	168	387	7.7	235	45.0	9.0×10^{27}
15	76	11	4	20	20	42.32	144.19	63	92	4.5	5	1.5	5.1×10^{22}
16		11	8	17	19	38.07	142.32*	30	440	6.2	17	3.9	5.1×10^{24}

Table 6. Continued.

No.	Date y	m	d	Time h	m	Lat. °N	Long. °E	H. km	Δ km	M_{JMA}	e_{s-9} 10^{-9}	τ_e sec	Moment dyne·cm
17	77	6	5	15	41	42.26	142.97	49	33	4.7	8	1.0	2.1×10^{22}
18	78	3	25	4	47	44.33	149.82*	40	620	7.3	287	14.0	1.6×10^{27}
19		5	16	16	35	40.95	141.47*	10	204	5.8	12	3.6	1.4×10^{24}
20		5	16	17	23	40.93	141.45*	10	204	5.8	27	3.1	2.3×10^{24}
21		6	21	20	10	47.68	149.23*	380	818	6.7	27	4.5	2.2×10^{25}
22	79	2	20	15	32	40.22	143.87*	0	234	6.5	213	7.0	1.1×10^{26}
23		4	24	17	5	41.41	142.10	89	111	5.2	47	2.4	1.7×10^{24}
24		5	26	6	11	42.30	143.00	61	32	4.9	32	1.4	1.9×10^{23}
25		10	22	16	3	41.97	142.33	79	69	4.3	6	1.1	3.2×10^{22}
26		12	7	3	29	42.03	142.56	67	49	3.6	4.2	0.56	4.9×10^{21}
27		12	7	4	58	40.72	144.92	72	207	4.4	11	0.73	5.9×10^{22}
28		12	14	16	19	42.83	144.28	44	129	5.7	169	2.0	4.1×10^{24}
29		12	14	21	50	41.16	142.76	31	101	3.6#	6.1	0.63	1.2×10^{22}
30		12	21	19	51	42.14	143.37	45	22	3.3#	3.2	0.37	9.9×10^{20}
31		12	25	6	7	42.43	143.89	49	76	4.0	23	0.60	3.4×10^{22}
32	80	2	14	21	1	40.18	142.15*	40	228	4.1	3.8	0.60	1.4×10^{22}
33		2	15	13	51	41.42	142.77*	50	91	4.1	13	0.74	3.1×10^{22}
34		2	15	23	25	44.77	149.83*	50	632	5.7	15	5.6	1.3×10^{25}
35		2	16	0	0	44.57	149.65*	0	651	5.5	10	3.3	3.2×10^{24}

Table 6. Continued.

No.	Date y	m	d	Time h	m	Lat. °N	Long. °E	H. km	Δ km	M_{JMA}	e_{s-9} 10^{-9}	τ_e sec	Moment dyne·cm
36	80	2	18	15	8	43.55	146.04	129	235	5.6	20	0.93	2.5×10^{23}
37		2	19	10	33	41.63	142.10	65	98	4.7	23	0.86	9.0×10^{22}
38		2	25	7	39	41.94	142.31	80	71	3.7	5.1	0.60	8.8×10^{21}
39		2	25	15	45	42.65	142.94	106	72	4.5	33	0.79	1.2×10^{23}
Aftershock sequence													
Mainshock													
40	80	2	23	14	51	43.46	146.73	30$	333	6.8	300	5.4	1.3×10^{26}
Aftershocks													
41		2	23	15	50	43.42	147.02	30$	353	5.7	67	2.2	5.1×10^{24}
42		2	24	3	55	43.69	146.57	30$	335	4.5	2.1	0.84	2.2×10^{22}
43		2	24	7	39	43.15	147.14	30$	350	5.9	80	2.3	6.7×10^{24}
44		2	24	11	27	43.15	147.26	30$	360	5.0	11	1.7	5.1×10^{23}
45		2	24	11	44	43.21	147.25	30$	362	4.9	2.0	1.0	3.2×10^{22}
46		2	24	12	13	43.11	147.31	30$	363	4.6	2.5	1.1	4.9×10^{22}
47		2	24	12	21	43.09	147.29	30$	359	4.8	3.8	0.84	4.4×10^{22}
48		2	24	13	38	43.76	146.99	30$	368	4.7	4.7	1.1	9.4×10^{22}
49		2	24	21	33	43.18	147.45	30$	376	4.8	3.6	1.8	1.9×10^{23}
50		2	25	0	32	43.21	148.31	30$	440	4.8	3.4	1.6	1.7×10^{23}
51		2	26	7	39	43.41	148.00	30$	437	4.5	1.3	1.5	5.8×10^{22}

Table 6. Continued.

No.	Date y	m	d	Time h	m	Lat. °N	Long. °E	H. km	Δ km	M_{JMA}	e_{s-9}	τ_e sec	Moment dyne·cm
52	80	2	26	18	56	43.29	147.15	30$	356	5.0	4.4	1.7	2.1×10^{23}
53		2	27	21	45	43.27	146.86	30$	334	5.7	57	2.1	3.7×10^{24}
54		2	28	8	3	43.25	146.88	30$	335	5.4	17	1.4	5.0×10^{23}
55		3	1	7	46	43.51	146.73	30$	337	4.6	3.4	0.84	3.6×10^{22}

Focal parameters are determined by the Research Center for Earthquake Prediction, Hokkaido University excluding thoes with * mark, which are determined by Japan Meteorological Agency (JMA).

e_s and τ_e are average amplitude and period of the first S-waves in the observed strain seismograms by three components of extensometers. Seismic moment estimated from the equation (12) is listed for each event.

Magnitude with # is estimated from F-P time.

Table 7. List of seismic moment and source process time data obtained by conventional seismological method and other related parameters

Event	Date			Moment	τ_e*	L.	Vr.	Mode	Ref.#
	y	m	d	dyne·cm	sec	km	km/s		
1 Tango	27	3	27	4.6×10^{26}	7.6	35	2.3	B	G
2 Saitama	31	9	21	6.8×10^{25}	4.3	20	2.3	B	G
3 Sanriku	33	3	2	4.3×10^{28}	58	185	3.2	U	G
4 Long Beach	33	3	11	2.8×10^{25}	13-6.5	30	2.3	?	G
5 South Izu	34	3	21	9.5×10^{23}	2.3	7	3.0	U	A
6 Tottori	43	9	10	3.6×10^{26}	7.2	33	2.3	B	G
7 Fukui	48	6	28	3.3×10^{26}	6.5	30	2.3	B	G
8 Chili	60	5	22	2.4×10^{30}	230	800	3.5	U	G
9 Kitamino	61	8	19	9.0×10^{25}	4.0	12	3.0	U	G
10 Wakasawan	63	3	27	3.3×10^{25}	4.3	20	2.3	B	G
11 Kurile	63	10	13	7.5×10^{28}	71	250	3.5	U	G
12 Alaska	64	3	28	5.2×10^{29}	143	500	3.5	U	G
13 Rat Island	65	2	4	1.4×10^{29}	125	500	4.0	U	G
14 Parkfield	66	6	28	3.2×10^{25}	9.6	26	2.7	U	G
15 Tokachioki	68	5	16	2.8×10^{28}	43	150	3.5	U	G
16 Saitama	68	7	1	1.9×10^{25}	2.9	10	3.4	U	G
17 Kurile	69	8	11	2.2×10^{28}	51	180	3.5	U	G
18 Gifu	69	9	9	3.5×10^{25}	3.6	18	2.5	U	G
19 Peru	70	5	31	1.0×10^{28}	52	130	2.5	U	G
20 San Fernando	71	2	9	1.2×10^{26}	8.3	20	2.4	U	G
21 Amagi	74	7	9	3.2×10^{23}	0.6	3.5	3.0	B	A
22 Kawazu	76	8	17	2.1×10^{24}	1.9	9	2.4	B	A

*τ_e is calculated from L/Vr·n (n=1 for Uni-lataral, =2 for Bi-lateral).

#Ref. G : Geller(1976) , A : Abe(1978).

Table 8. Source parameters of multiple shock sequence

No.	P-time* (sec.)	Source process time (sec.)	Seismic moment (dyne.cm)
long-period event			
	0.0	60.0	45 x 10^{26}
short-period events			
1	0.0	5.0	0.43 x 10^{26}
2	10.1	7.1	3.9
3	11.1	2.6	0.26
4	15.6	8.6	3.8
5	19.3	3.0	0.95
6	24.0	2.9	0.40
7	27.4	8.6	3.4
8	28.3	3.7	1.6
9	31.7	2.4	0.54
10	34.3	2.3	0.80
11	36.0	8.6	3.7
12	36.4	3.0	0.46
13	40.3	3.1	0.95
14	45.9	3.2	0.90
15	48.9	2.9	1.1
16	51.4	3.0	0.77
17	55.2	2.4	0.30
18	57.9	3.9	0.95
Total moment for short-period events			25 x 10^{26}
Over-all moment			70 x 10^{26}

* refer to the first P-wave arrival.

Table 9. Comparison of seismic moments of the Kunashiri event by analyses of strain seismogram in this study and of WWSSN long period-seismogram by Sudo and Sasatani (1979)

Strain seismogram	WWSSN long period-seismogram
dynamic motion	
Multiple shock sequence 18 short-period events and a long-period event estimated	*Multiple-shock analysis for body waves*
S.P. events 2.5×10^{27} dyne·cm	2.5×10^{27} dyne·cm
L.P. event 4.5×10^{27} dyne·cm	
Over-all moment 7.0×10^{27} dyne·cm	Over-all moment estimated from surface waves 9.6×10^{27} dyne·cm
permanent deformation	
Strain step 6.0×10^{27} dyne·cm	Unknown

FIGURE CAPTIONS

Fig. 1. Schematic representation of a horizontal linear extensometer. Examples of rod supporting system : (A) is an inverted pendulum system; (B) a hanging system.

Fig. 2. Schematic diagrams showing the fixer (left), rod supporting system (middle), and free end (right). Specification for pedestal settlement is also shown (left,bottom).

Fig. 3. Geological sketch map around EGO (after Funahashi and Hashimoto,1951), vertical and horizontal cross section views of the observational vault are shown in the upper, middle, and lower parts, respectively.

Fig. 4. Schematic representation of signal flow and influence factors on the crustal movement observation using the extensometer in the vault.

Fig. 5. Examples of records of three components by loading test for the extensometer.

Fig. 6. Plots of load given at the fixed end point versus resultant strain at the free end point by loading test for each component of the extensometer.

Fig. 7. Block diagram of the observational system.

Fig. 8. Daily variations of crustal strains observed by three components of the extensometer in the vault during the period from August, 1971 to March, 1981. Daily variations of water-discharge from the vault and of precipitation are also shown at the lower part.

Fig. 9. Estimated secular strain accumulations subtracting exponential decay drifts of the E-AB and E-CD components from Fig.8 (an upper curve for each component). Low-pass filtered records longer than 1 year (middle curve) 4 years (lower curve) are also shown for each component. Arrows denote the occurrence of the 1973 Earthquake off the Nemuro Peninsula.

Fig.10. Configuration of the long base-line network around EGO.

Fig.11. Repeated length measurements of each base-line (in Fig.10) are shown as a function of time. A least squares fit to the data excluding open circle data (see text) is also shown. Error bars represent one standard deviation on either side of the plotted point.

Fig.12. Plot of the standard deviation of the residual of a least squares linear fit to the data in Fig.11 versus

base-line length.

Fig.13. Plot of the accumulated strain during the period from 1972 to 1980 versus the azimuth of base-line. Error bars represent one standard deviation on either side of the plotted point. The solid curve is the least squares solution for homogeneous plane strain excluding open circles. The results obtained by the extensometers are also shown by open square marks.

Fig.14. Comparison of principal strains of the accumulated crustal strain obtained by the extensometers in the vault and by the long base-line network around EGO during the period from 1971 to 1980. Extension and contraction reckoned solid and dashed lines, respectively.

Fig.15. Map showing the location of EGO and the aftershock area of the 1973 Earthquake off the Nemuro Peninsula.

Fig.16. Daily variations of crustal strains observed by the extensometers, water-discharge from the vault , and precipitation at EGO during the period from 1972 to 1974. Arrows and dotted lines denote the occurrence time of the event and the co-seismic strain steps, respectively. Three periods holded between a pair of dashed lines in each year will be used for comparison in Fig.17.

Fig.17. Strain variations in each component of the extensometer as a function of the logarithm of water-discharge for the periods shown in Fig.16. Closed circles, open circles, and crosses indicate the case of 1972, 1973, and 1974. The mark "EQ" for each component in the case of 1973 denotes the occurrence of the 1973 earthquake.

Fig.18. Residual strain changes subtracting the effect due to the water-discharge. Light and dark shaded areas represent the pre-seismic and post-seismic abnormal changes related to the 1973 earthquake, respectively.

Fig.19 Epicenter distribution of the earthquakes accompanied by strain steps observed at EGO.

Fig.20. Seven examples of the observed strain steps. The event number of each record is the same one given in Table 4.

Fig.21. Plot of the calculated strain steps versus the observed ones. Open and solid marks indicate consistent and inconsistent polarities between the observed and the calculated strain steps, respectively. Numerals denote the earthquake numbers given in Table 4.

Fig.22. Plot of the observed strain step as a function of hypocentral distance (abscissa) and earthquake magnitude (ordinate). Straight lines show the least squares solution for the equation (1). Numerals attached to the plots correspond to events in Table 4.

Fig.23. Geometry of an arbitrarily orientated buried double couple point source to the surface.

Fig.24. A parabolic ramp function with rise time, τ_e and final moment, Mo as a moment rate function assumed.

Fig.25. A strain seismogram observed by newly improved recording system.

Fig.26. Map showing epicenters with focal solutions for 14 earthquakes of which strain seismograms were compared with the synthetic ones. Numerals denote the earthquake numbers given in Table 6.

Fig.27. Focal mechanism solutions for eight earthquakes which were newly added in this study. Numbers correspond to events in Table 6. Equal area projection (upper hemisphere) of the P-wave first-motion data are shown. Solid and open circles indicate compressional and dilatational first motions, respectively.

Fig.28. Comparison of the observed strain seismograms with the optimal synthetic ones for the Hidaka Mountains earthquake on October 31, 1976.

Fig.29. Observed strain seismograms and synthetic ones calculated for various values of source process time τ_e for the earthquake off Erimo on January 19, 1979.

Fig.30. Observed strain seismogram of the South of Chubu earthquake on March 7, 1978 (upper part). Comparison of the S-wave part between observed and synthetic strain seismograms calculated for various values of source process time τ_e.

Fig.31. Observed and synthetic strain seismograms for the Earthquake of Miyagi-ken-oki on June 12, 1978.

Fig.32. Comparison of the observed strain seismograms with the optimal synthetic ones for the earthquakes occurring near EGO.

Fig.33. Plot of seismic moment estimated from strain seismogram versus that obtained by the conventional seismological method (solid circle) and estimated from the empirical relationship to magnitude (open circle).

Fig.34. The relationship between seismic moment to a product of S-wave amplitude and a second power of period of S-wave and a hypocentral distance.

Fig.35. Map showing epicenters of 55 earthquakes of which strain seismograms were analyzed and listed in Table 6.

Fig.36. Comparison of the observed strain seismogram for the earthquake with the smallest magnitude in this study (middle part) with the low-pass filtered seismograms observed by short-period horizontal seismometers (upper and lower parts).

Fig.37 Examples of strain seismograms for small earthquakes. The first one-cycle of S-waves are shown by a pair of short horizontal lines. Numbers correspond to events in Table 6.

Fig.38. Plot of source process time versus seismic moment. Circle and triangle denote uni-lateral and bi-lateral rupture modes, respectively. Solid marks denote the results obtained by this study and listed in Table 6. Open marks are obtained by conventional seismological method listed in Table 7. Straight lines are calculated by the assumed fault model (see text).

Fig.39. Map showing the location of EGO and the epicenters of the mainshock (cross) and aftershocks (solid circle) of the 1978 Kunashiri Strait earthquake located by ISC. Solid elipsoid is the epicenter of the 1978 Etorofu earthquake. Thick and thin dashed lines denote fracture zones (after Hilde et al.,1976) and contour of hypocentral depth of deep seismic zone, respectively.

Fig.40. Hypocentral distribution of the mainshock (large solid circle) and aftershocks (small circle) with magnitude greater than 4 determined by ISC. (a) : epicentral distribution, (b) : vertical cross section of northwest-southeast direction.

Fig.41. Focal mechanism solution of the Kunashiri event determined from the P-wave first-motion data of WWSSN long-period seismograms (after Sudo and Sasatani,1979). Equal area projection on a lower hemisphere.

Fig.42. The strain seismograms of the 1978 Kunashiri earthquake observed at EGO: (a) routine record traces, (b) reproduced records, (c) low-pass filtered records with a short-period cut-off 30 seconds.

Fig.43. Comparison of the observed strain seismograms between the 1978 Kunashiri earthquake (upper) and the 1978 Etorofu earthquake (lower).

Fig.44. P-wave arrival times of short-period events identified are shown by small circles on the observed strain seismogram of the E-CD component (upper). A synthetic strain seismogram of the component with a source process time of 5 seconds is also shown (lower).

Fig.45. Synthetic strain seismograms (upper) and their low-pass filtered records (lower) due to a source model A for the 1978 Kunashiri event.

Fig.46. Synthetic strain seismograms due to a source Model B.

Fig.47. Synthetic strain seismograms (solid curves) of ultra-low frequency component for various values of source process time in comparison with the observed ones (dashed curve) are shown for the E-CD component. The curve with source process time of 60 seconds is the best fit to the observed ones in three components.

Fig.48. Reproduced high gain records for the E-AB and E-CD components about 3 minutes before the P-arrival of the 1978 Kunashiri earthquake. Note that any pre-seismic movement beyond the capability of the EGO extensometer did not occurred.

Fig.49. Plot of seismic moment versus source process time for multiple shock sequence of the 1978 Kunashiri earthquake. Straight lines denote equal stress drop for the event with the same rupture velocity. Double open and solid circles denote the long-period and the short-period events in multiple shock sequence, respectively.

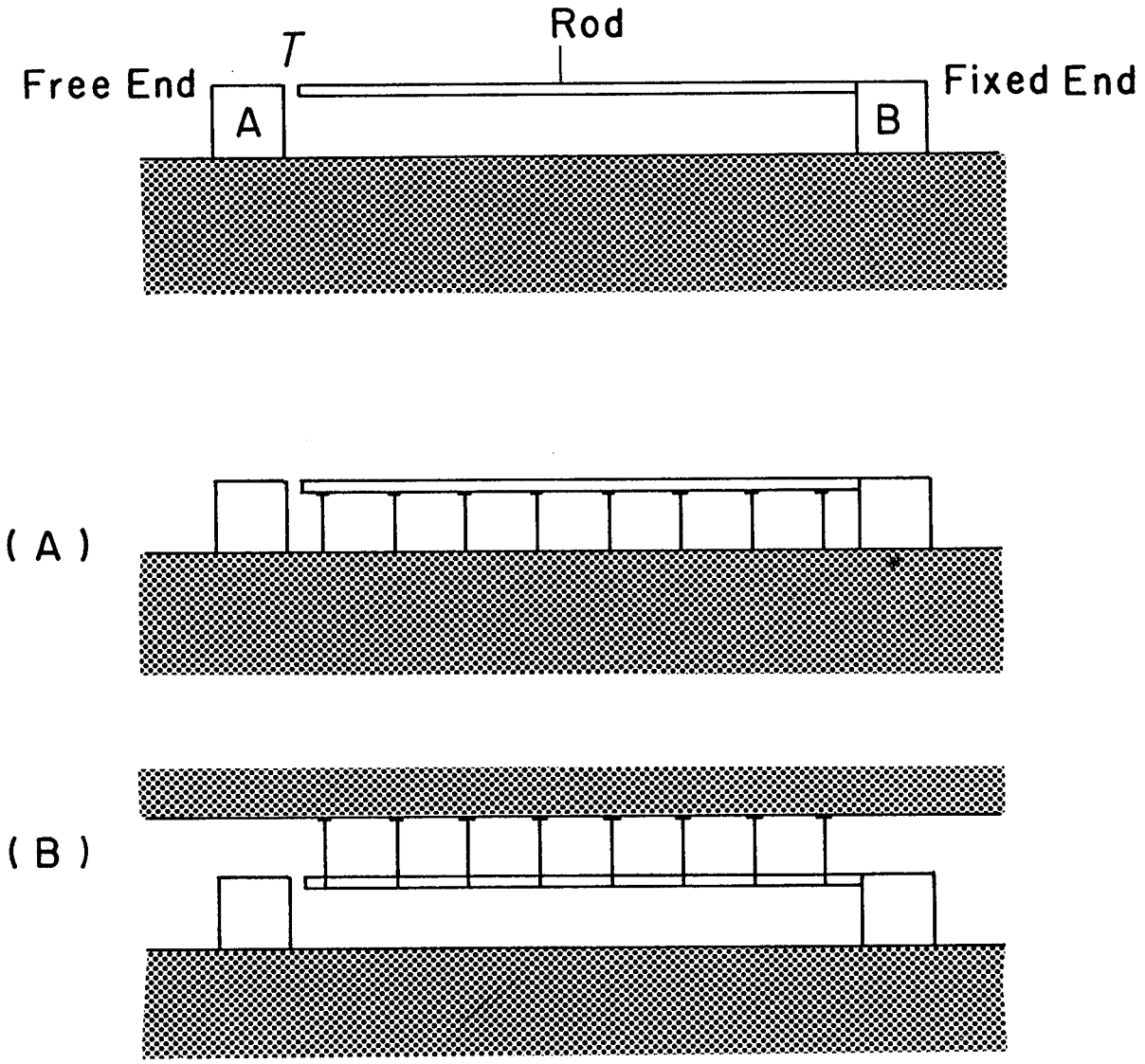

Fig. 1

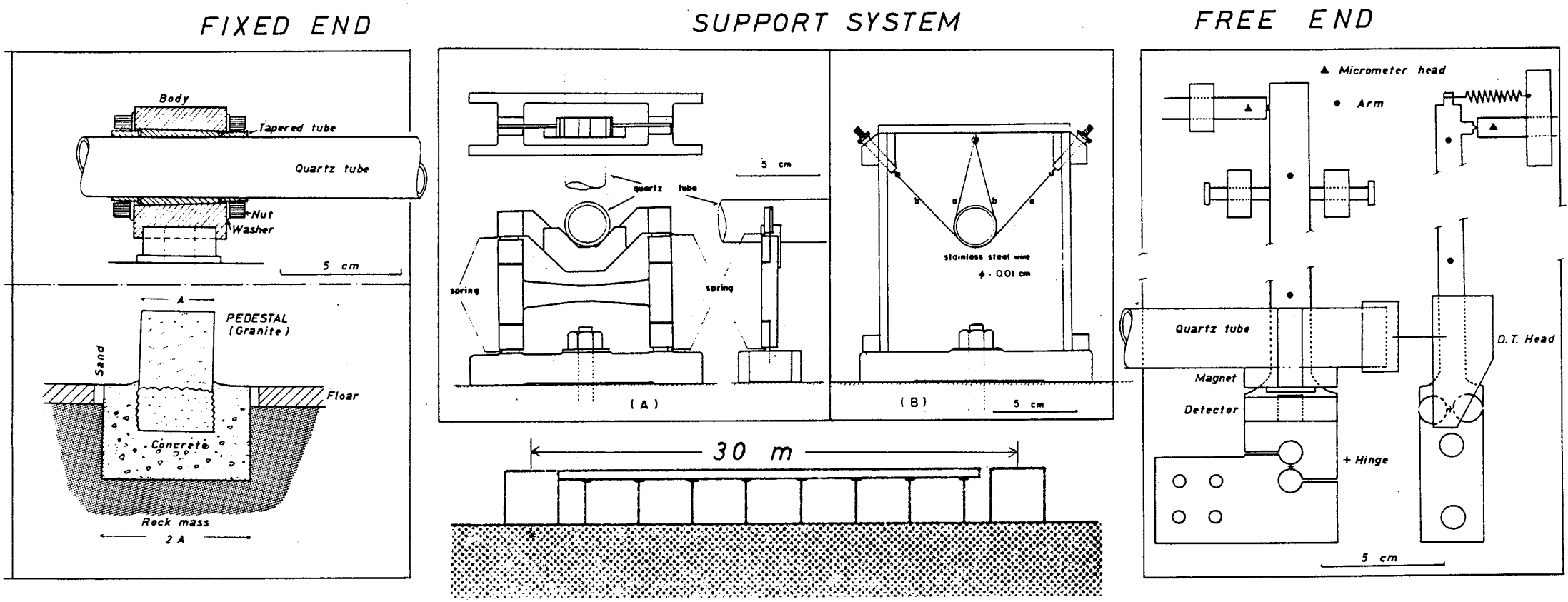
FIXED END
SUPPORT SYSTEM
FREE END
Body
Tapered tube
Quartz tube
Nut
Washer
5 cm
A
PEDESTAL
(Granite)
Sand
Floar
Concrete
Rock mass
2 A
quartz tube
5 cm
spring
spring
(A)
stainless steel wire
ϕ - 0.01 cm
(B)
5 cm
30 m
Micrometer head
Arm
Quartz tube
D.T. Head
Magnet
Detector
+ Hinge
5 cm

Fig. 2

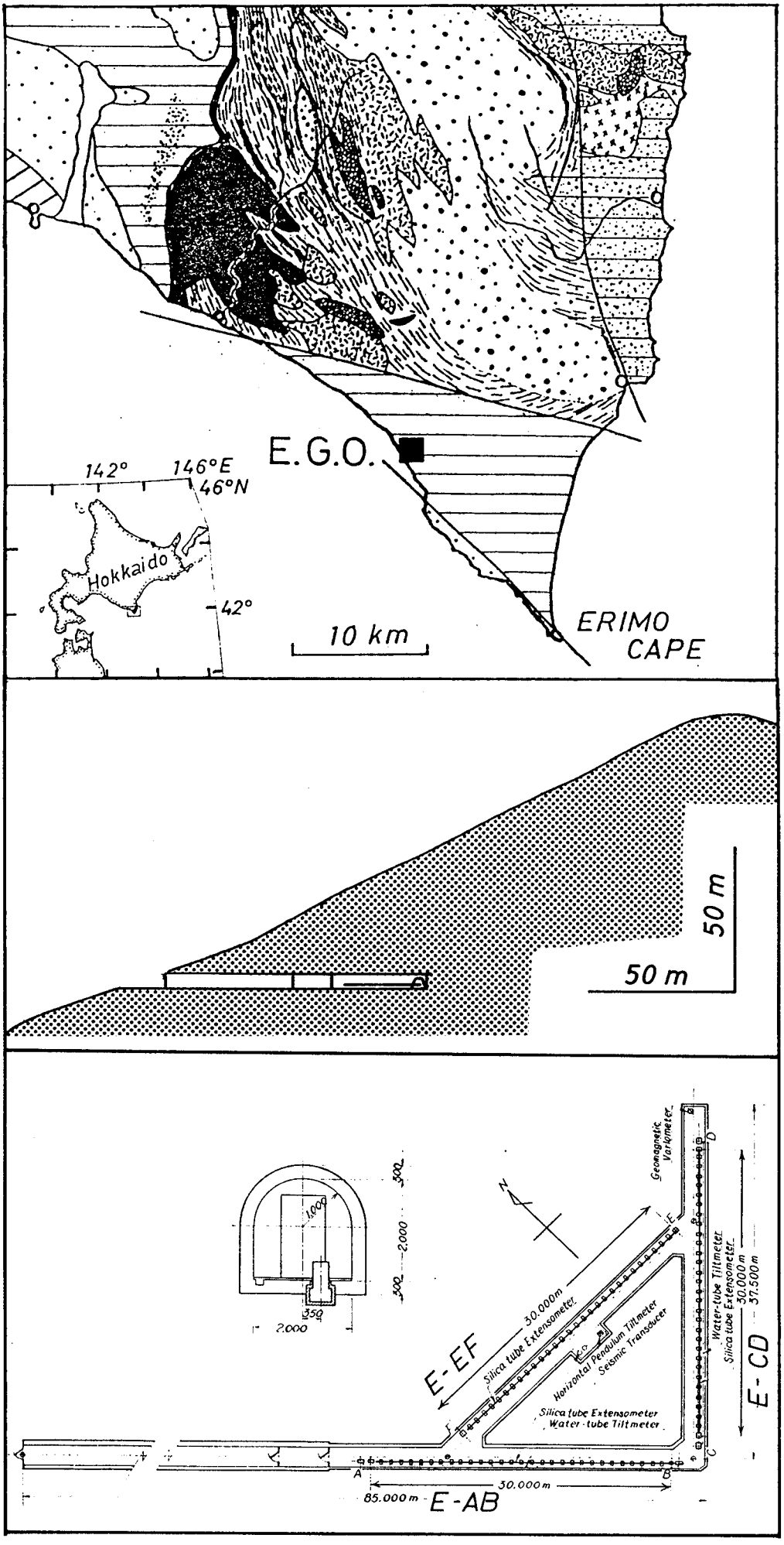
E.G.O.
142°
146°E
46°N
Hokkaido
42°
10 km
ERIMO
CAPE
50 m
50 m
E-EF
30.000m
Silica tube Extensometer
Horizontal Pendulum Tiltmeter
Seismic Transducer
Silica tube Extensometer
Water-tube Tiltmeter
Geomagnetic Variometer
Water-tube Tiltmeter
Silica tube Extensometer
30.000 m
37.500 m
E-CD
85.000 m
E-AB
30.000 m
2.000
300
2.000
300
350
1000

Fig. 3

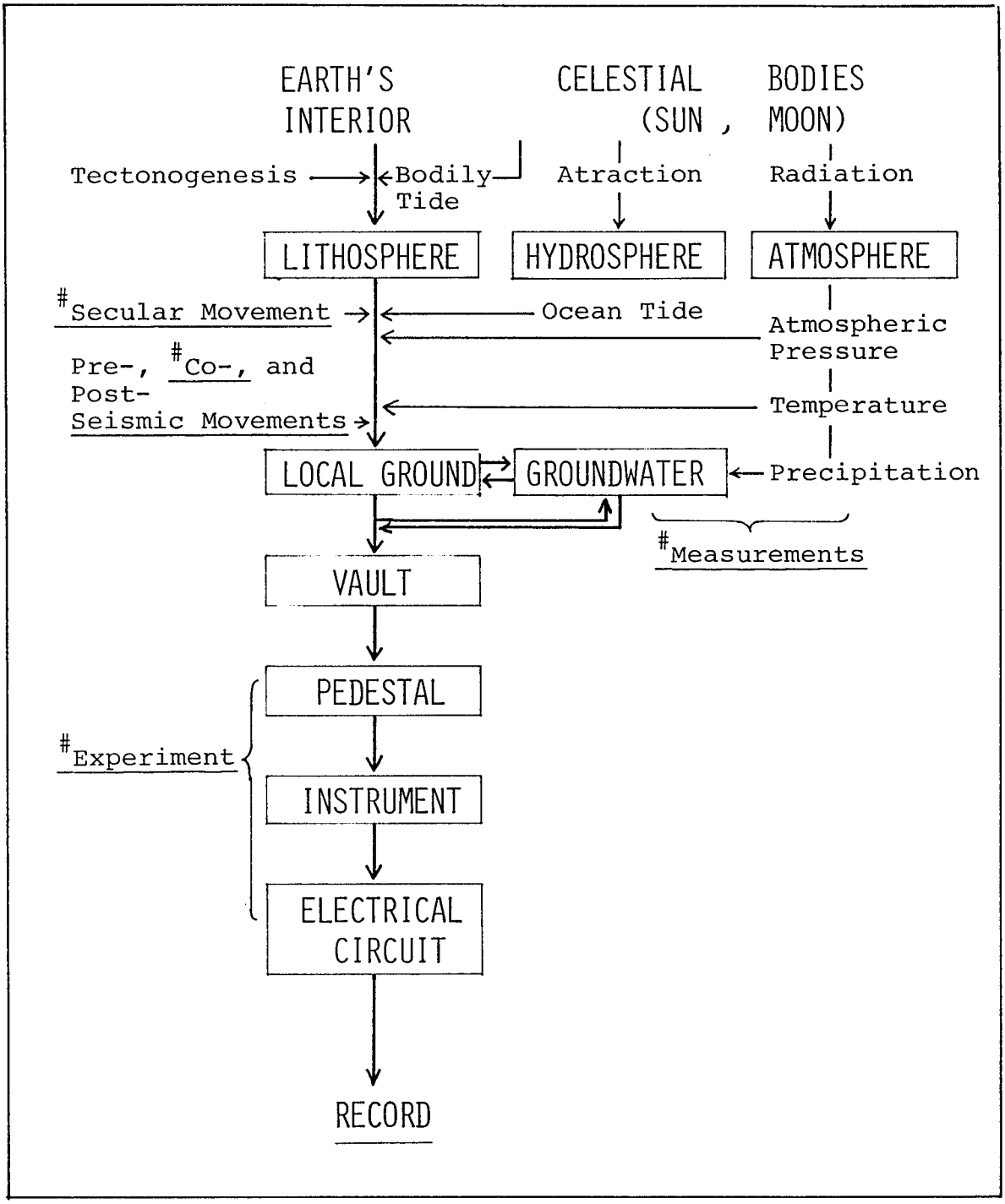
EARTH'S INTERIOR
CELESTIAL (SUN, MOON)
BODIES
Tectonogenesis
Bodily Tide
Atraction
Radiation
LITHOSPHERE
HYDROSPHERE
ATMOSPHERE
#Secular Movement
Ocean Tide
Atmospheric Pressure
Pre-, #Co-, and Post-Seismic Movements
Temperature
LOCAL GROUND
GROUNDWATER
Precipitation
#Measurements
VAULT
PEDESTAL
#Experiment
INSTRUMENT
ELECTRICAL CIRCUIT
RECORD

Fig. 4

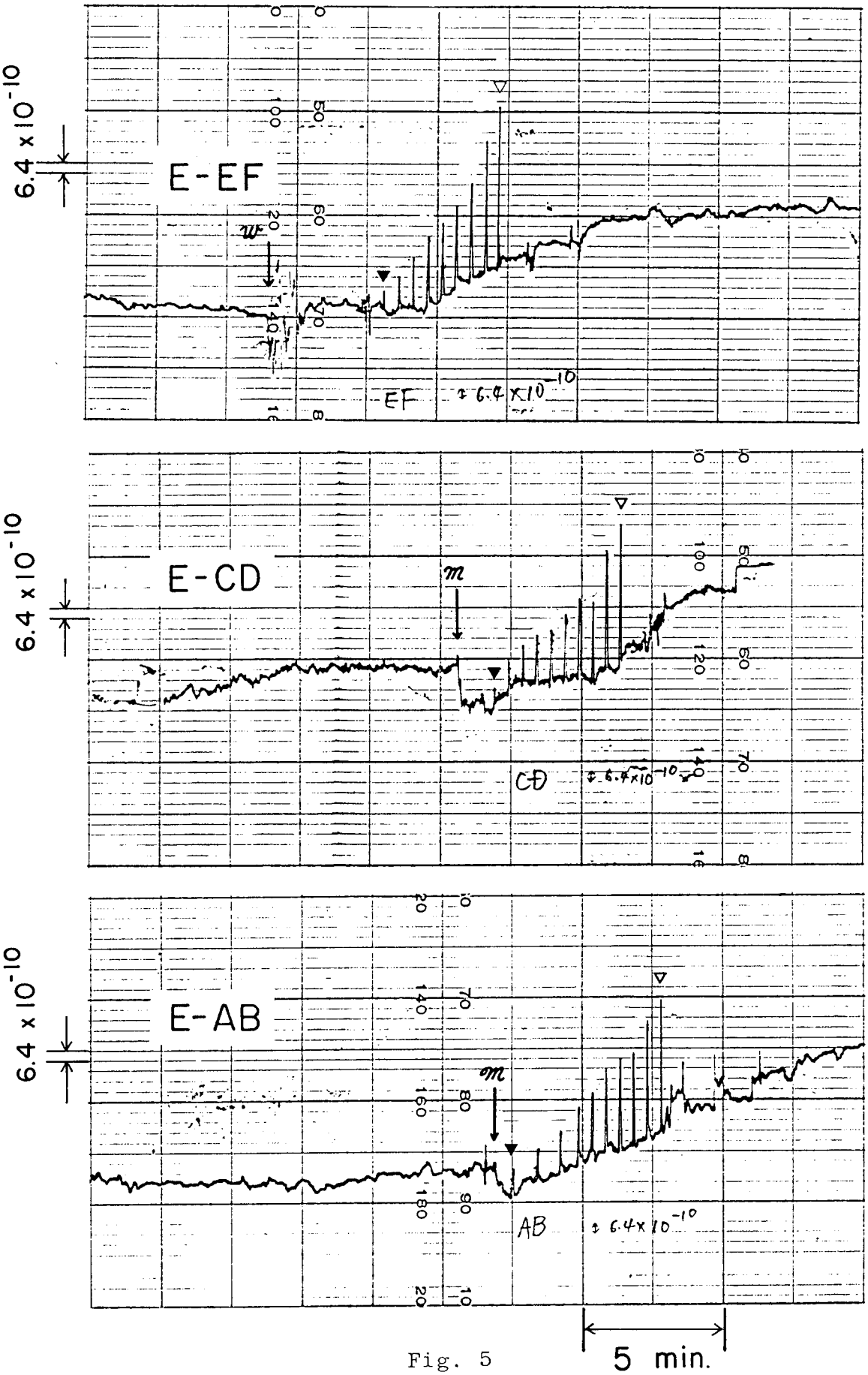
6.4 x 10⁻¹⁰
E-EF
w
EF
± 6.4×10⁻¹⁰
6.4 x 10⁻¹⁰
E-CD
m
CD
± 6.4×10⁻¹⁰
6.4 x 10⁻¹⁰
E-AB
m
AB
± 6.4×10⁻¹⁰
5 min.

Fig. 5

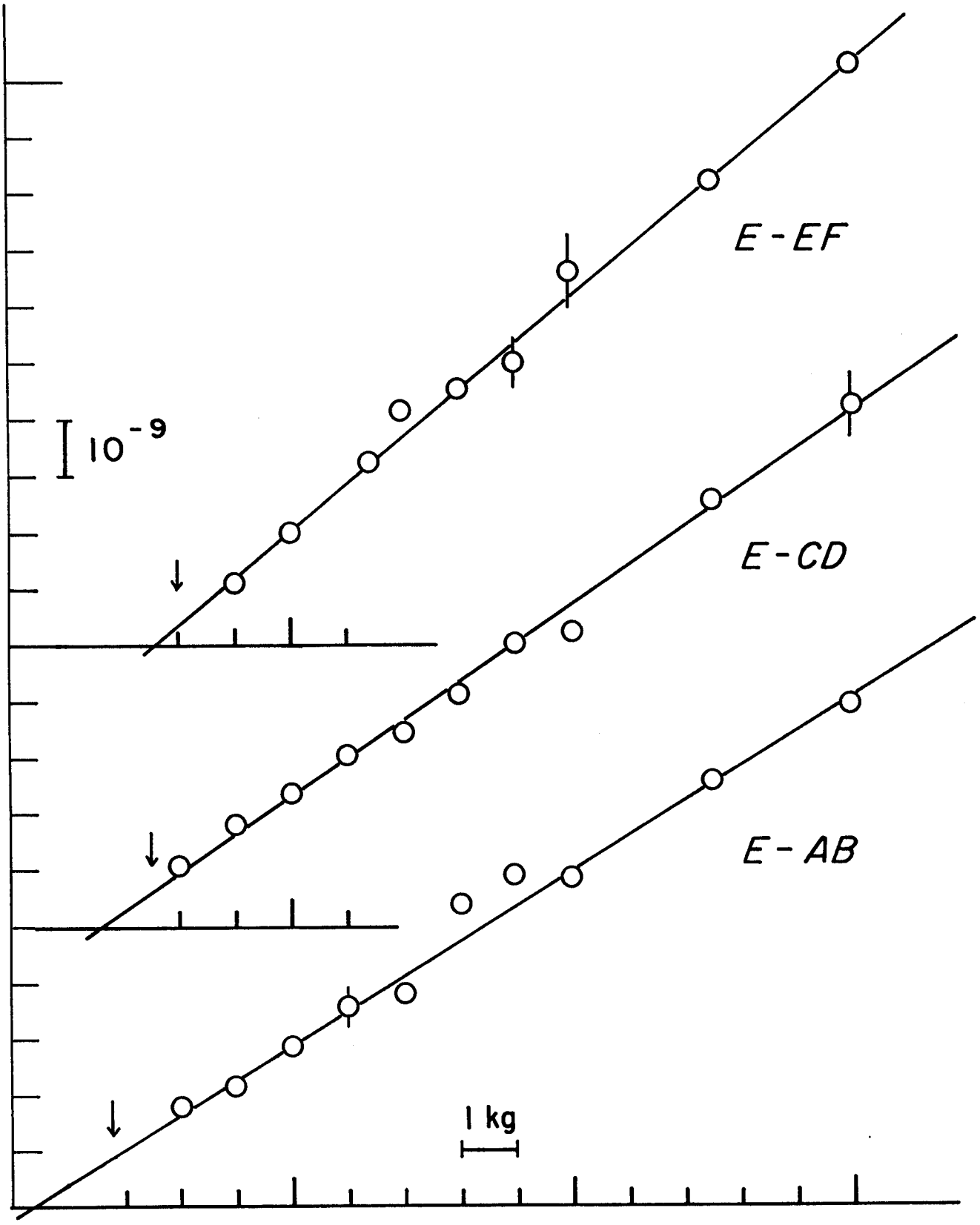

Fig. 6

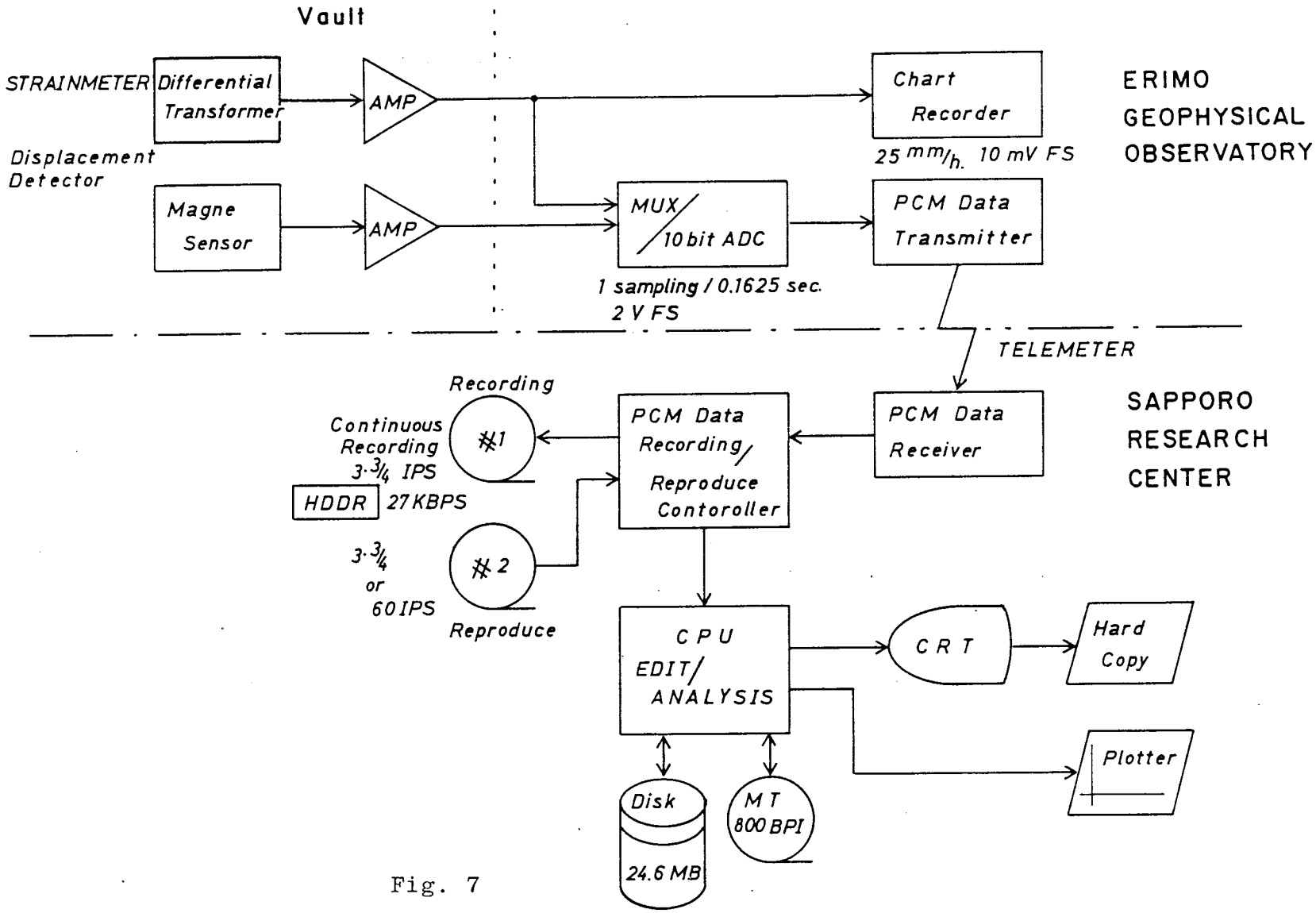
Vault
STRAINMETER
Differential Transformer
Displacement Detector
AMP
Magne Sensor
AMP
Chart Recorder
25 mm/h. 10 mV FS
ERIMO GEOPHYSICAL OBSERVATORY
MUX / 10 bit ADC
1 sampling / 0.1625 sec.
2 V FS
PCM Data Transmitter
TELEMETER
PCM Data Receiver
SAPPORO RESEARCH CENTER
PCM Data Recording / Reproduce Contoroller
Recording
Continuous Recording
3·3/4 IPS
#1
HDDR
27 KBPS
3·3/4 or 60 IPS
#2
Reproduce
C P U EDIT/ ANALYSIS
C R T
Hard Copy
Plotter
Disk
24.6 MB
M T
800 BPI

Fig. 7

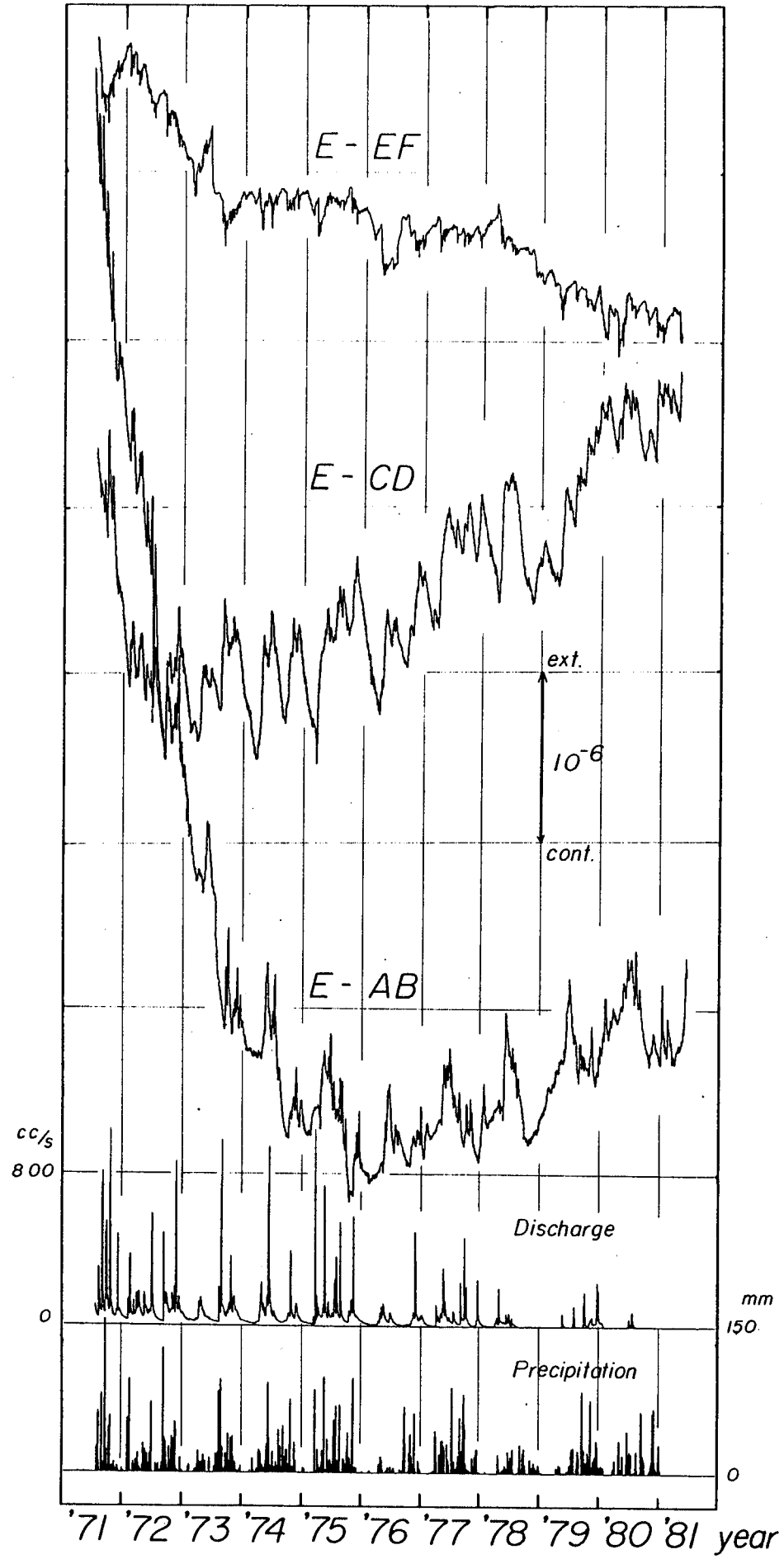
E - EF
E - CD
ext.
10⁻⁶
cont.
E - AB
cc/s
800
Discharge
0
mm
150
Precipitation
0
'71 '72 '73 '74 '75 '76 '77 '78 '79 '80 '81 year

Fig. 8

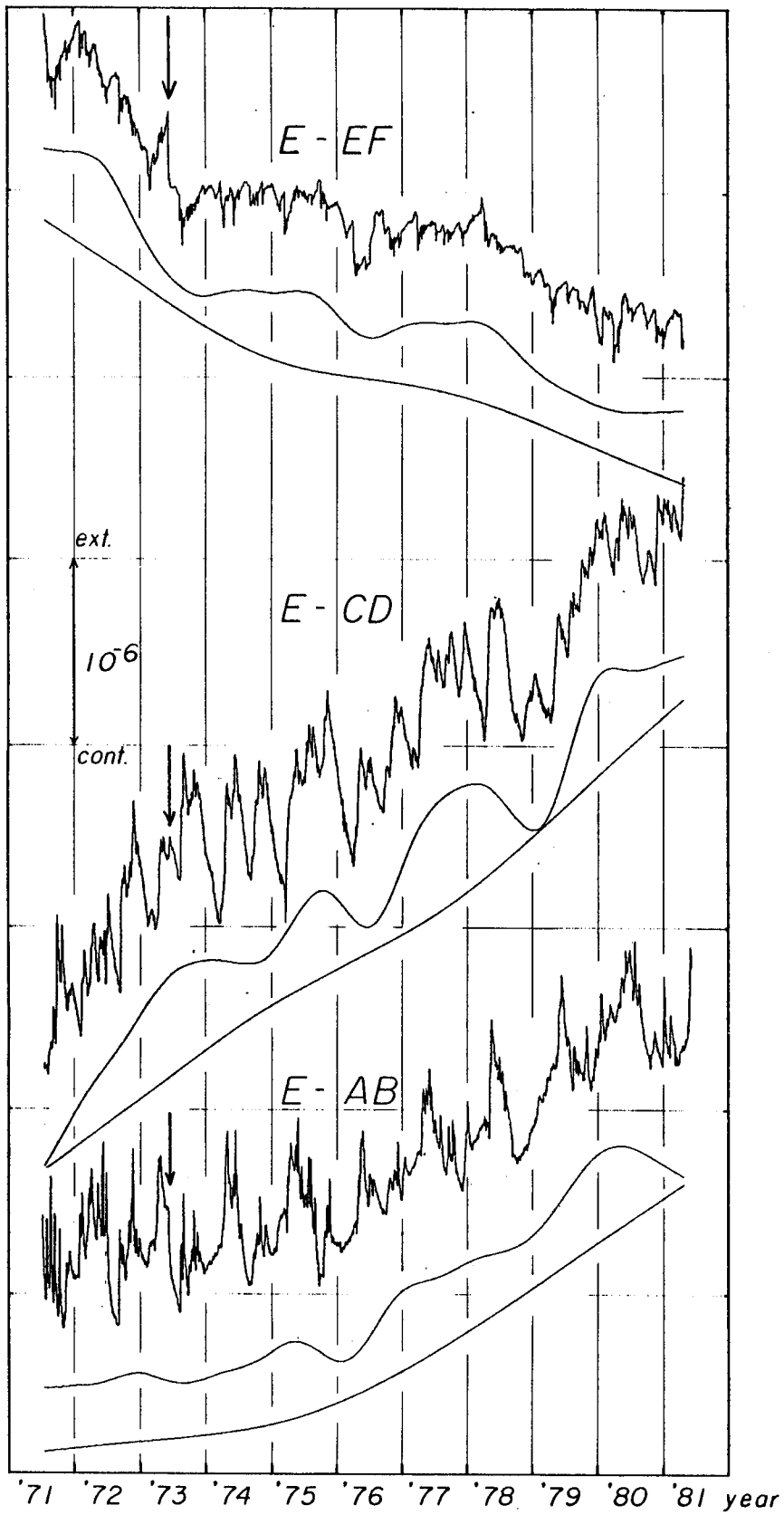

Fig. 9

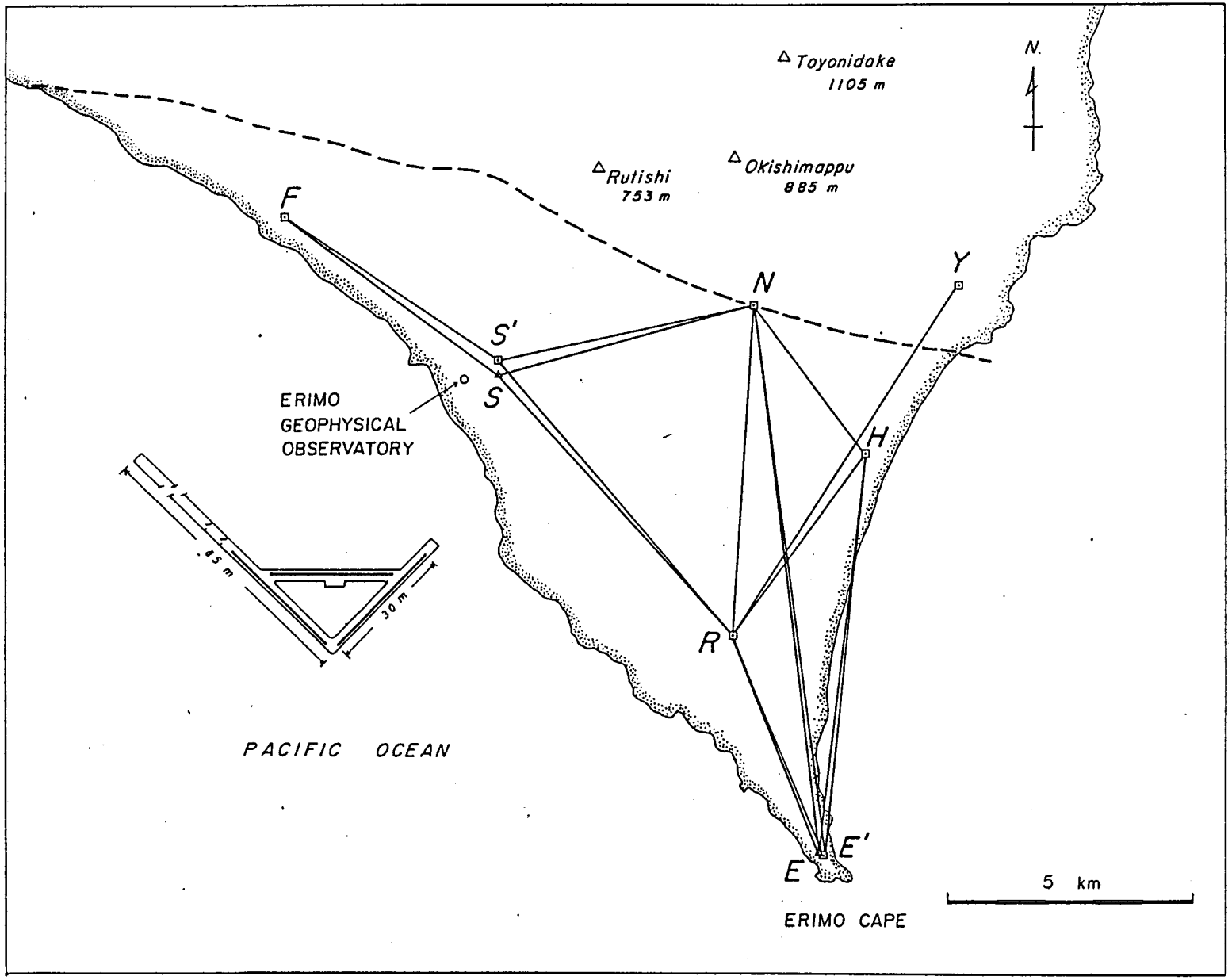
△Toyonidake
1105 m
N.
△Rutishi
753 m
△Okishimappu
885 m
F
N
Y
S'
S
ERIMO
GEOPHYSICAL
OBSERVATORY
H
85 m
30 m
R
PACIFIC OCEAN
E
E'
5 km
ERIMO CAPE

Fig.10

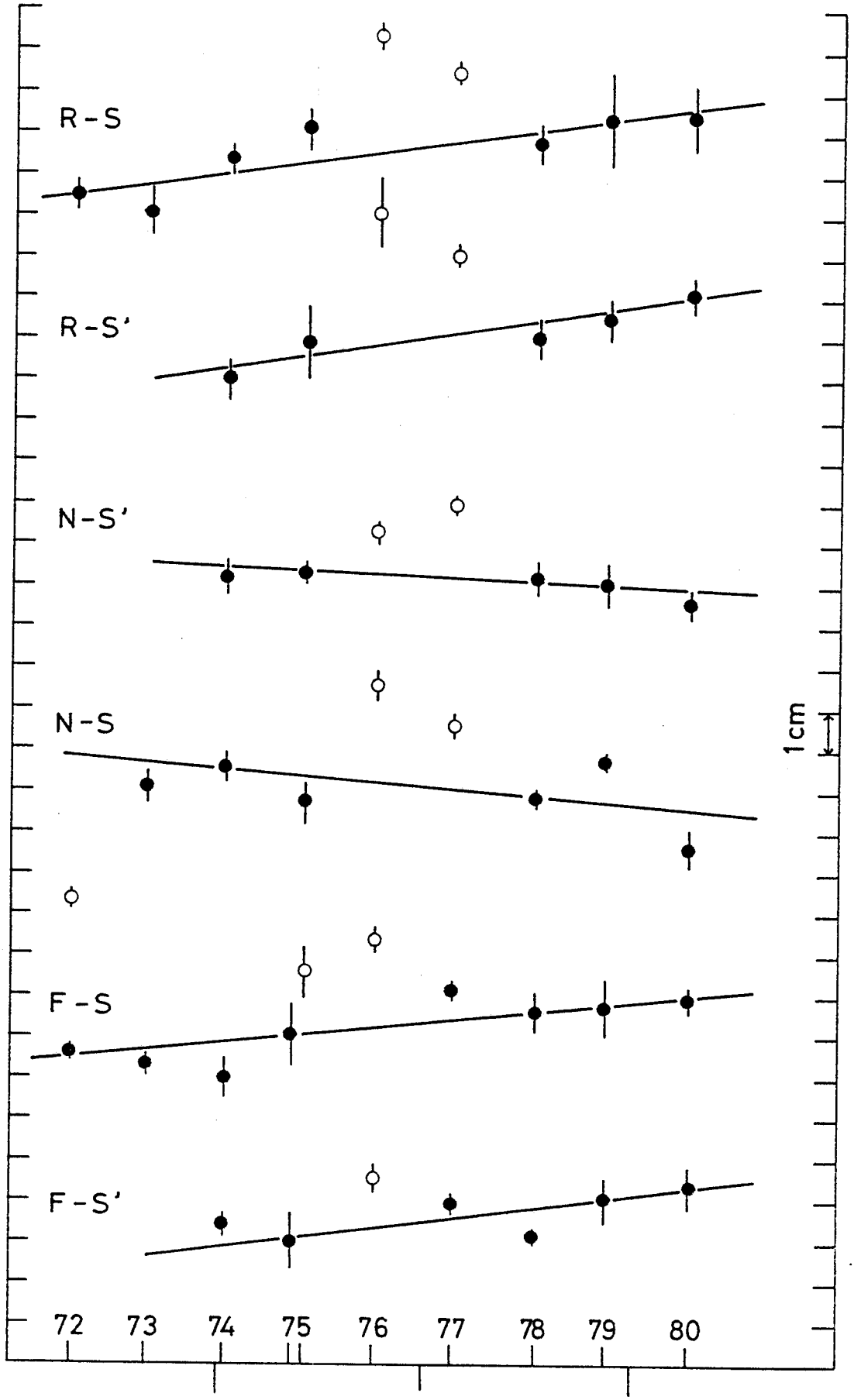

Fig.11

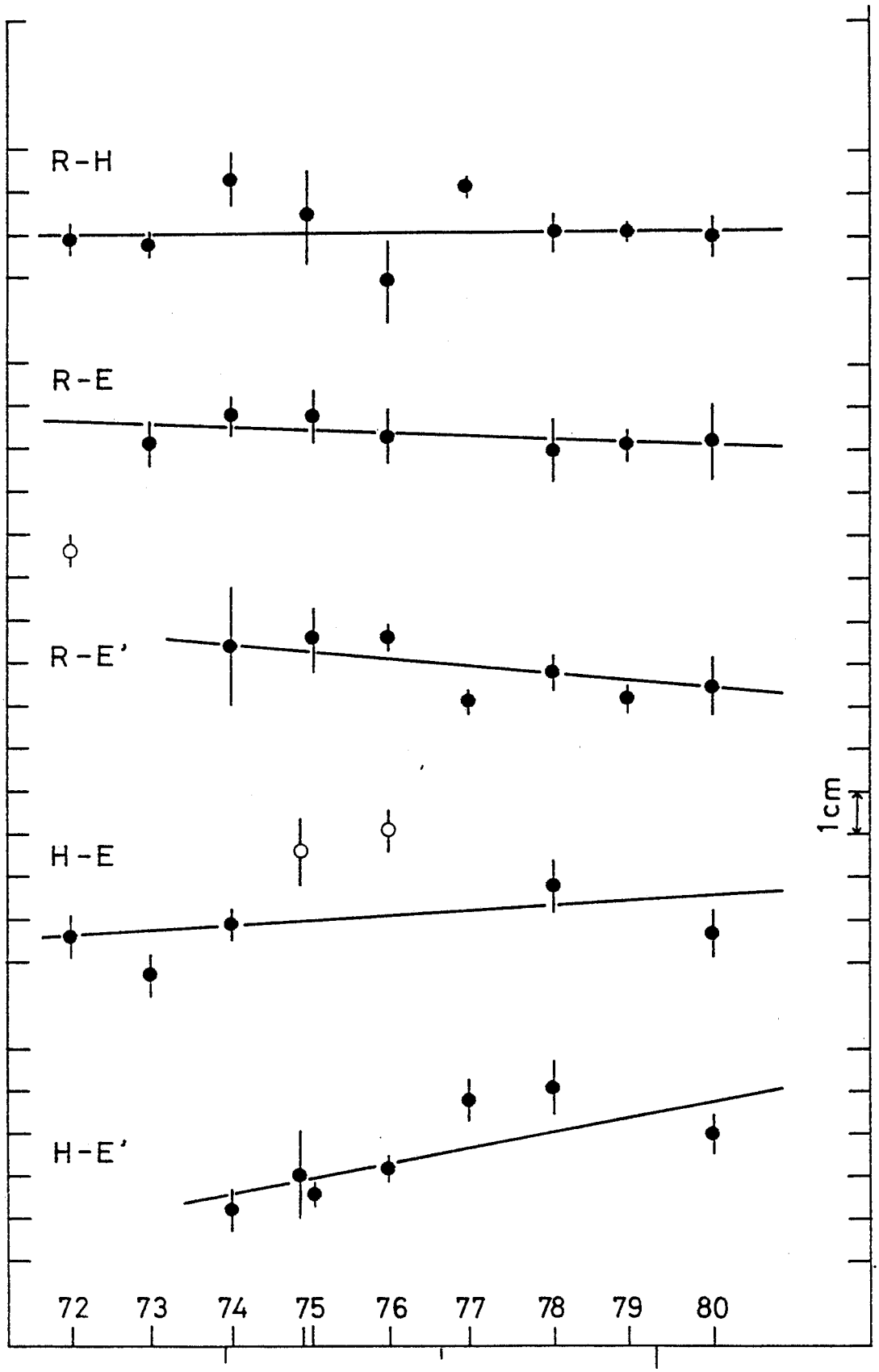

Fig.11. continued.

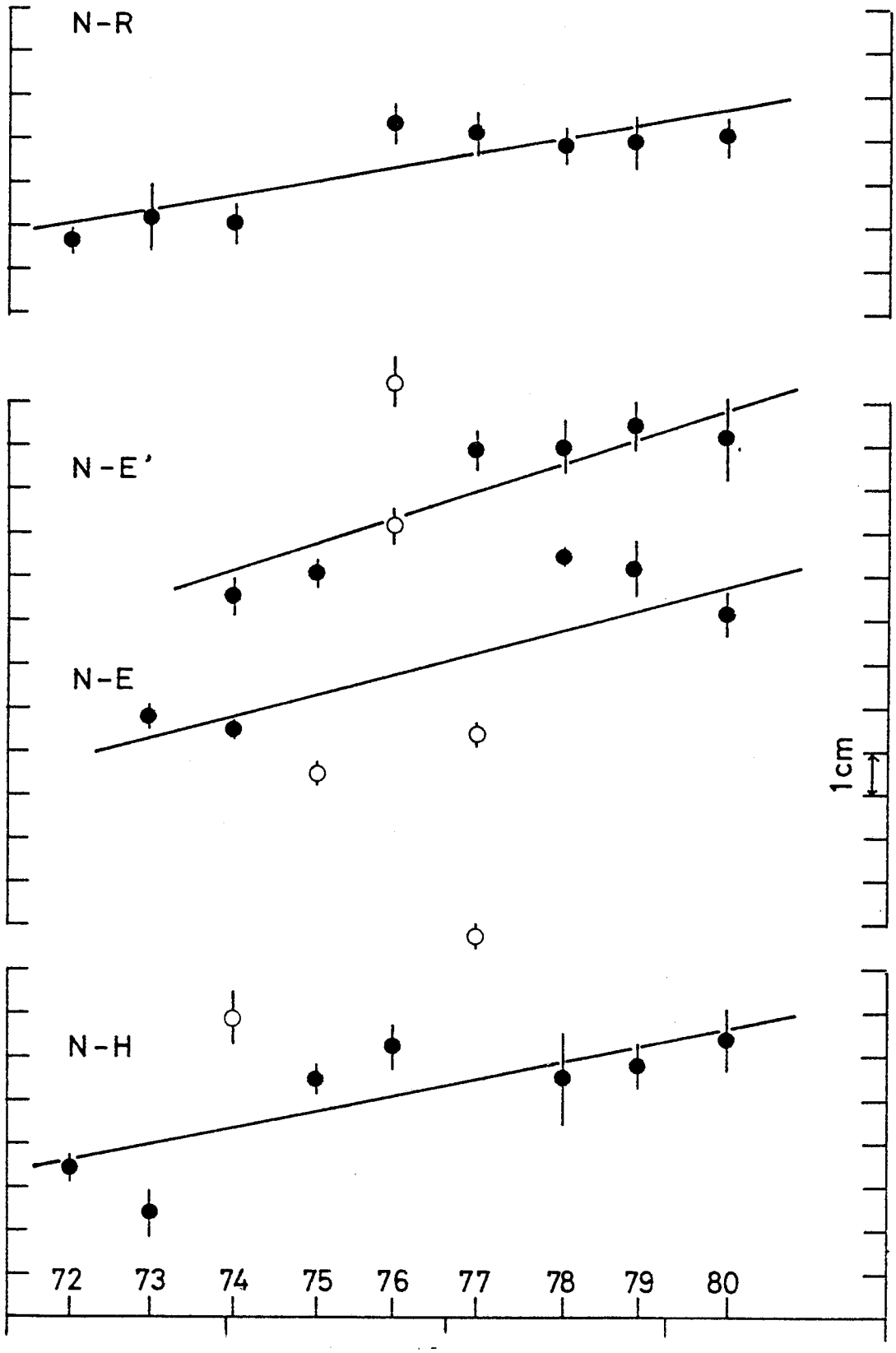

Fig.11 continued.

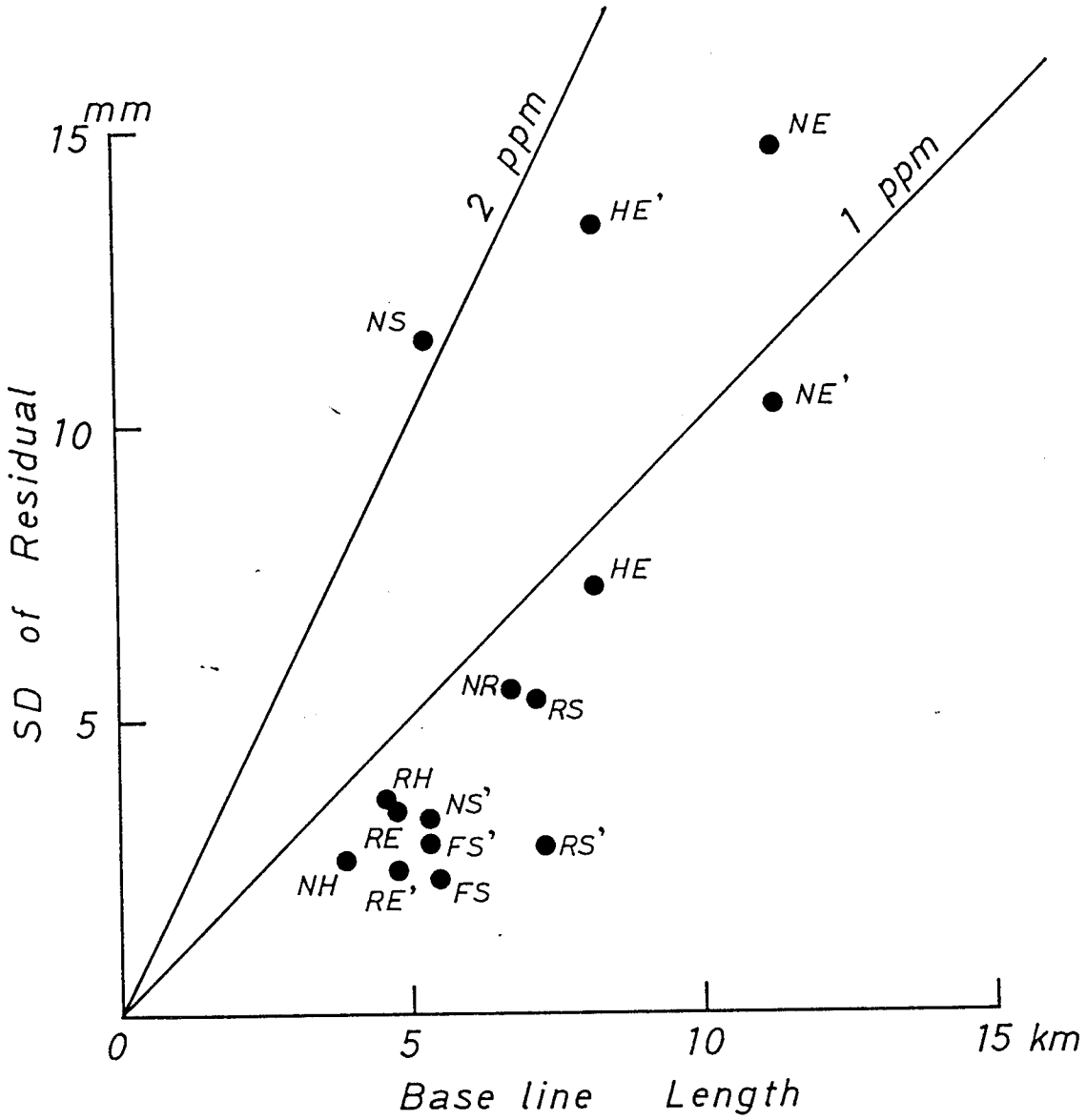
mm
15
10
5
SD of Residual
2 ppm
1 ppm
NE
HE'
NS
NE'
HE
NR
RS
RH
NS'
RE
FS'
RS'
NH
RE'
FS
0
5
10
15 km
Base line Length

Fig.12

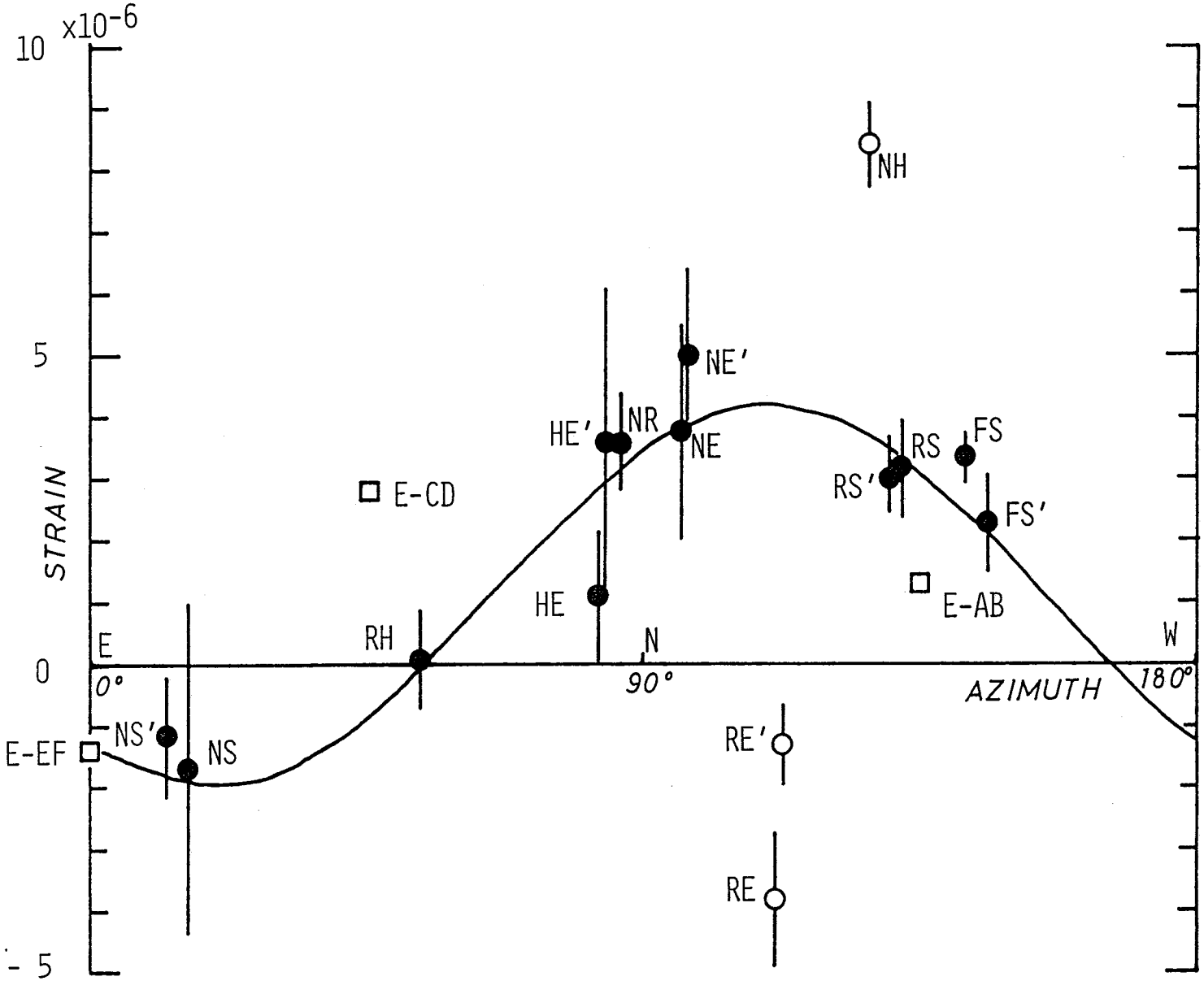
10
x10-6
5
0
- 5
STRAIN
E
0°
N
90°
W
180°
AZIMUTH
NH
NE'
HE'
NR
NE
E-CD
RS
FS
RS'
FS'
HE
E-AB
RH
RE'
RE
E-EF
NS'
NS

Fig.13

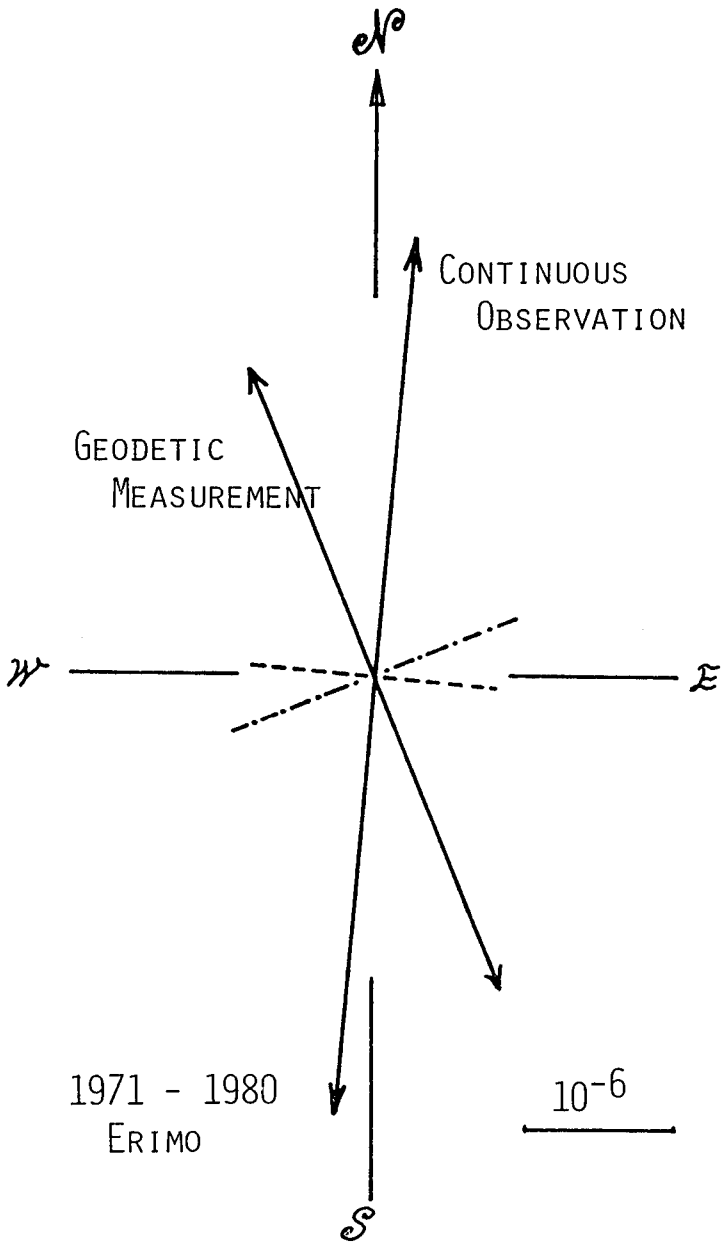
N
CONTINUOUS
OBSERVATION
GEODETIC
MEASUREMENT
W
E
1971 - 1980
ERIMO
10^{-6}
S

Fig.14

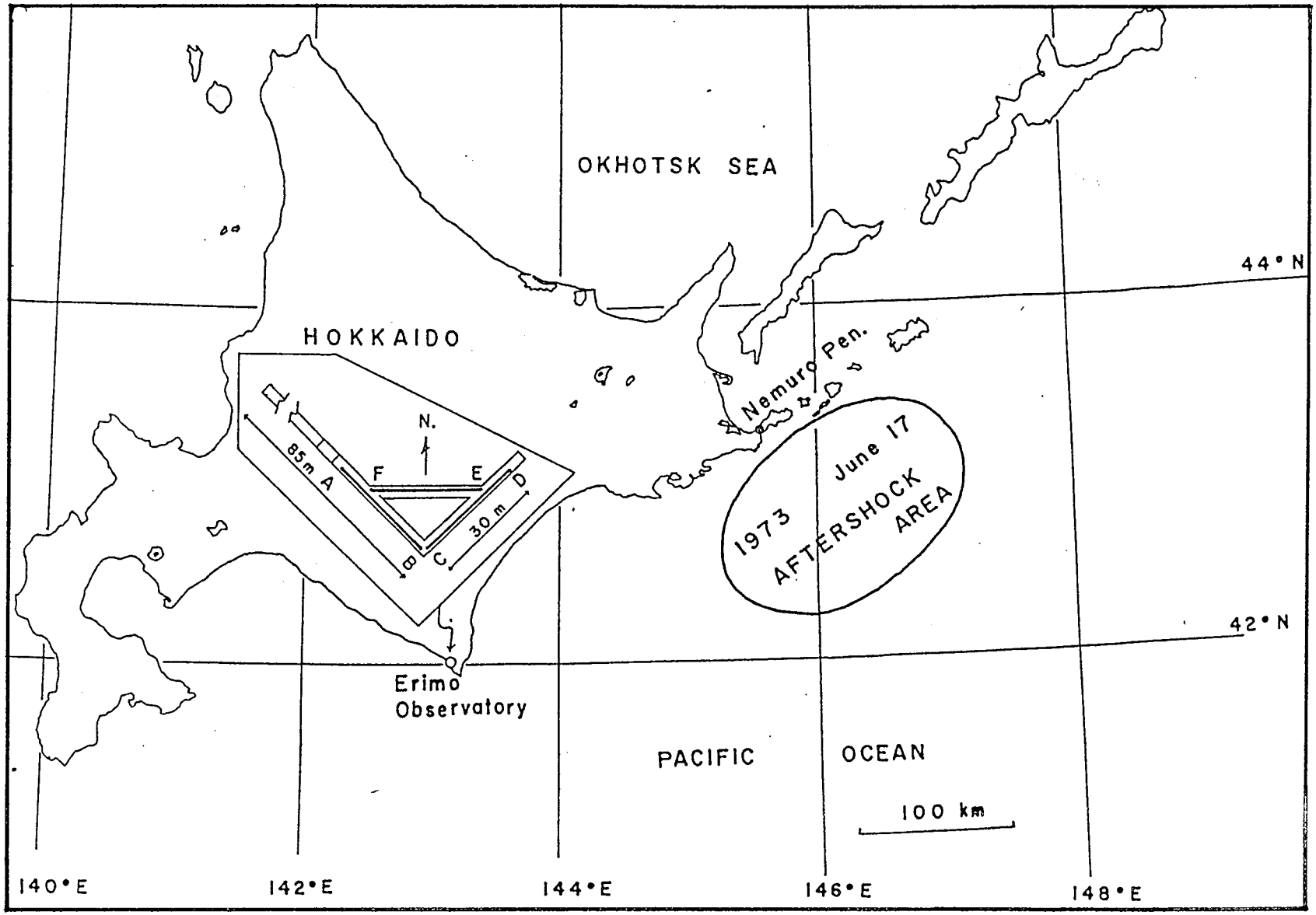
OKHOTSK SEA
HOKKAIDO
Nemuro Pen.
N.
85m
A
F
E
D
30m
B
C
1973
June 17
AFTERSHOCK
AREA
Erimo
Observatory
PACIFIC
OCEAN
100 km
44°N
42°N
140°E
142°E
144°E
146°E
148°E

Fig.15

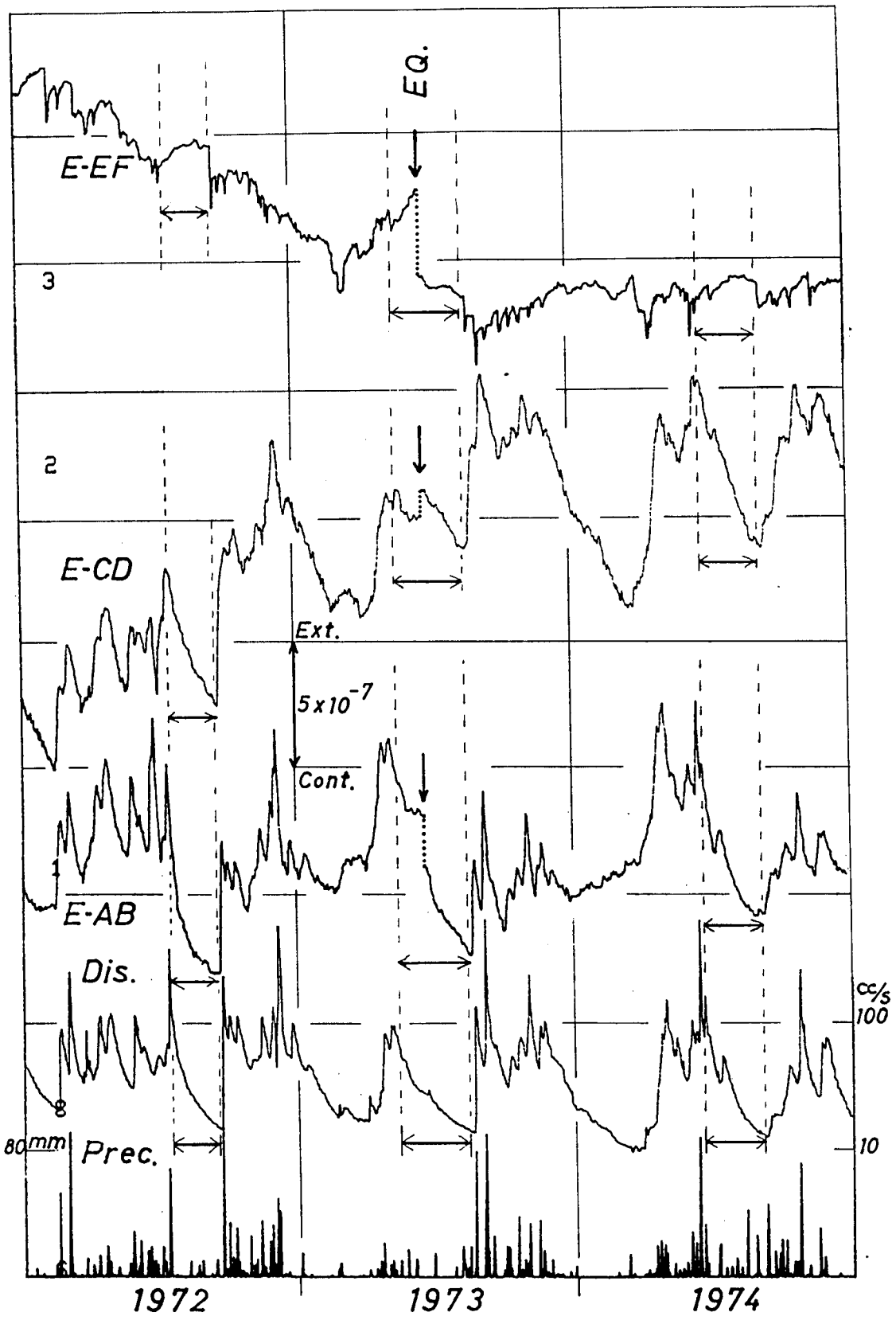
EQ.
E-EF
3
2
E-CD
Ext.
5x10⁻⁷
Cont.
1
E-AB
Dis.
cc/s
100
8
80mm
Prec.
10
1972
1973
1974

Fig.16

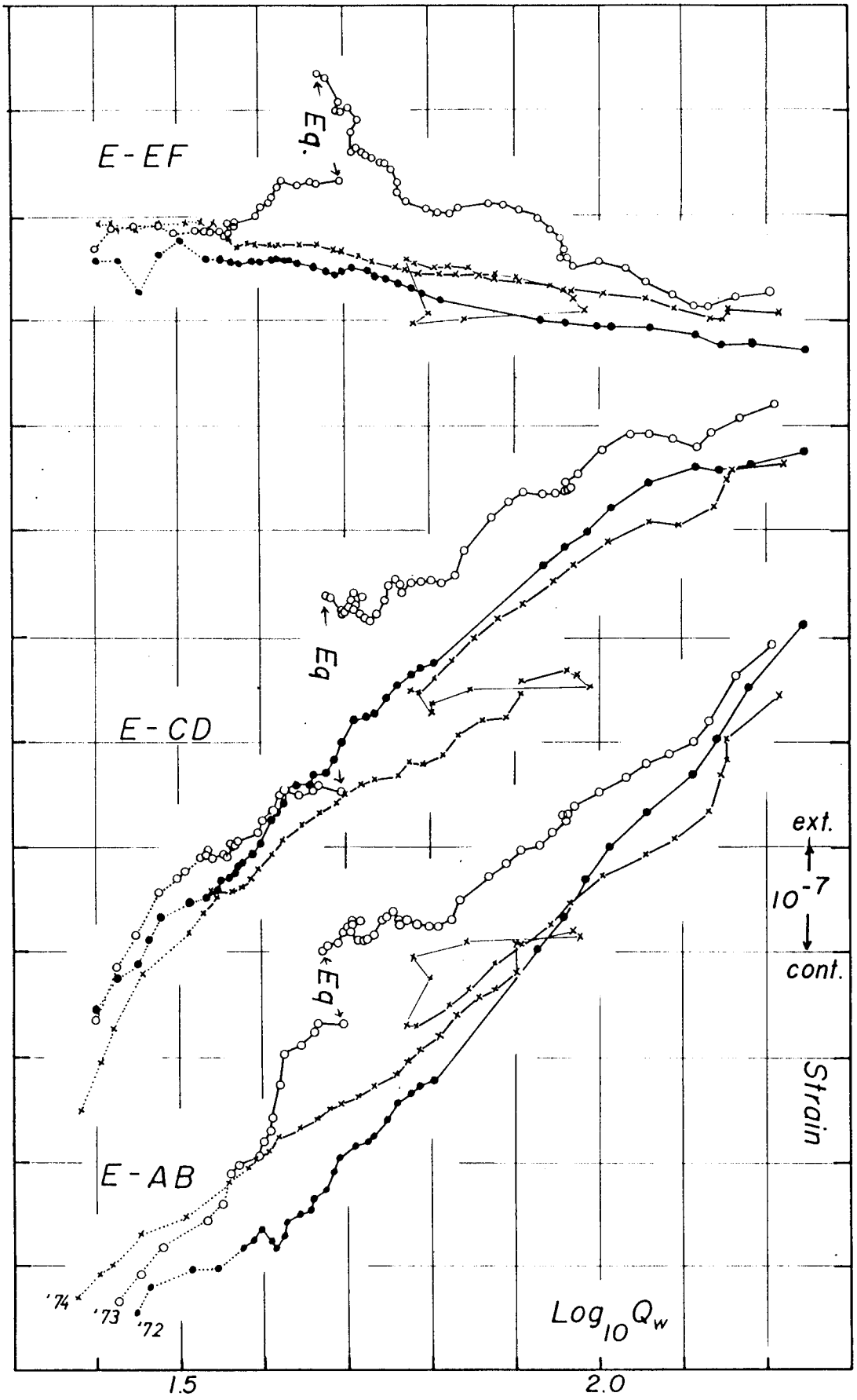

Fig.17

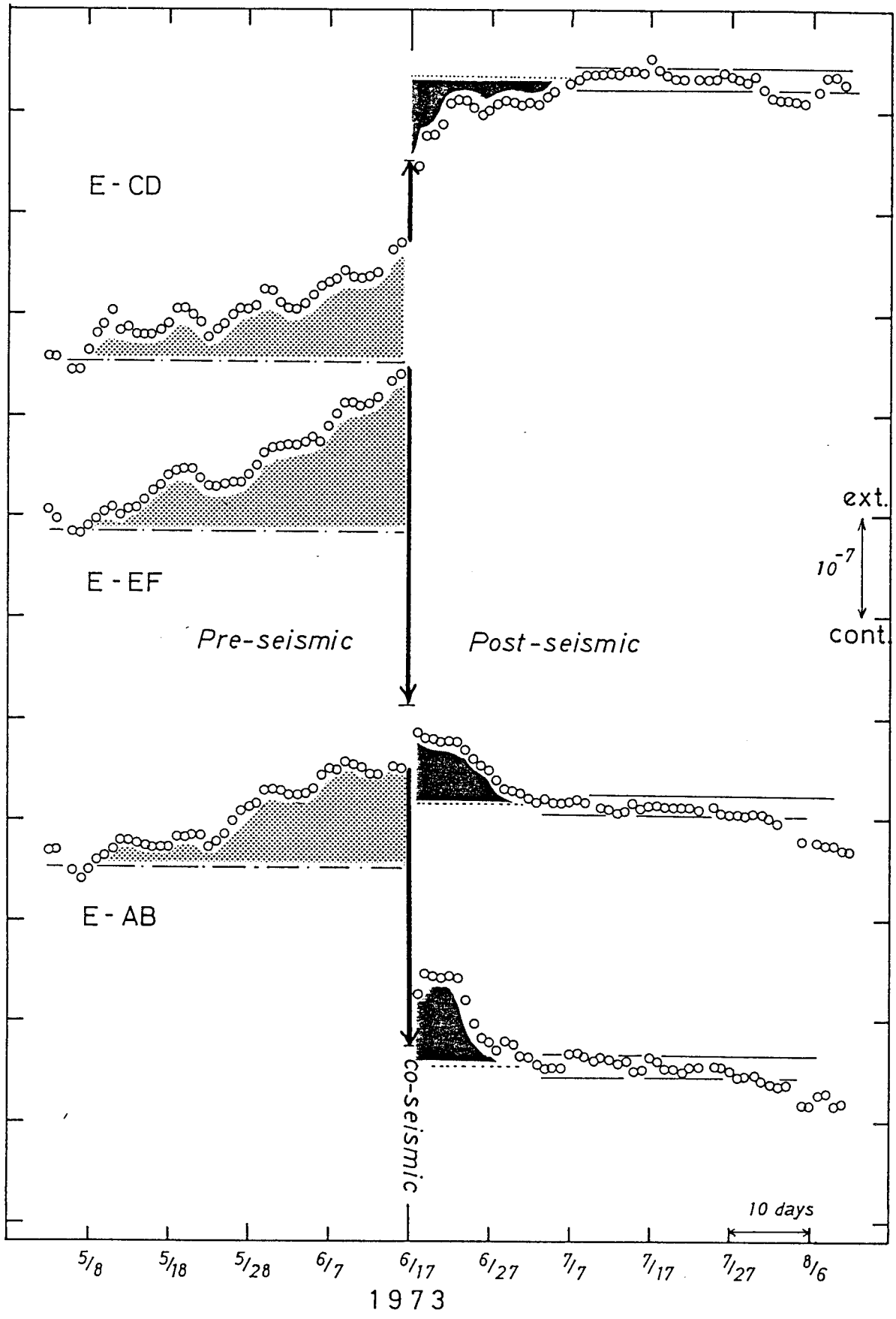
E - CD
E - EF
E - AB
Pre-seismic
Post-seismic
co-seismic
ext.
10^{-7}
cont.
10 days
5/8
5/18
5/28
6/7
6/17
6/27
7/7
7/17
7/27
8/6
1973

Fig.18

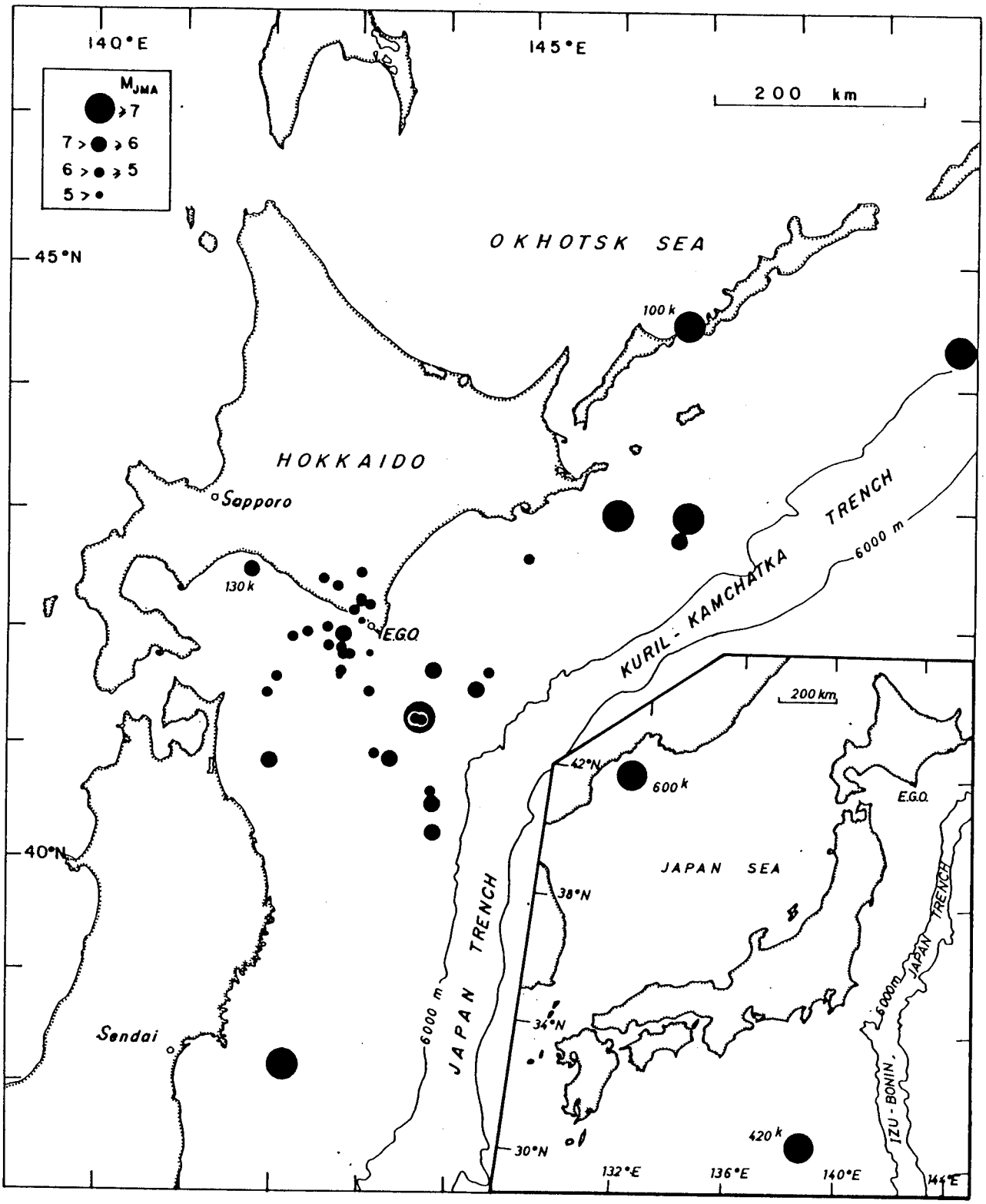
140°E
145°E
200 km
M_{JMA}
≥7
7 > ● ≥6
6 > ● ≥5
5 > ●
45°N
OKHOTSK SEA
100 k
HOKKAIDO
Sapporo
130 k
E.G.Q.
KURIL - KAMCHATKA TRENCH
6000 m
200 km
42°N
600 k
E.G.Q.
40°N
JAPAN SEA
38°N
JAPAN TRENCH
6000 m
Sendai
34°N
6000m JAPAN TRENCH
IZU - BONIN
420 k
30°N
132°E
136°E
140°E
144°E

Fig.19

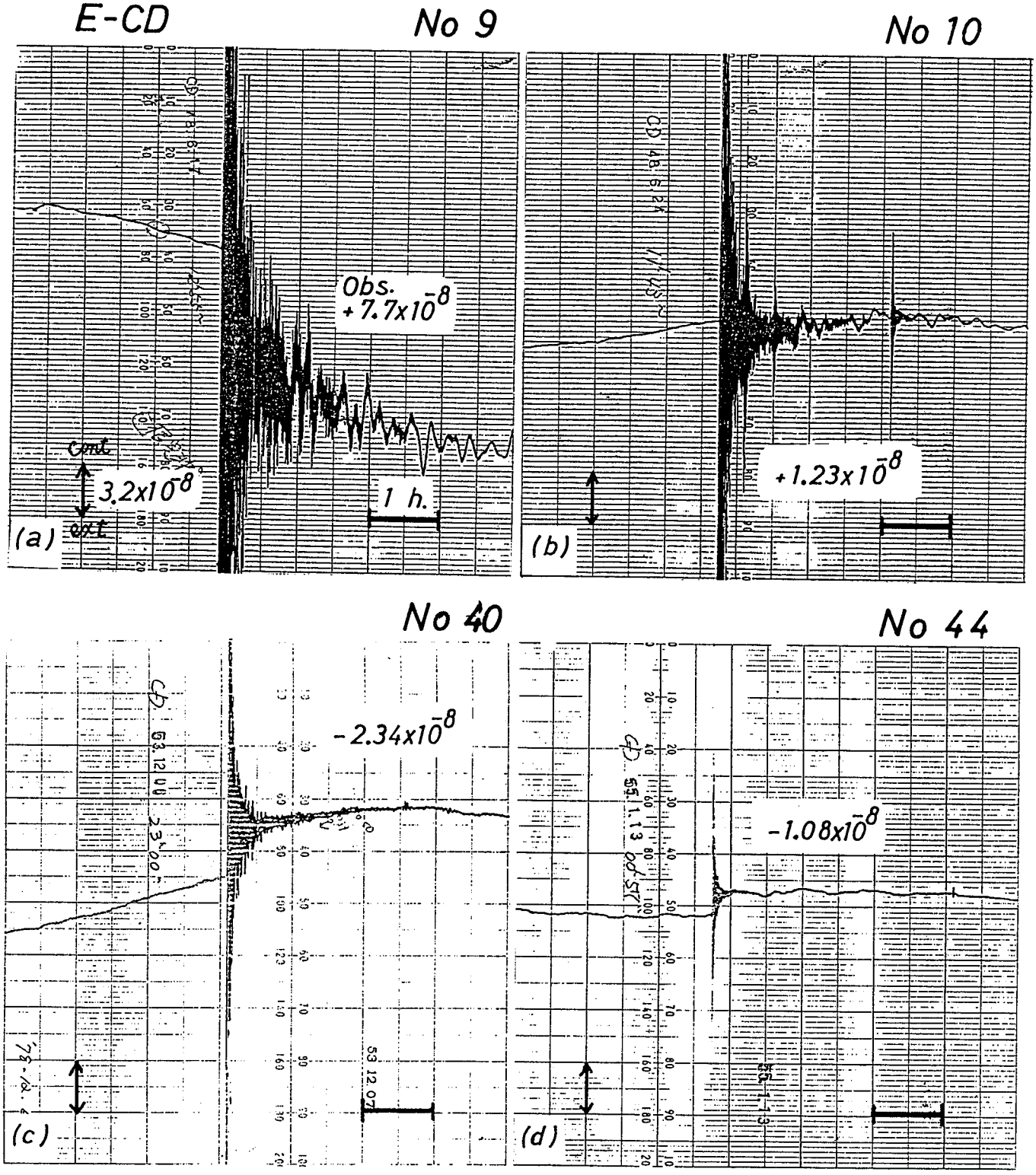
E-CD
No 9
No 10
Obs.
+7.7x10⁻⁸
cmt
3.2x10⁻⁸
ext
1 h.
(a)
+1.23x10⁻⁸
(b)
No 40
No 44
-2.34x10⁻⁸
(c)
-1.08x10⁻⁸
(d)

Fig.20

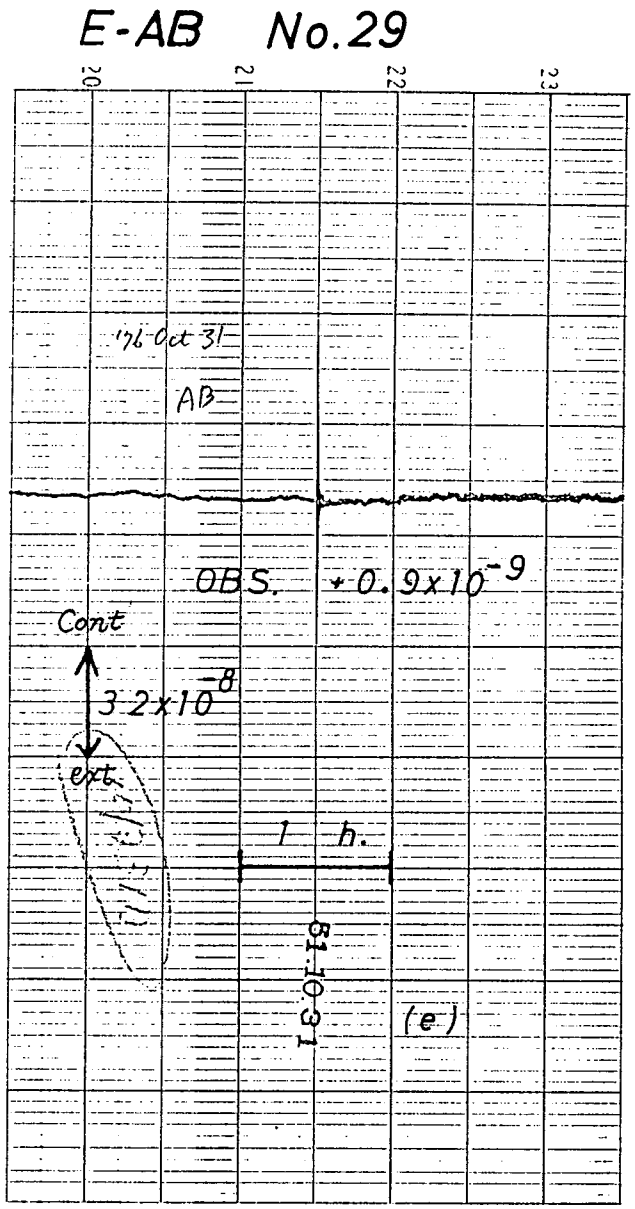

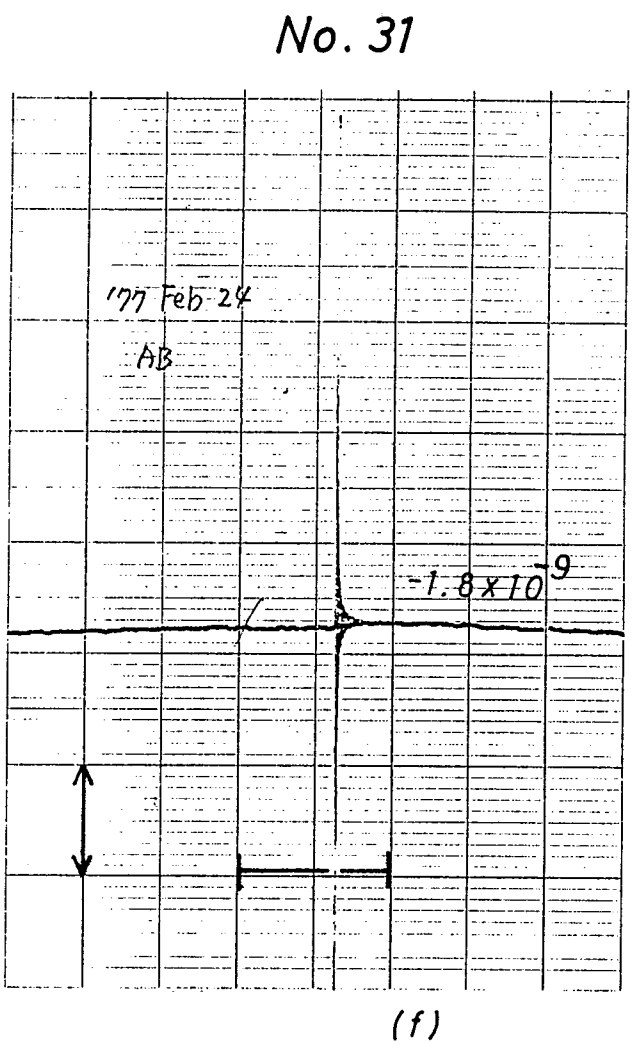

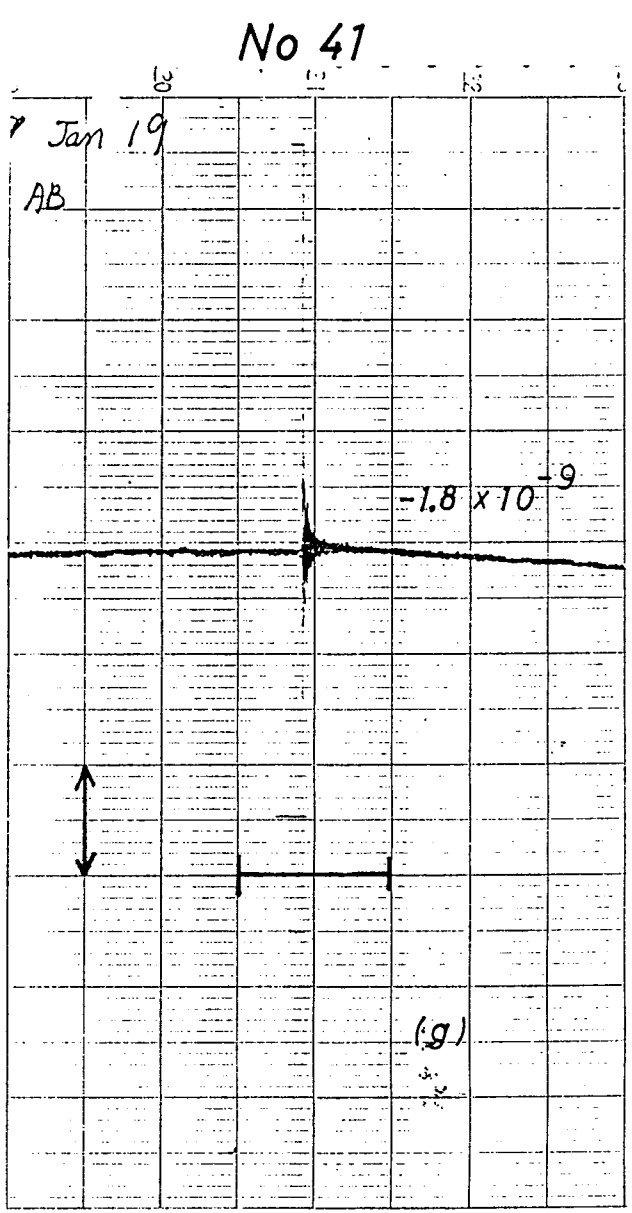

Fig.20 continued.

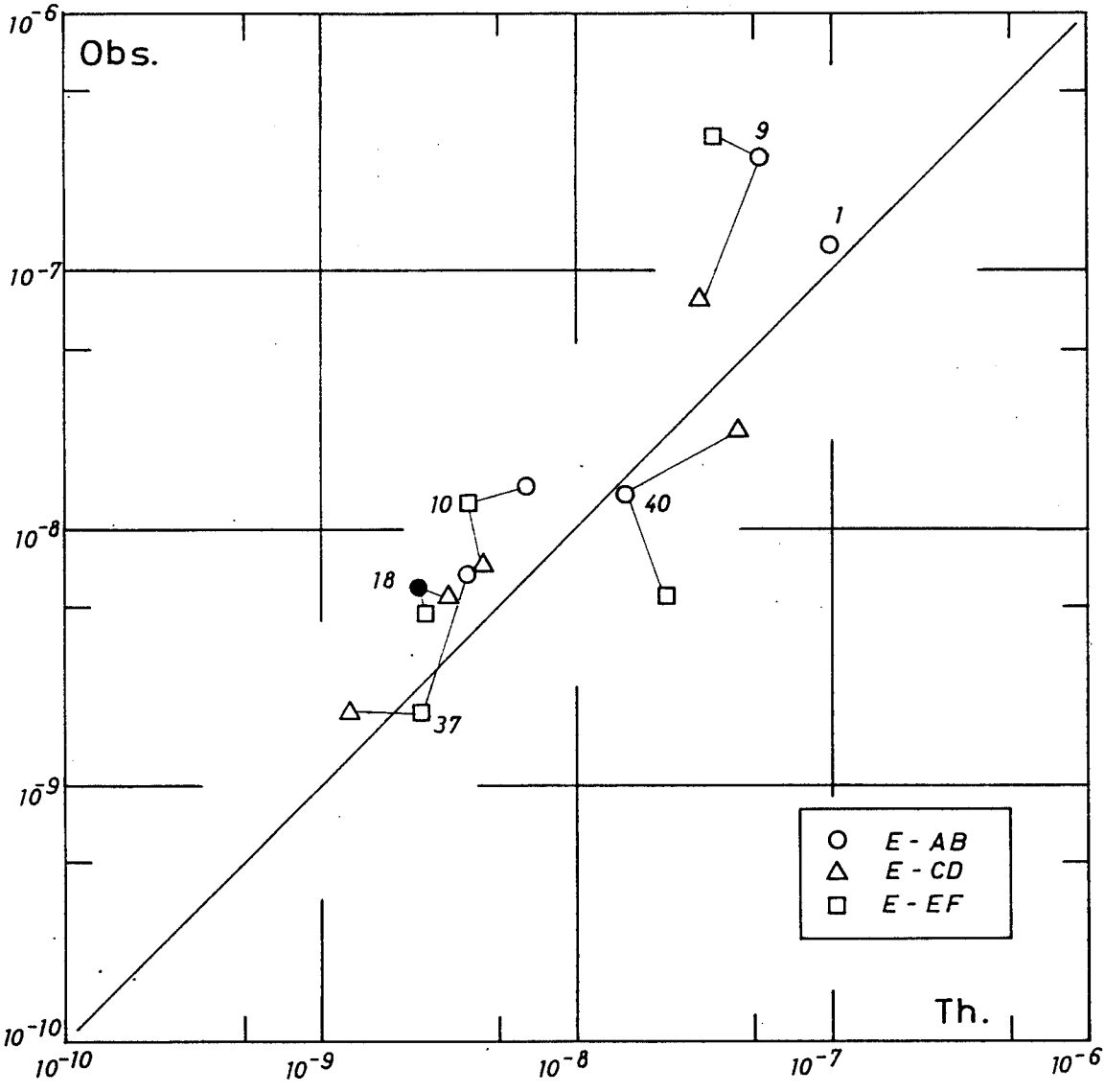

Fig.21

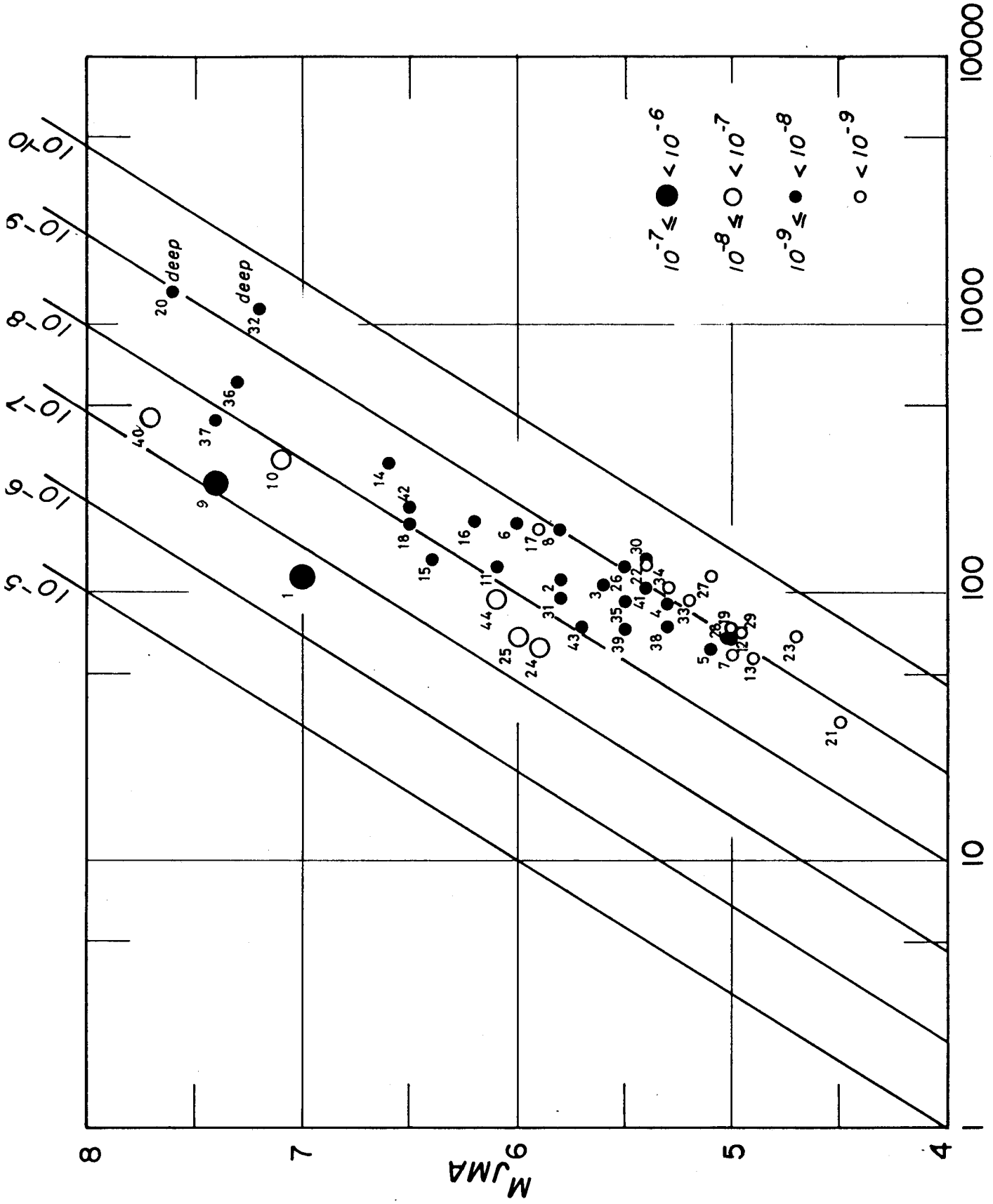
$10^{-7} \leq \bullet < 10^{-6}$
$10^{-8} \leq \circ < 10^{-7}$
$10^{-9} \leq \bullet < 10^{-8}$
$\circ < 10^{-9}$
deep
deep
M_{JMA}
R. km
10000
1000
100
10
1
8
7
9
5
4

Fig.22

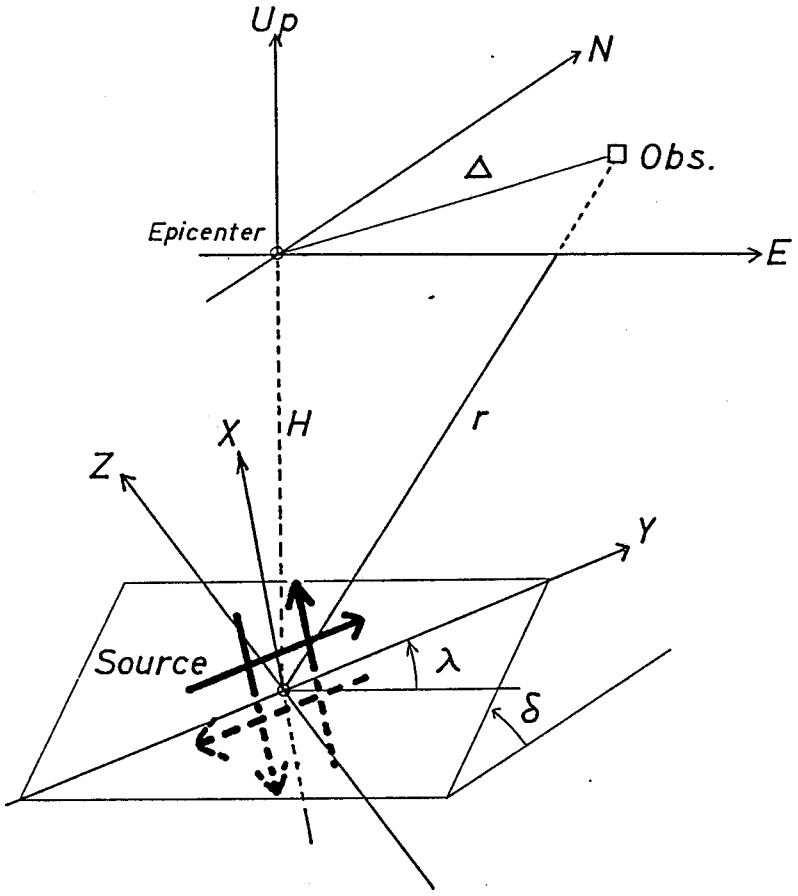

Fig.23

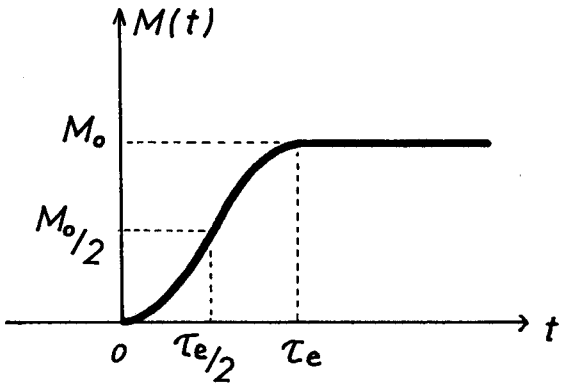

Fig.24

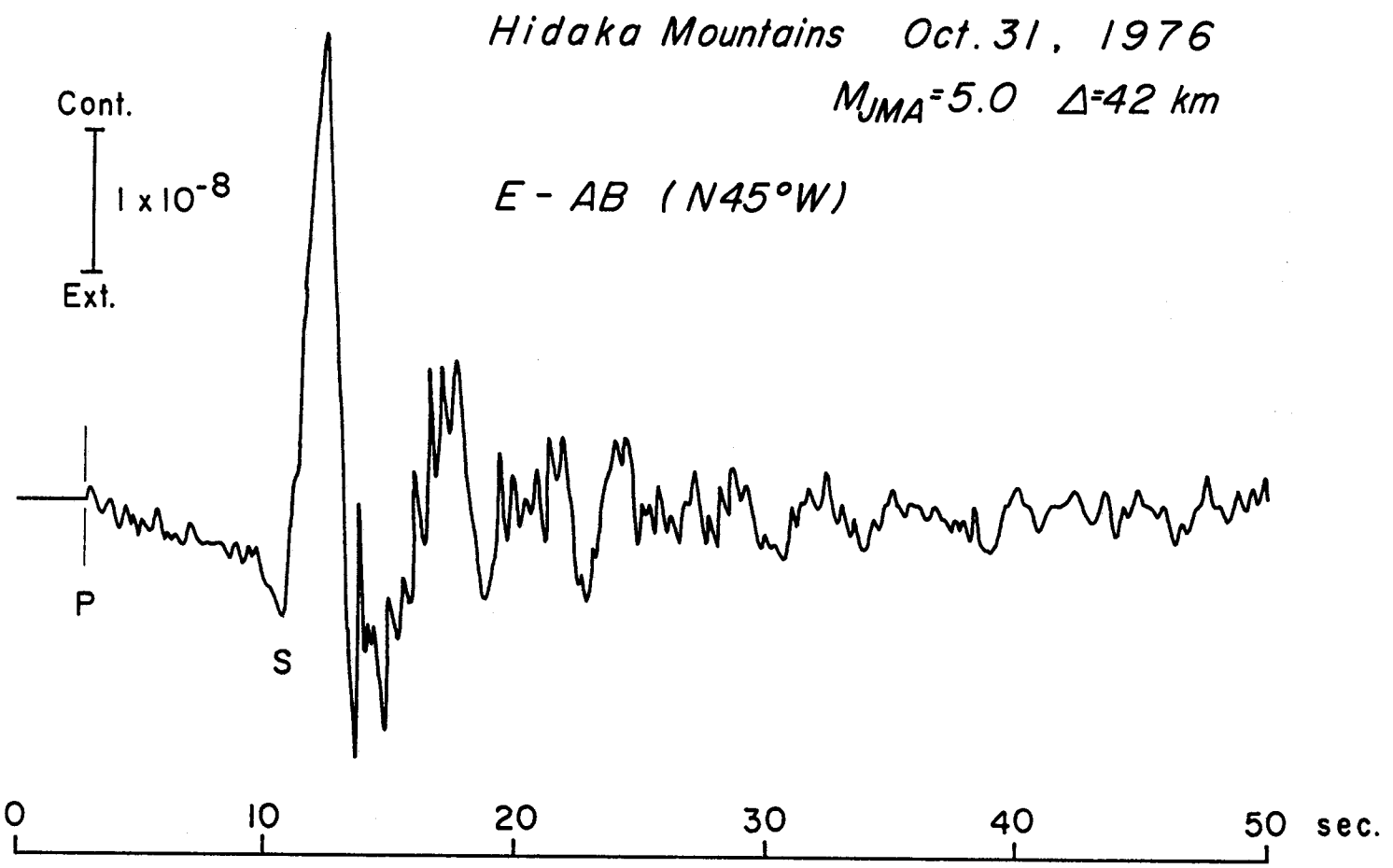
Hidaka Mountains Oct. 31, 1976
M_{JMA}=5.0 Δ=42 km
E - AB (N45°W)
Cont.
1 x 10^{-8}
Ext.
P
S
0
10
20
30
40
50 sec.

Fig.25

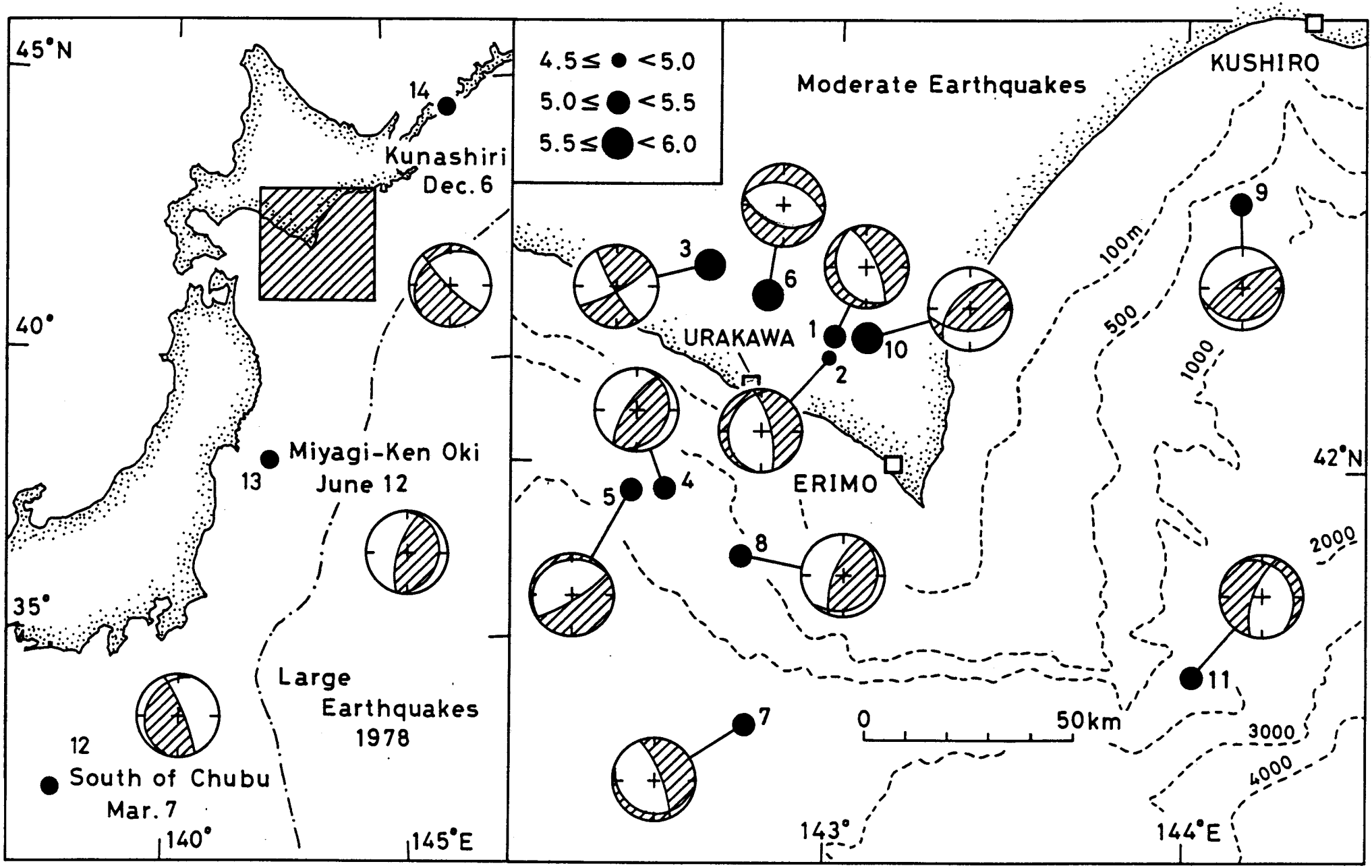
45°N
40°
35°
140°
145°E
143°
144°E
42°N
4.5≤ ● <5.0
5.0≤ ● <5.5
5.5≤ ● <6.0
Moderate Earthquakes
KUSHIRO
URAKAWA
ERIMO
Kunashiri
Dec. 6
Miyagi-Ken Oki
June 12
South of Chubu
Mar. 7
Large
Earthquakes
1978
100m
500
1000
2000
3000
4000
0
50km
1
2
3
4
5
6
7
8
9
10
11
12
13
14

Fig.26

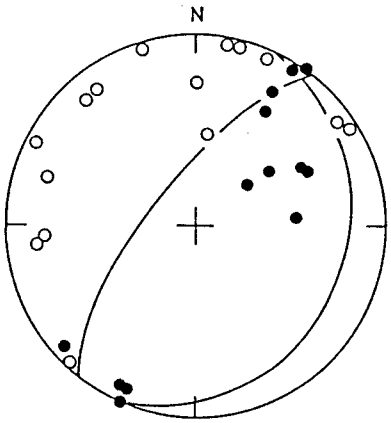

4. May 6, 1977

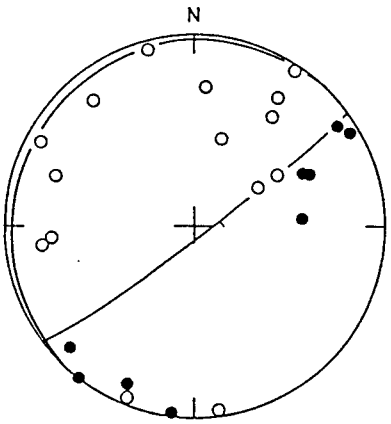

5. Nov. 17, 1977

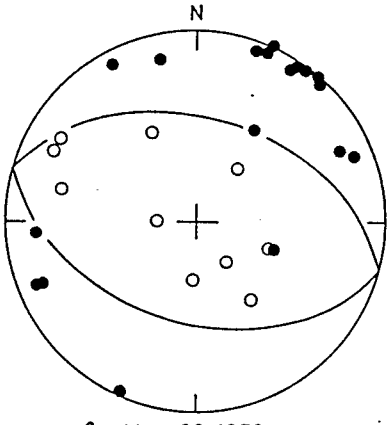

6. Mar. 20, 1978

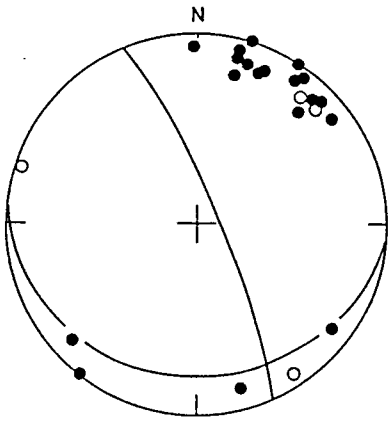

7. Apr. 6, 1978

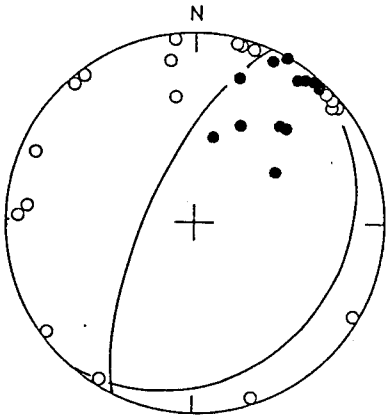

8. July 16, 1978

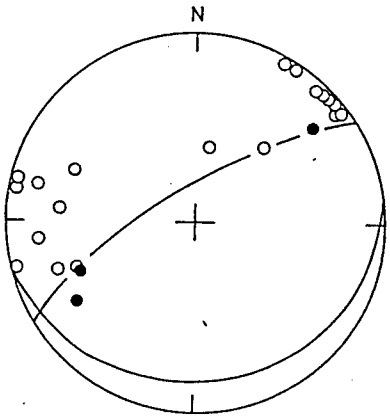

9. Oct. 29, 1978

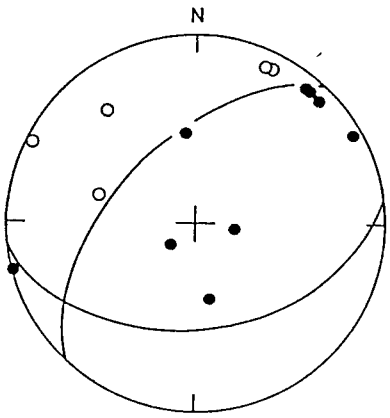

10. Nov. 7, 1978

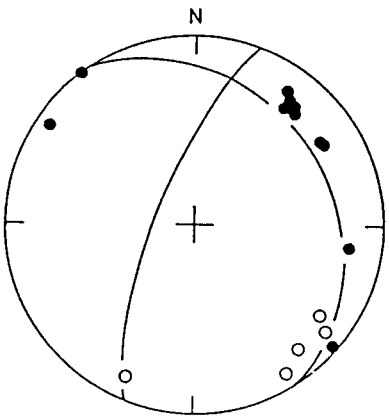

11. Jan. 19, 1979

Fig. 27

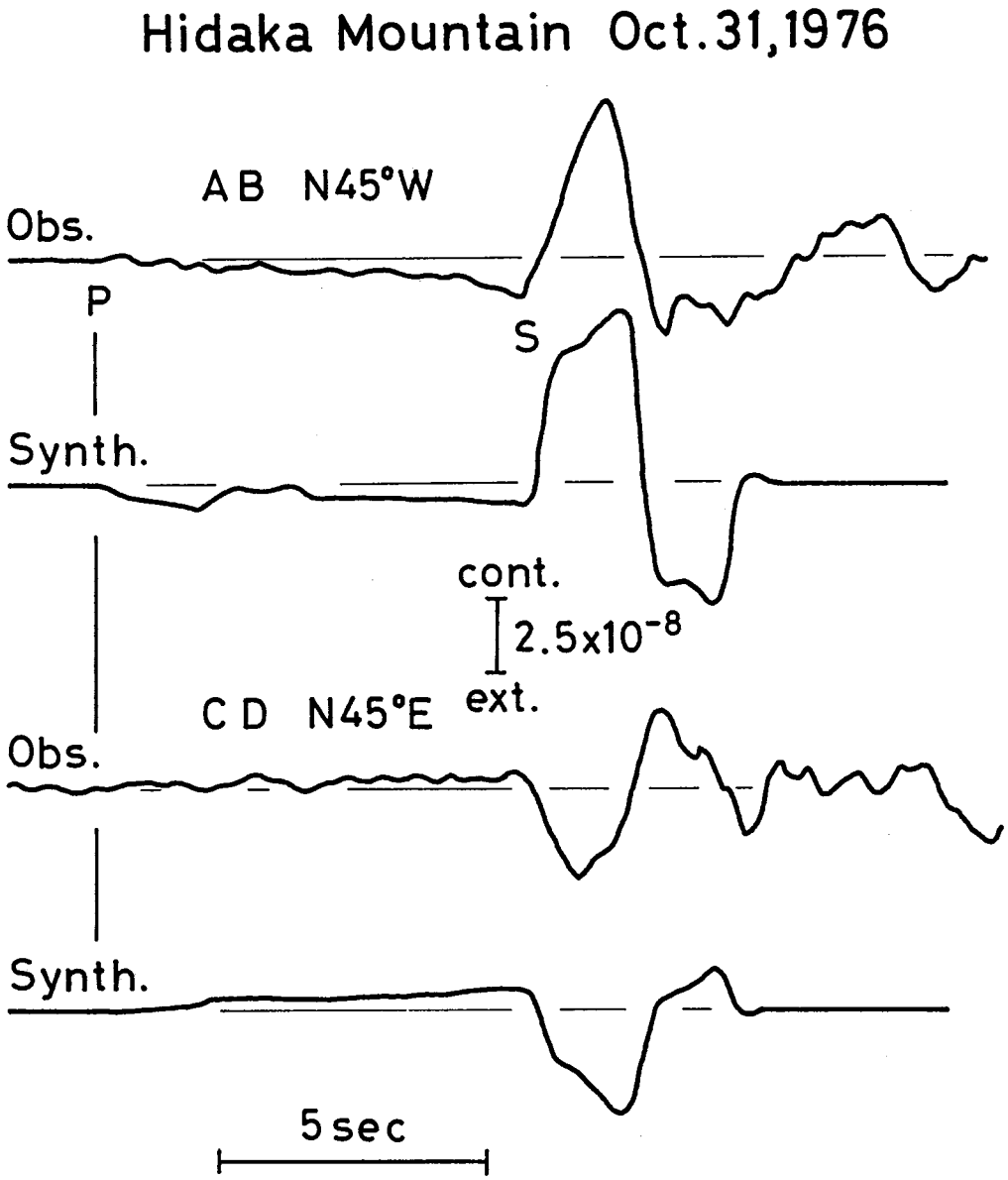
Hidaka Mountain Oct.31,1976
AB N45°W
Obs.
P
S
Synth.
cont.
2.5x10⁻⁸
ext.
CD N45°E
Obs.
Synth.
5 sec

Fig.28

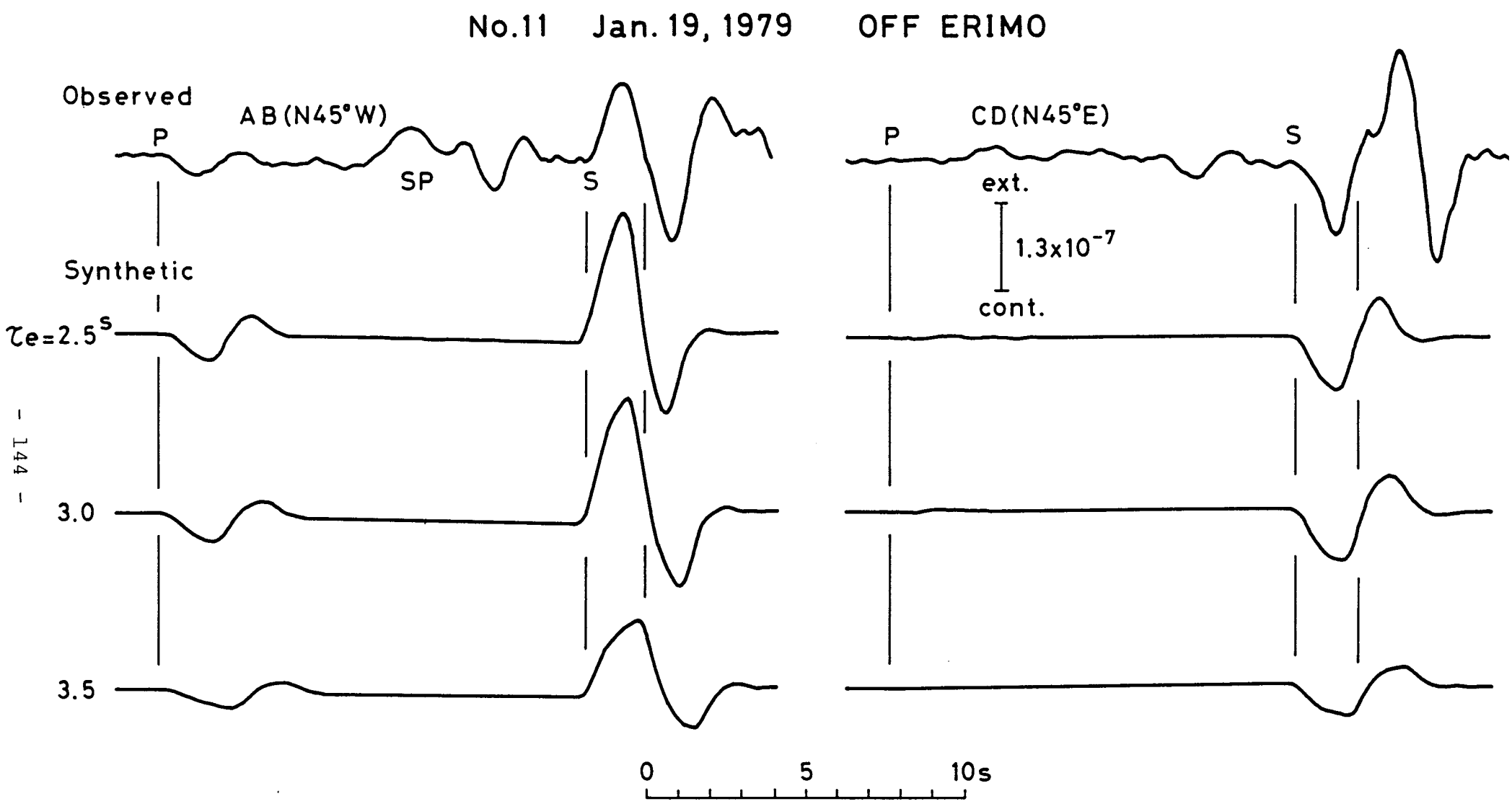
No.11 Jan. 19, 1979 OFF ERIMO
Observed
AB(N45°W)
P
SP
S
CD(N45°E)
P
S
ext.
1.3x10⁻⁷
cont.
Synthetic
τe=2.5s
3.0
3.5
0
5
10s

Fig.29

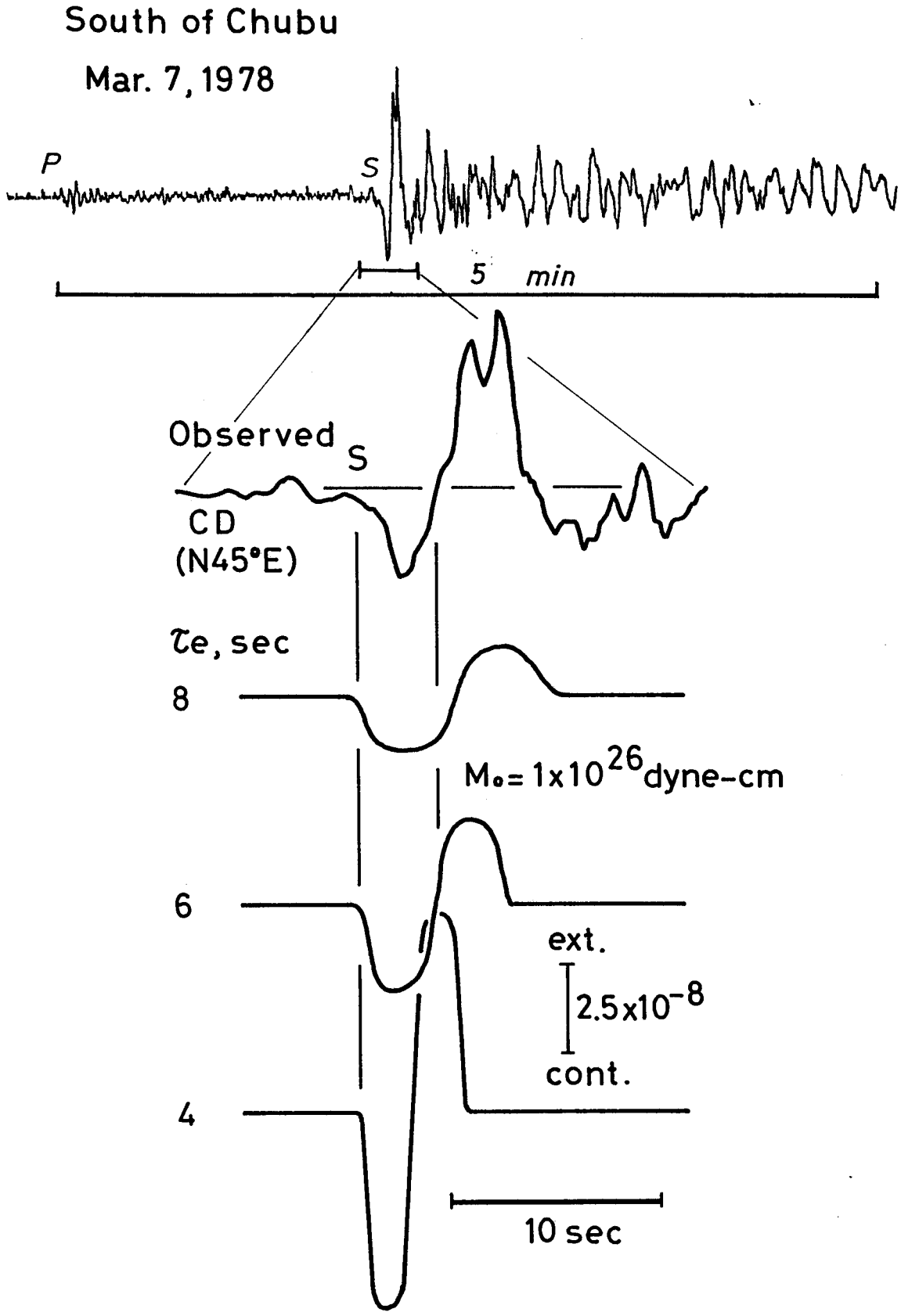
South of Chubu
Mar. 7, 1978
P
S
5 min
Observed
S
CD
(N45°E)
τe, sec
8
Mo= 1x10^26 dyne-cm
6
ext.
2.5x10^-8
cont.
4
10 sec

Fig.30

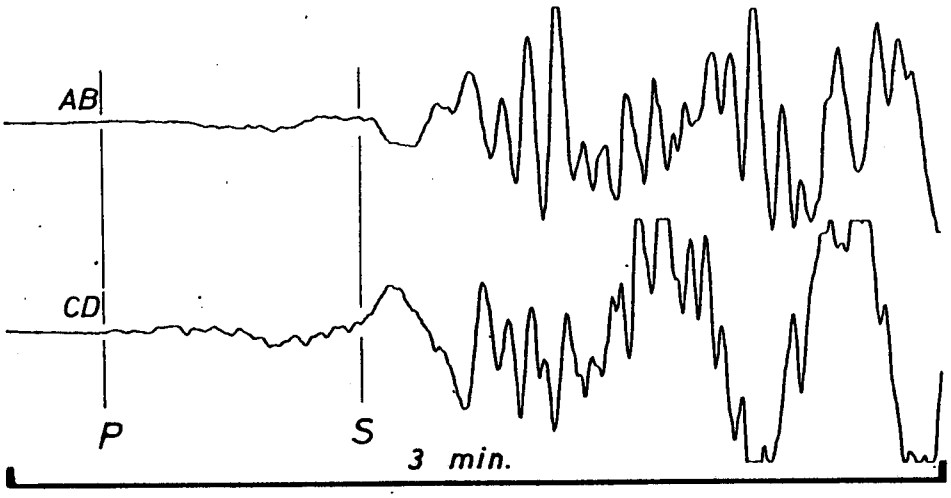

Miyagi-Ken Oki June 12,1978

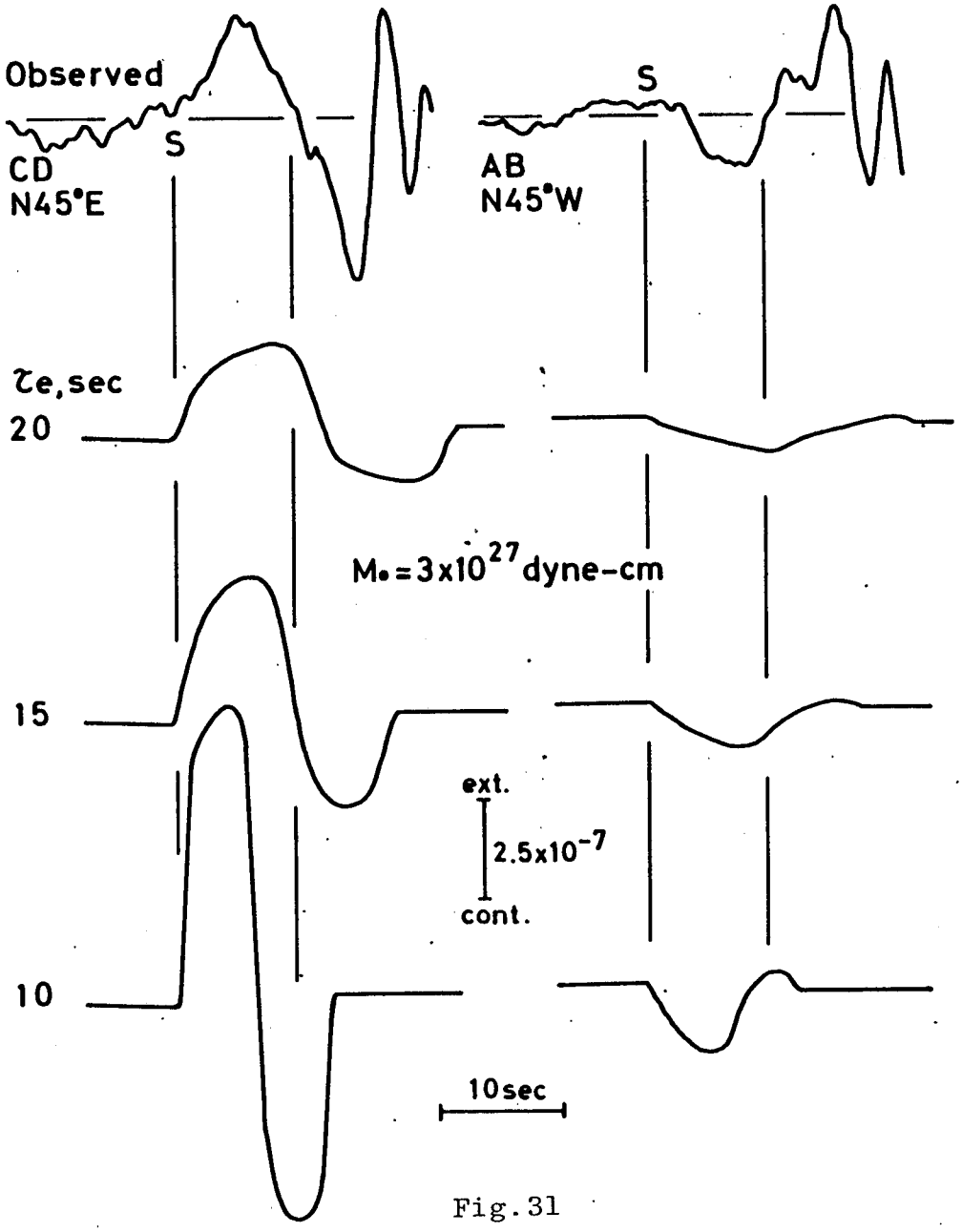

Fig.31

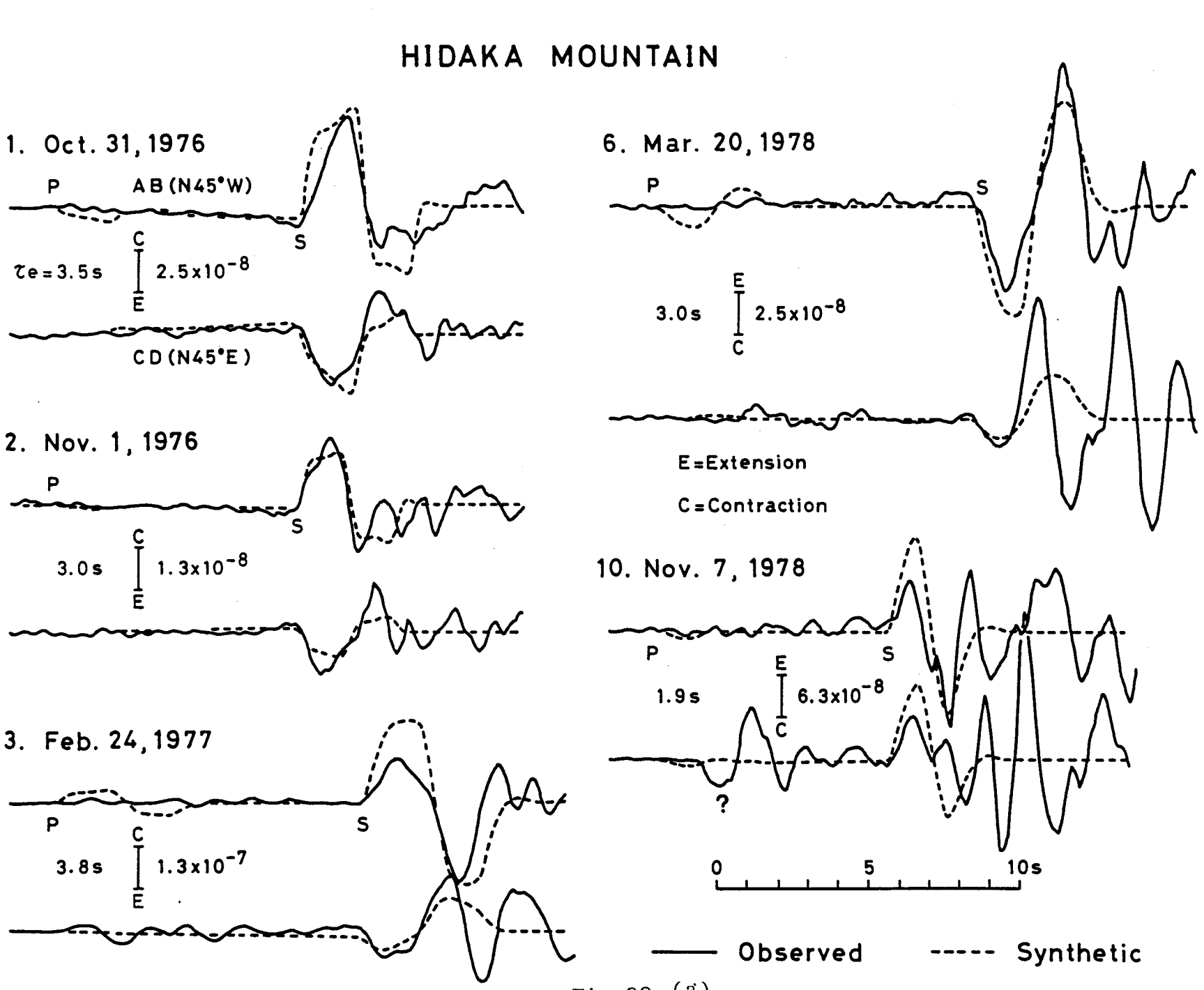
HIDAKA MOUNTAIN
1. Oct. 31, 1976
P
AB (N45°W)
S
C
τe=3.5s
2.5x10⁻⁸
E
CD (N45°E)
2. Nov. 1, 1976
P
S
C
3.0s
1.3x10⁻⁸
E
3. Feb. 24, 1977
P
S
C
3.8s
1.3x10⁻⁷
E
6. Mar. 20, 1978
P
S
E
3.0s
2.5x10⁻⁸
C
E=Extension
C=Contraction
10. Nov. 7, 1978
P
S
E
1.9s
6.3x10⁻⁸
C
?
0
5
10s
Observed
Synthetic

Fig.32 (a)

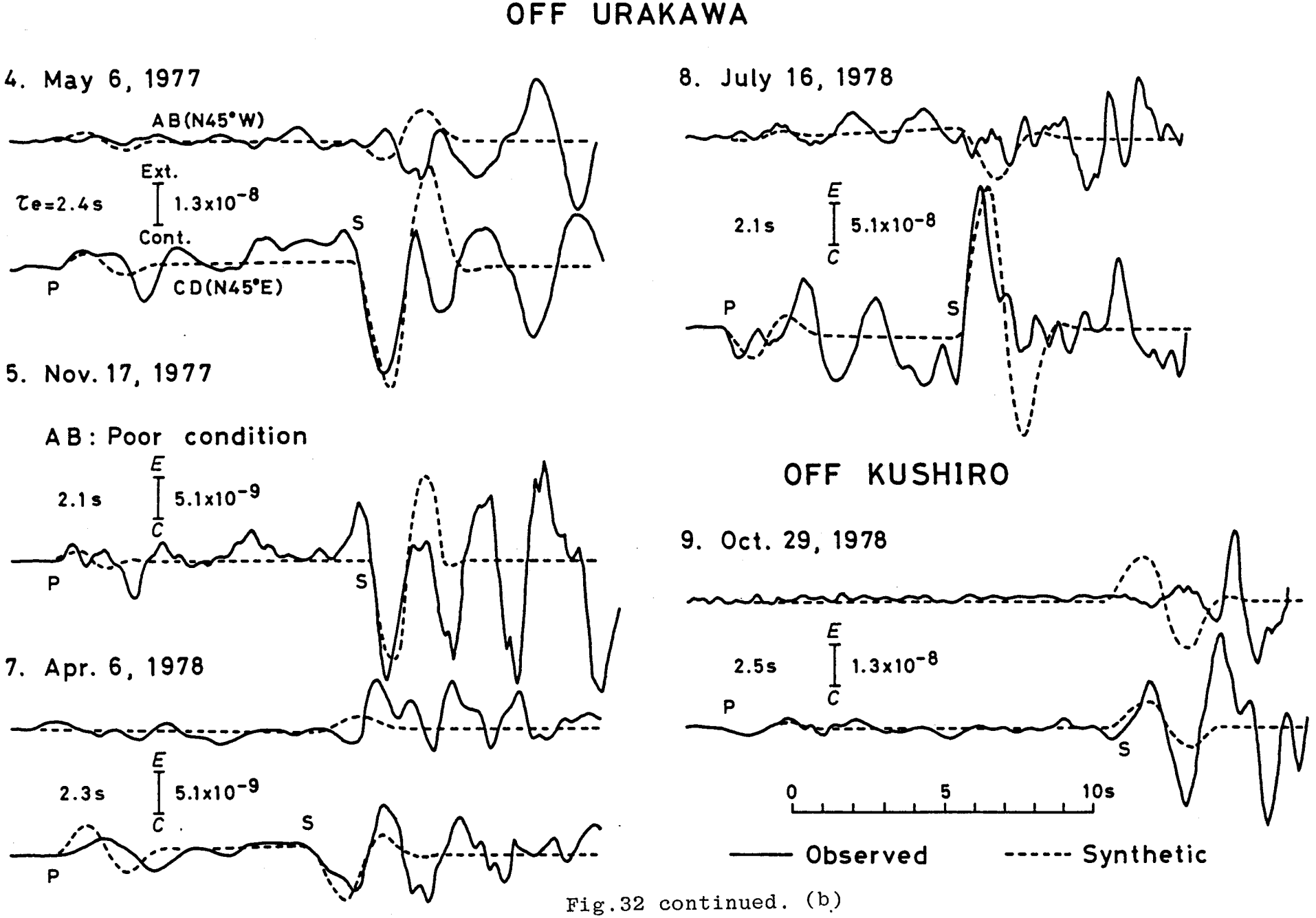

Fig.32 continued. (b)

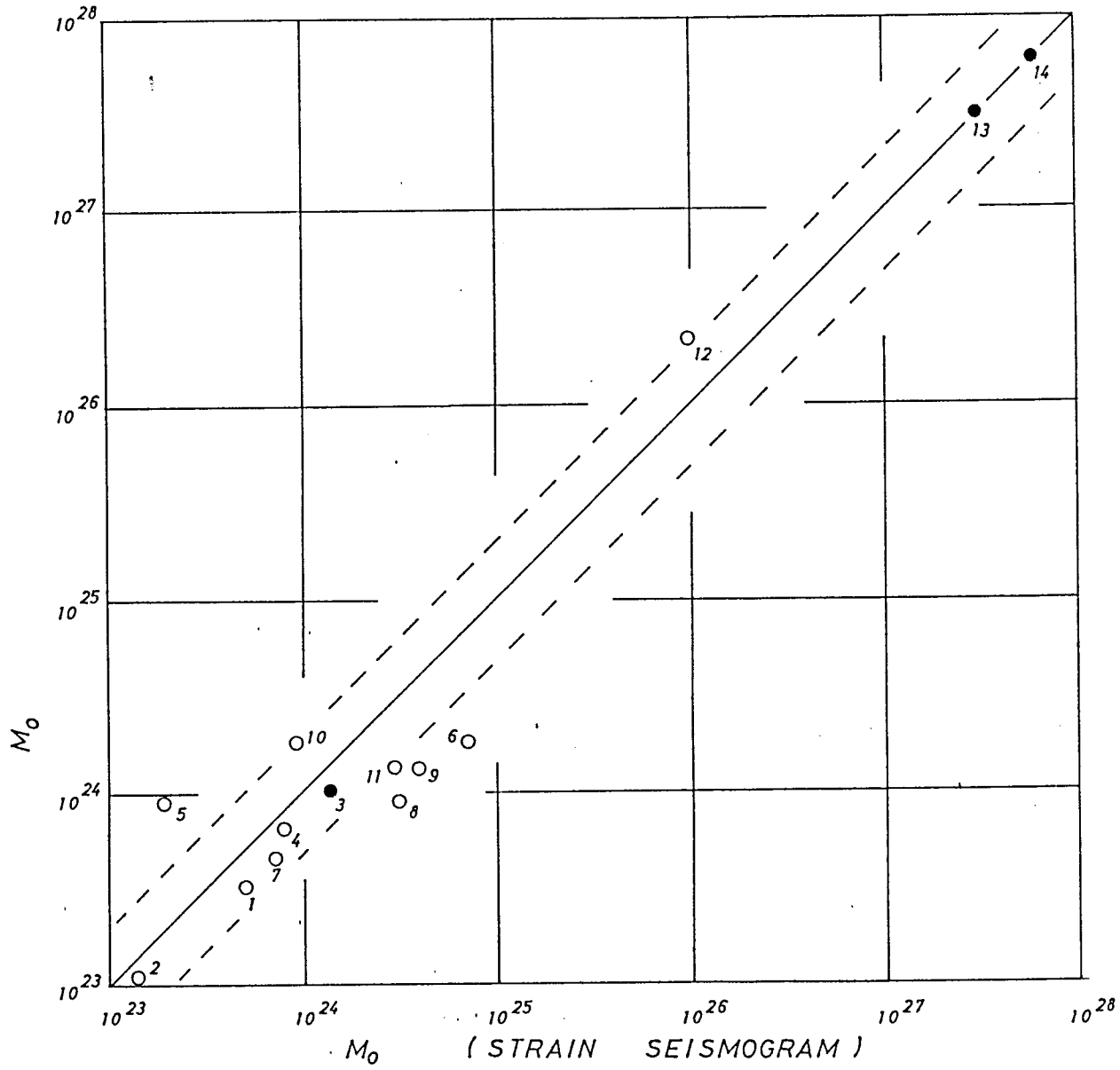
10^{28}
10^{27}
10^{26}
10^{25}
10^{24}
10^{23}
M_o
10^{23}
10^{24}
10^{25}
10^{26}
10^{27}
10^{28}
M_o (STRAIN SEISMOGRAM)
1
2
3
4
5
6
7
8
9
10
11
12
13
14

Fig.33

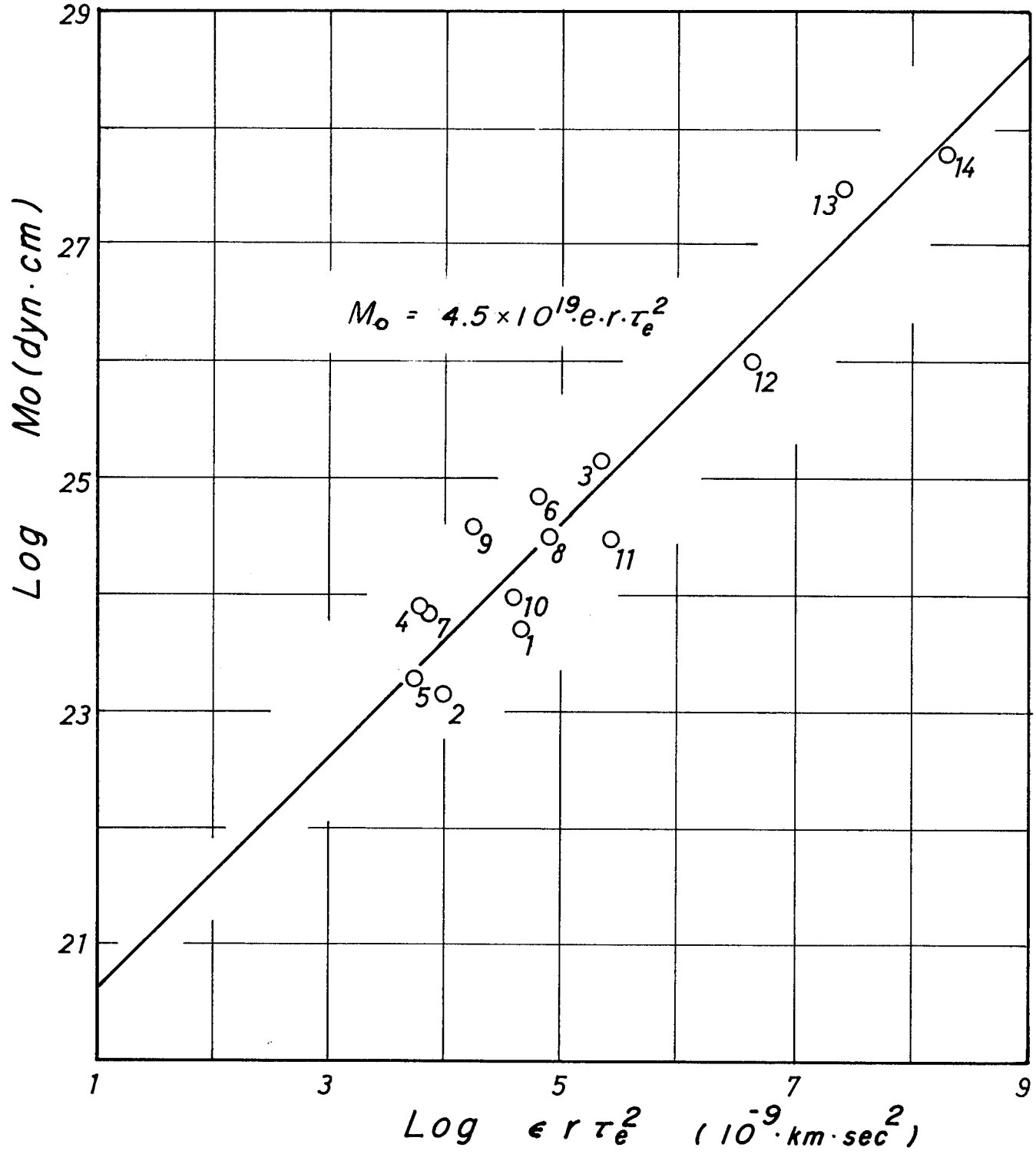
29
27
25
23
21
Log Mo (dyn·cm)
$M_o = 4.5 \times 10^{19} e \cdot r \cdot \tau_e^2$
1
3
5
7
9
Log $\epsilon r \tau_e^2$ (10^{-9}·km·sec^2)
1
2
3
4
5
6
7
8
9
10
11
12
13
14

Fig.34

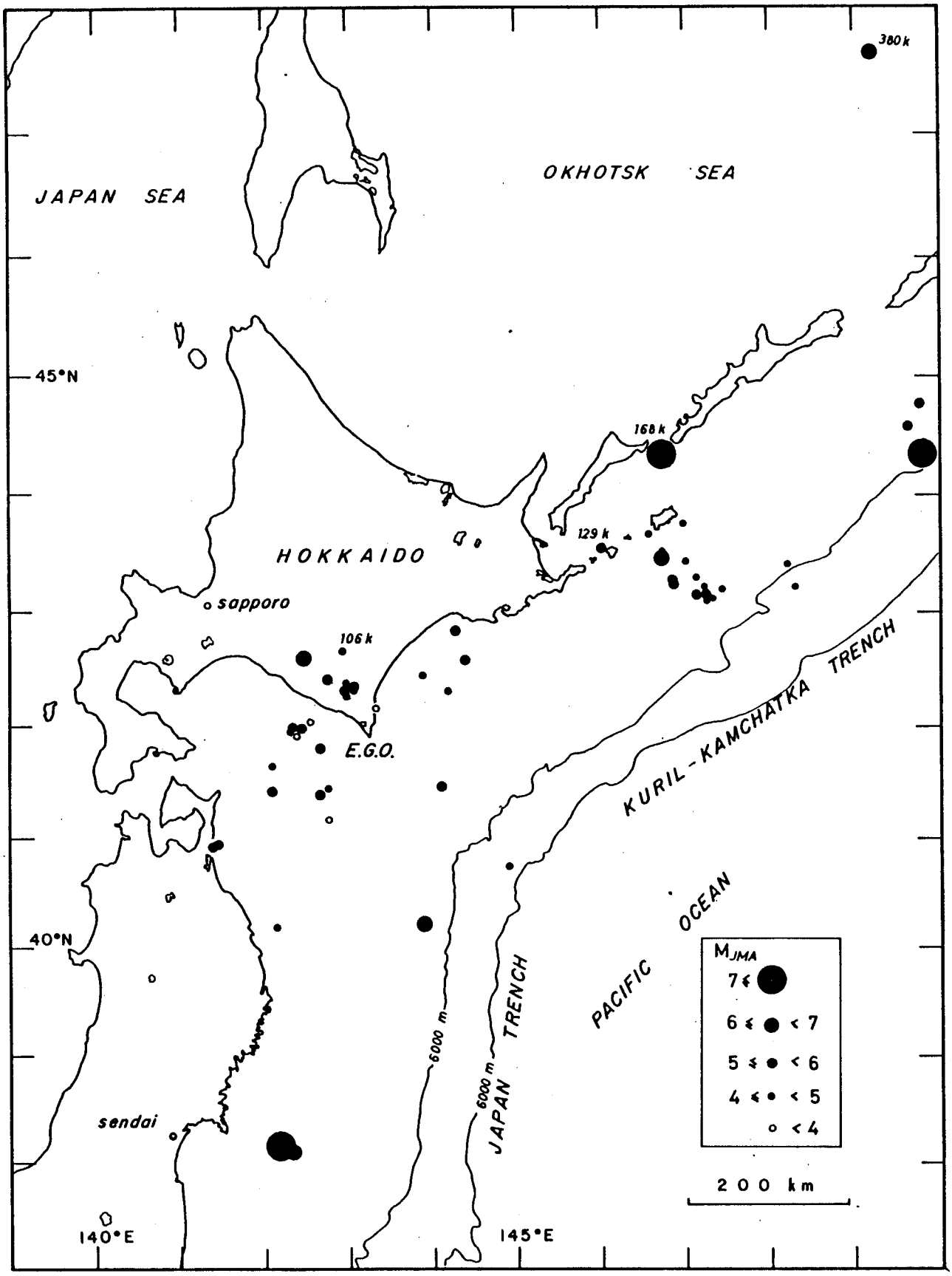
380k
JAPAN SEA
OKHOTSK SEA
45°N
168k
129k
HOKKAIDO
sapporo
106k
E.G.O.
KURIL-KAMCHATKA TRENCH
40°N
PACIFIC OCEAN
6000 m
6000 m
JAPAN TRENCH
sendai
M JMA
7 ≤
6 ≤ ● < 7
5 ≤ ● < 6
4 ≤ ● < 5
○ < 4
200 km
140°E
145°E

Fig.35

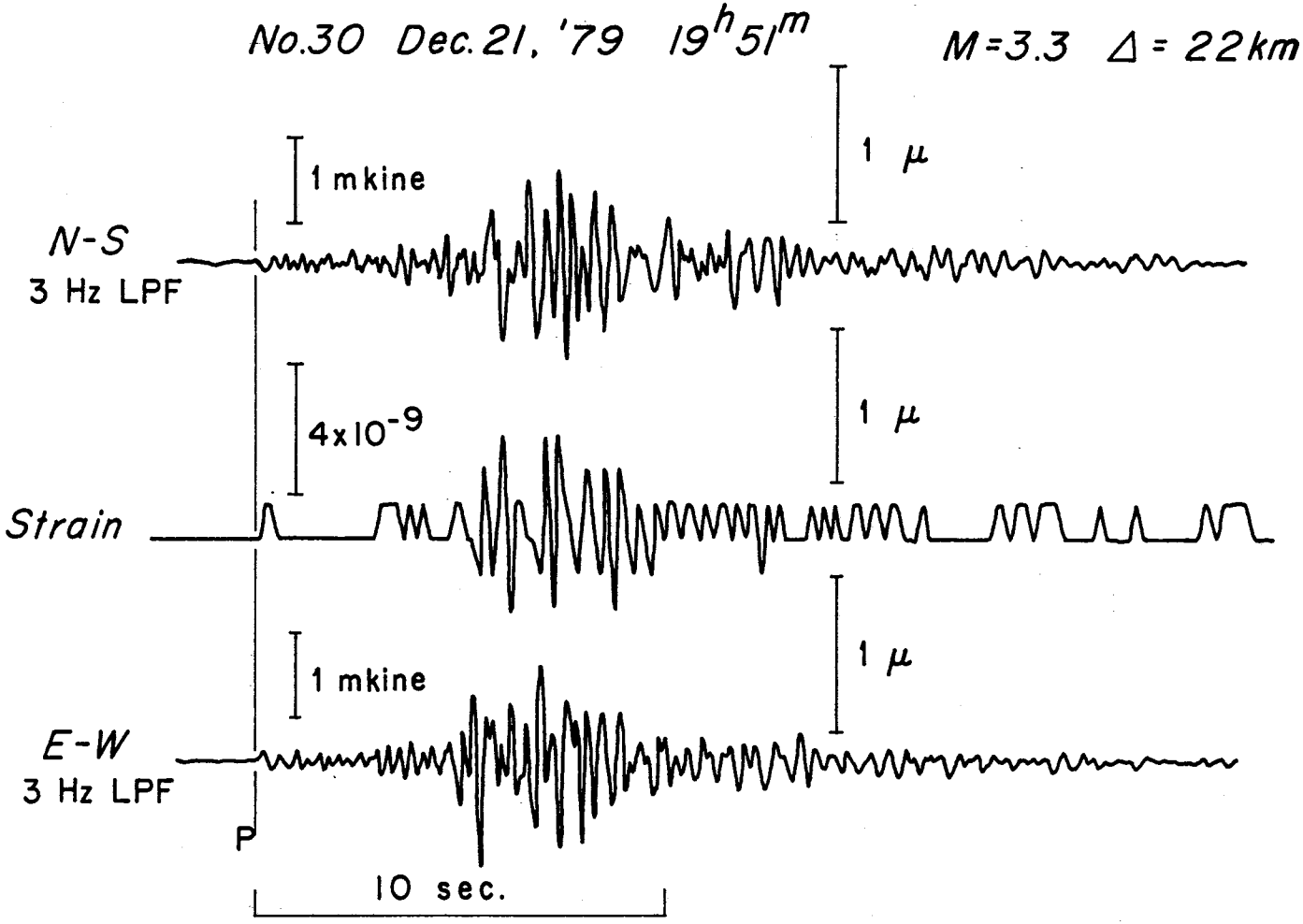
No.30 Dec.21, '79 19h51m
M=3.3 Δ = 22km
1 mkine
1 μ
N-S
3 Hz LPF
4x10-9
1 μ
Strain
1 mkine
1 μ
E-W
3 Hz LPF
P
10 sec.

Fig.36

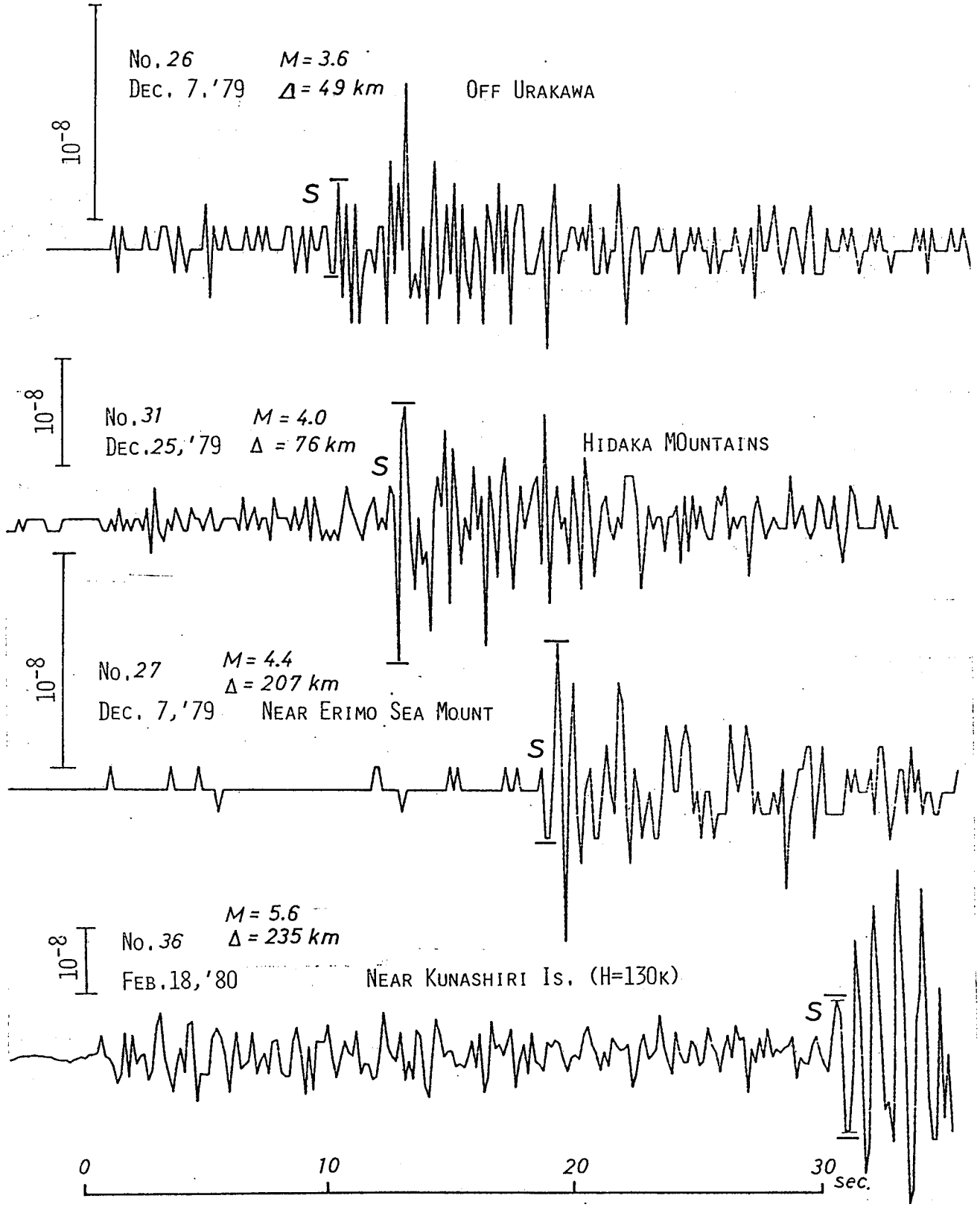
No. 26
DEC. 7, '79
M = 3.6
Δ = 49 km
OFF URAKAWA
10⁻⁸
S
No. 31
DEC. 25, '79
M = 4.0
Δ = 76 km
HIDAKA MOUNTAINS
10⁻⁸
S
No. 27
DEC. 7, '79
M = 4.4
Δ = 207 km
NEAR ERIMO SEA MOUNT
10⁻⁸
S
No. 36
FEB. 18, '80
M = 5.6
Δ = 235 km
NEAR KUNASHIRI IS. (H=130K)
10⁻⁸
S
0
10
20
30
sec.

Fig. 37.

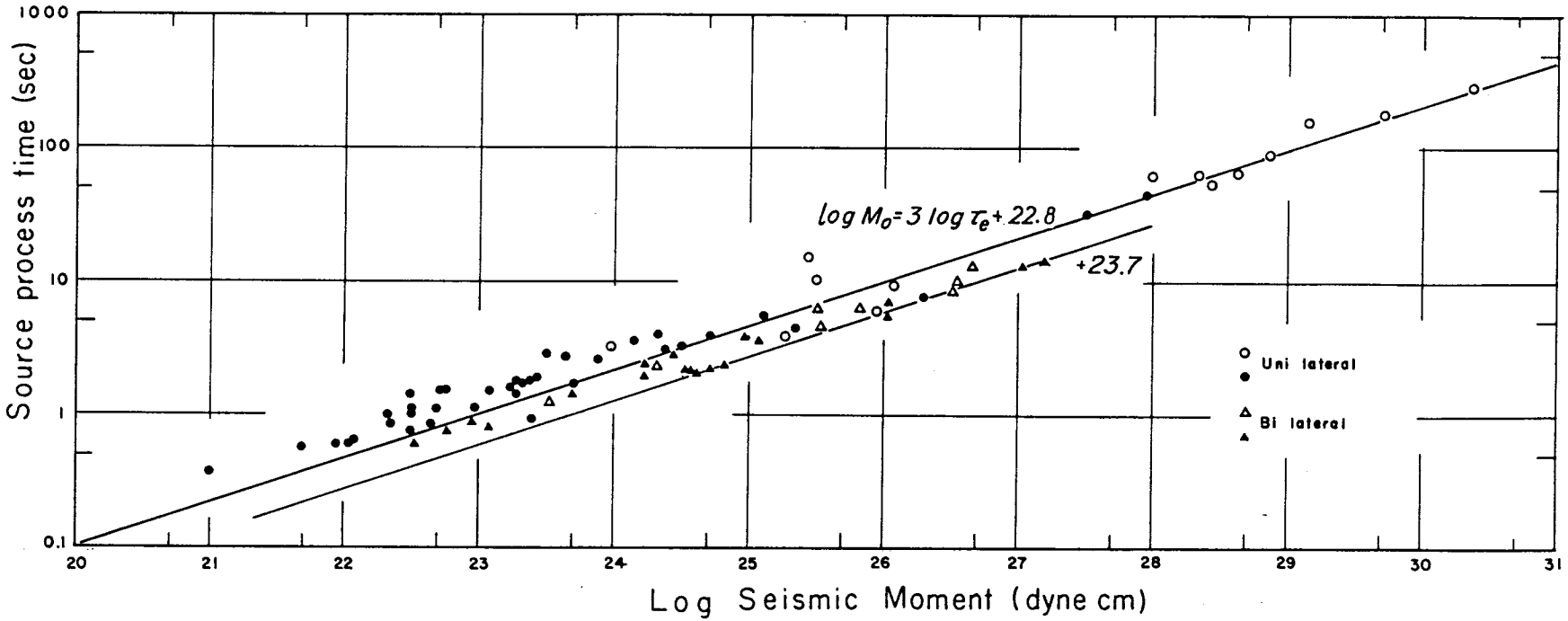
Source process time (sec)
1000
100
10
1
0.1
20
21
22
23
24
25
26
27
28
29
30
31
Log Seismic Moment (dyne cm)
log M_0= 3 log τ_e + 22.8
+23.7
Uni lateral
Bi lateral

Fig. 38

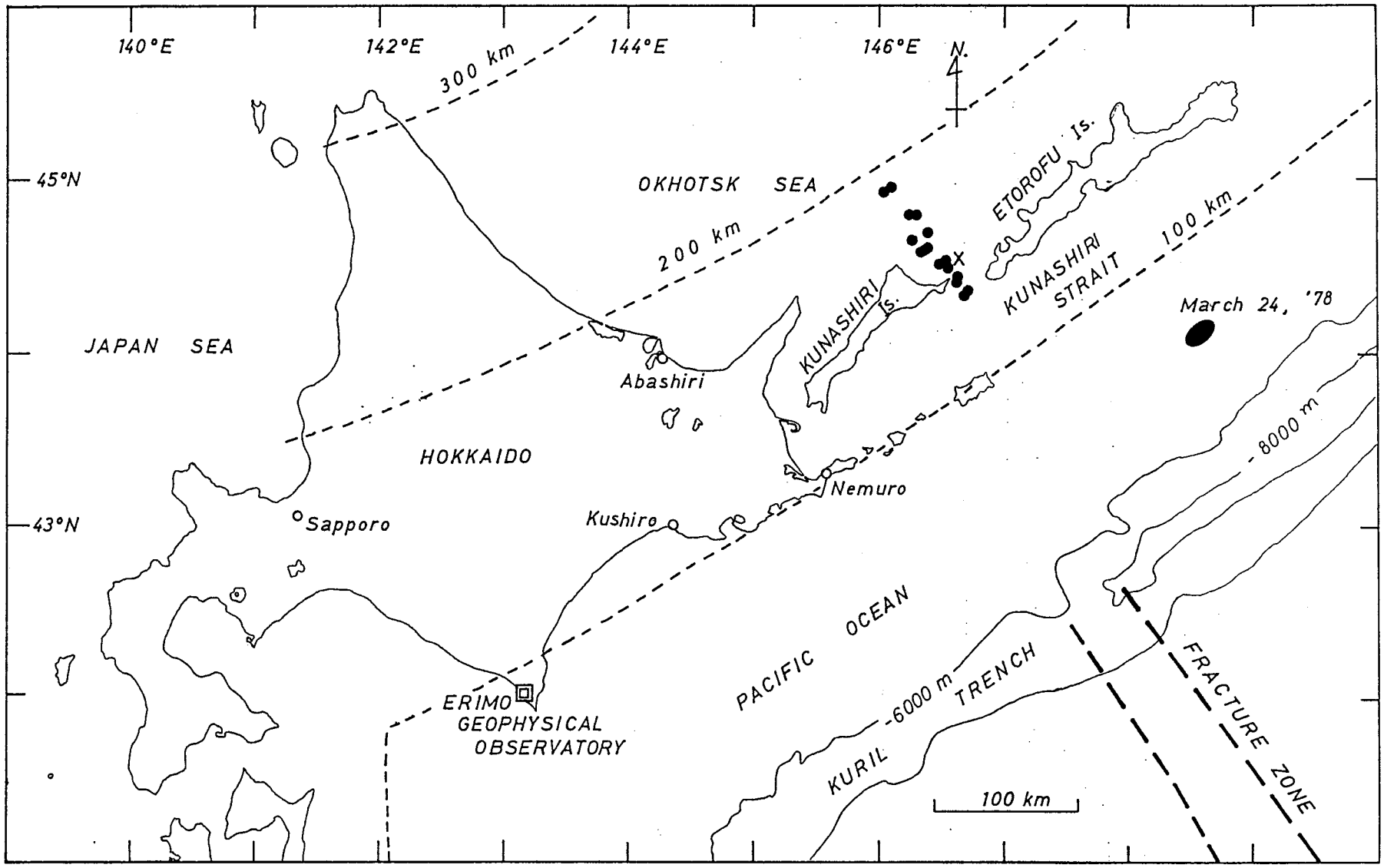
140°E
142°E
144°E
146°E
N.
300 km
200 km
100 km
45°N
43°N
OKHOTSK SEA
JAPAN SEA
PACIFIC OCEAN
ETOROFU Is.
KUNASHIRI Is.
KUNASHIRI STRAIT
March 24, '78
Abashiri
HOKKAIDO
Nemuro
Kushiro
Sapporo
ERIMO GEOPHYSICAL OBSERVATORY
8000 m
6000 m
KURIL TRENCH
FRACTURE ZONE
100 km

Fig.39

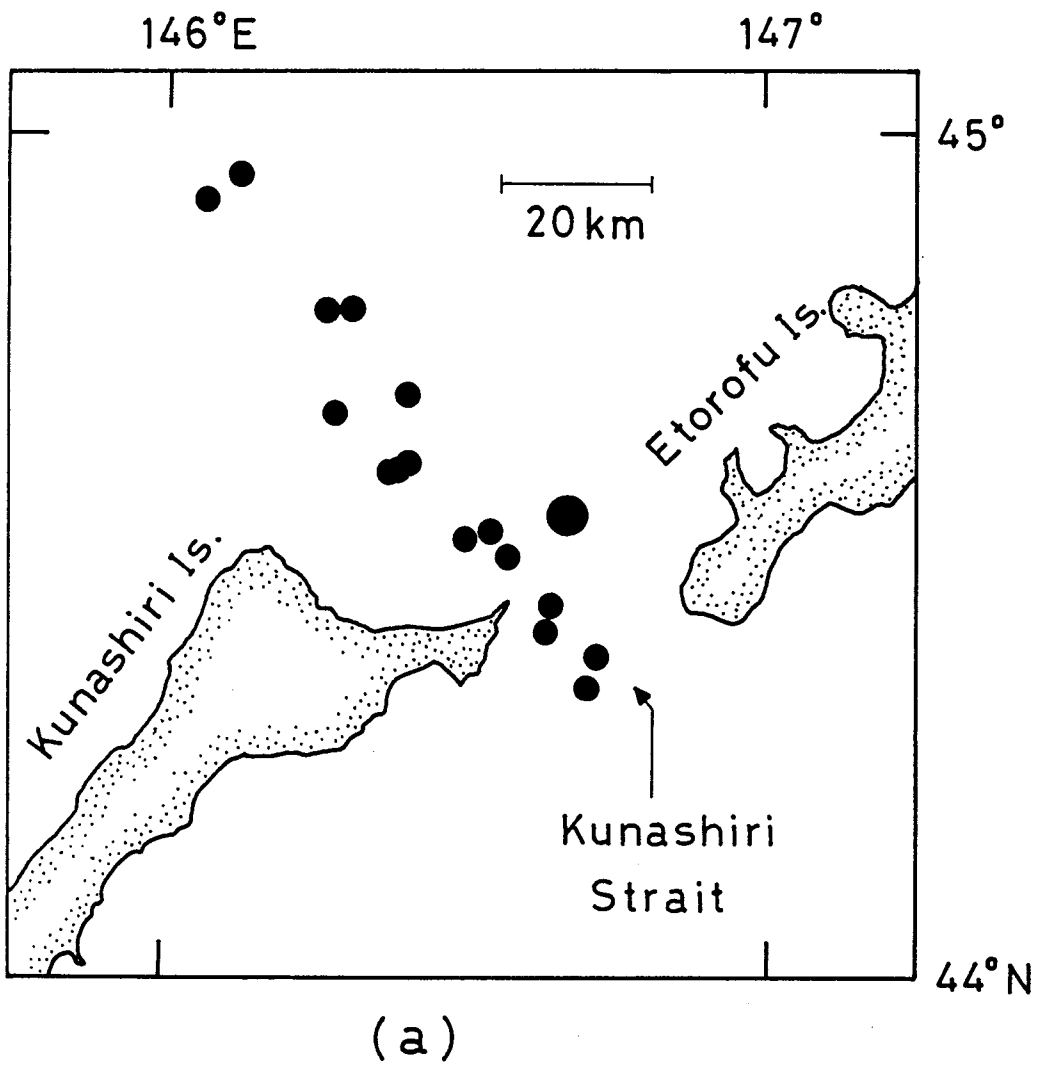
146°E
147°
45°
20km
Etorofu Is.
Kunashiri Is.
Kunashiri
Strait
44°N
(a)

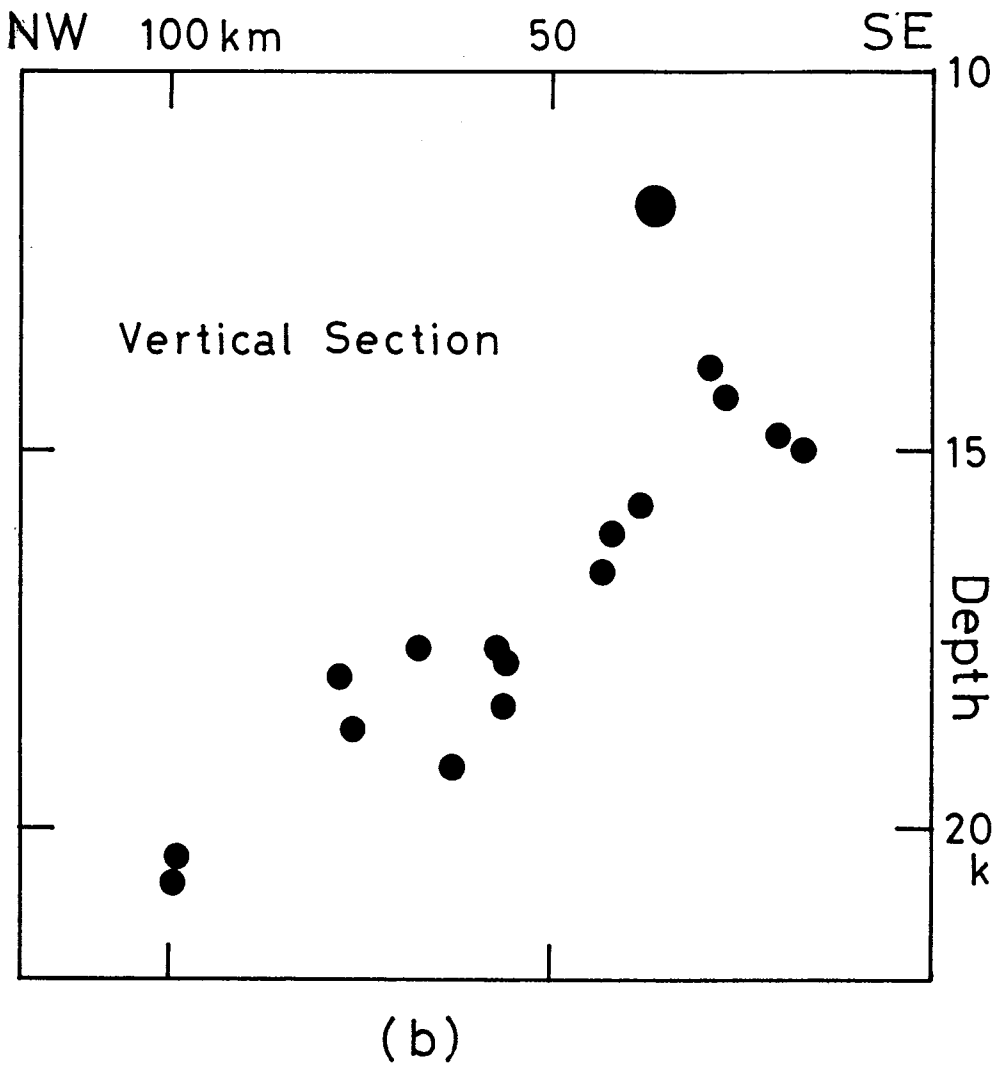
NW
100km
50
SE
Vertical Section
10
15
20
Depth
k
(b)

Fig.40

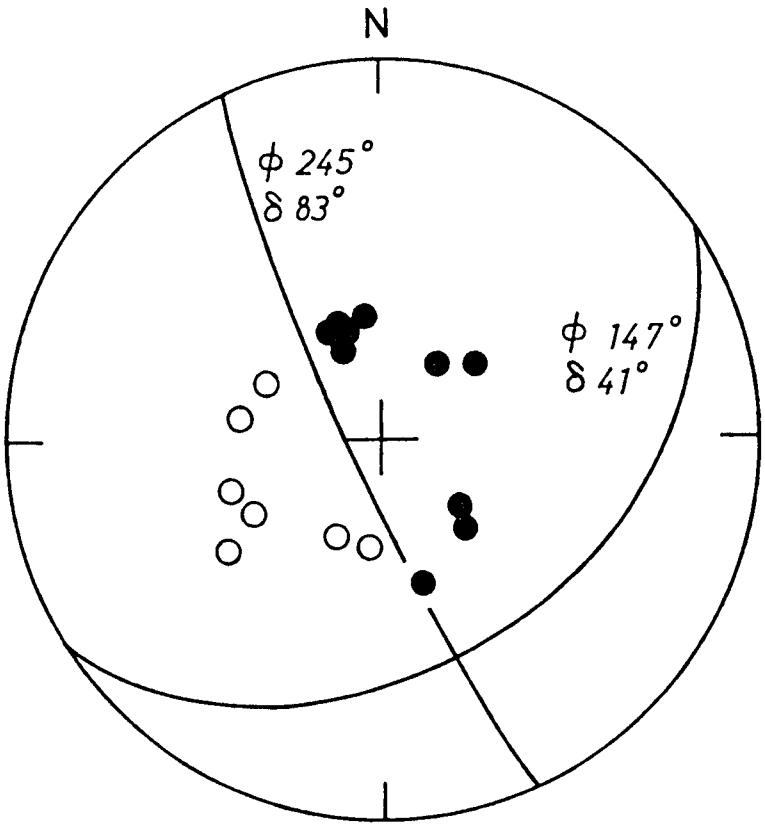

Fig.41

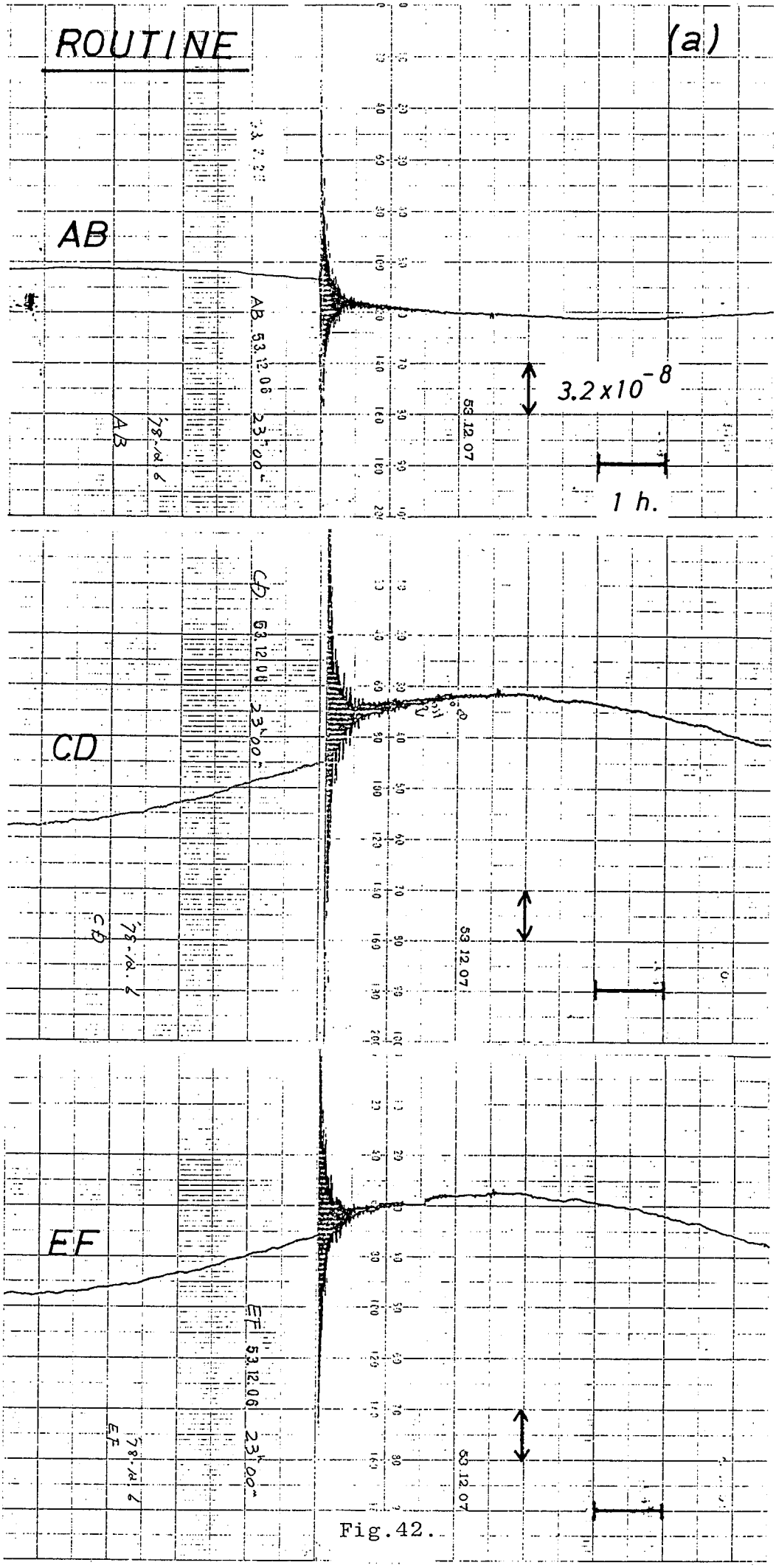

Fig.42.

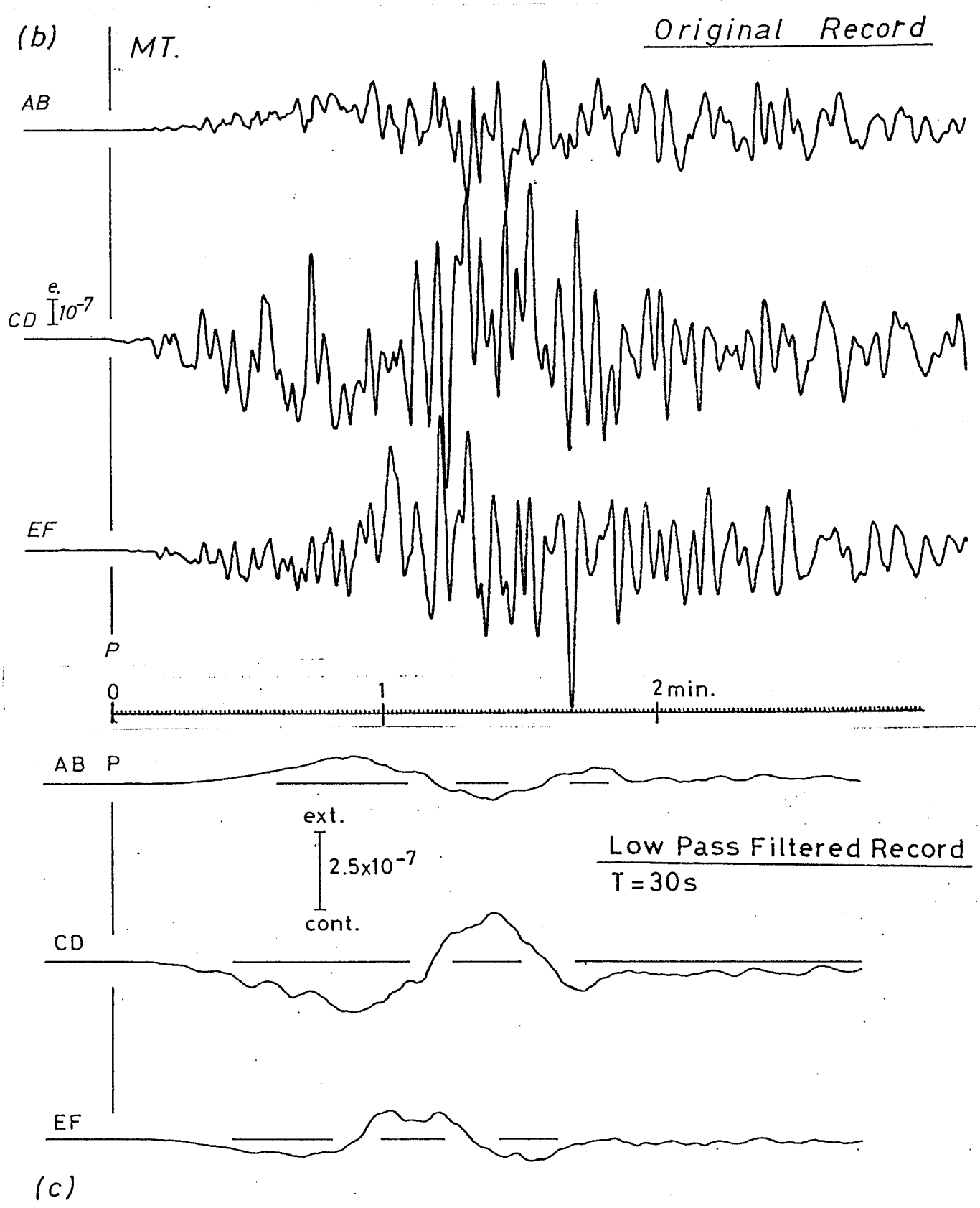

Fig.42. continued.

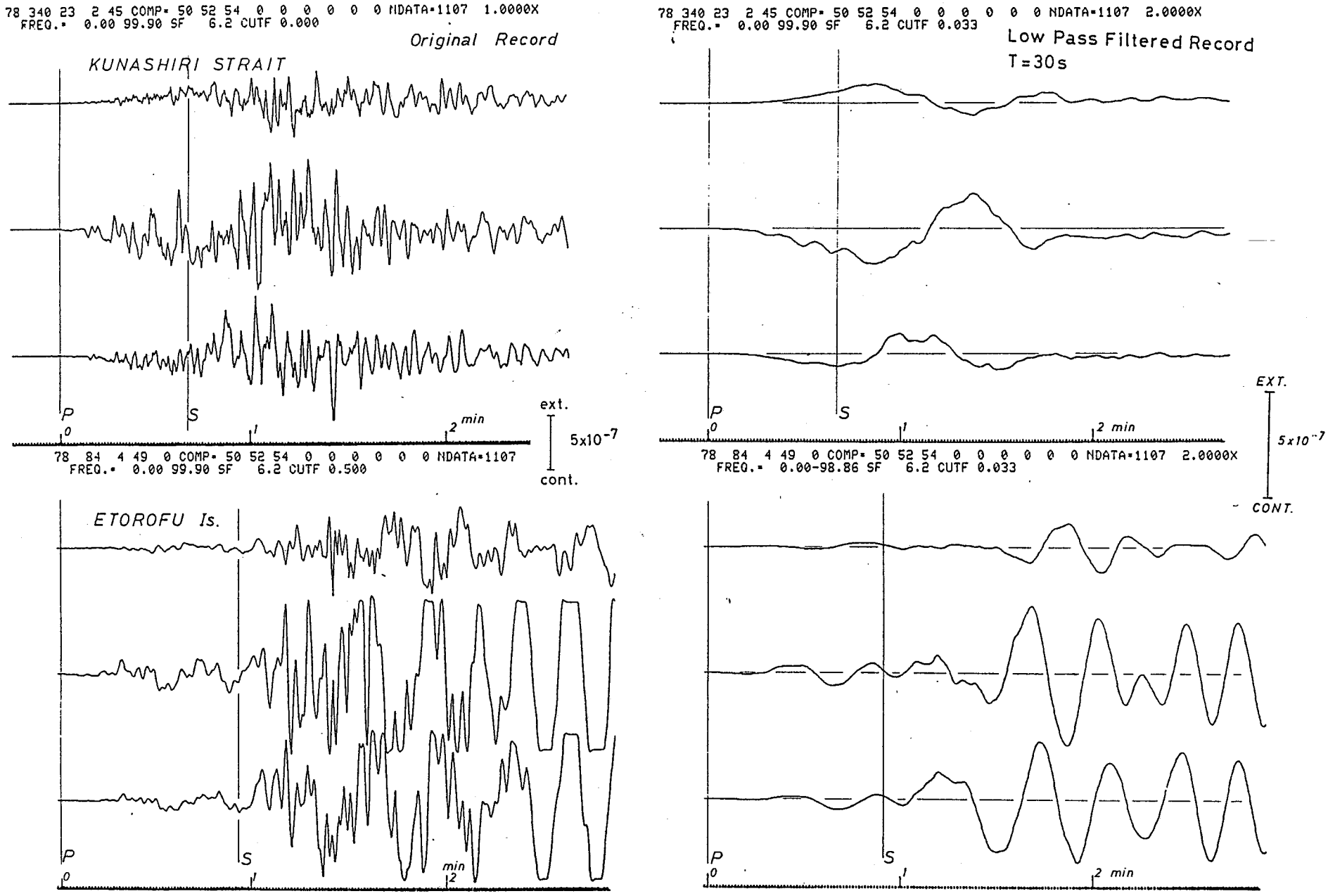
78 340 23 2 45 COMP= 50 52 54 0 0 0 0 0 0 NDATA=1107 1.0000X
FREQ.= 0.00 99.90 SF 6.2 CUTF 0.000
Original Record
KUNASHIRI STRAIT
P
S
0
1
2 min
78 84 4 49 0 COMP= 50 52 54 0 0 0 0 0 0 NDATA=1107
FREQ.= 0.00 99.90 SF 6.2 CUTF 0.500
ext.
5x10-7
cont.
78 340 23 2 45 COMP= 50 52 54 0 0 0 0 0 0 NDATA=1107 2.0000X
FREQ.= 0.00 99.90 SF 6.2 CUTF 0.033
Low Pass Filtered Record
T=30s
78 84 4 49 0 COMP= 50 52 54 0 0 0 0 0 0 NDATA=1107 2.0000X
FREQ.= 0.00-98.86 SF 6.2 CUTF 0.033
EXT.
5x10-7
CONT.
ETOROFU Is.
min

Fig.43

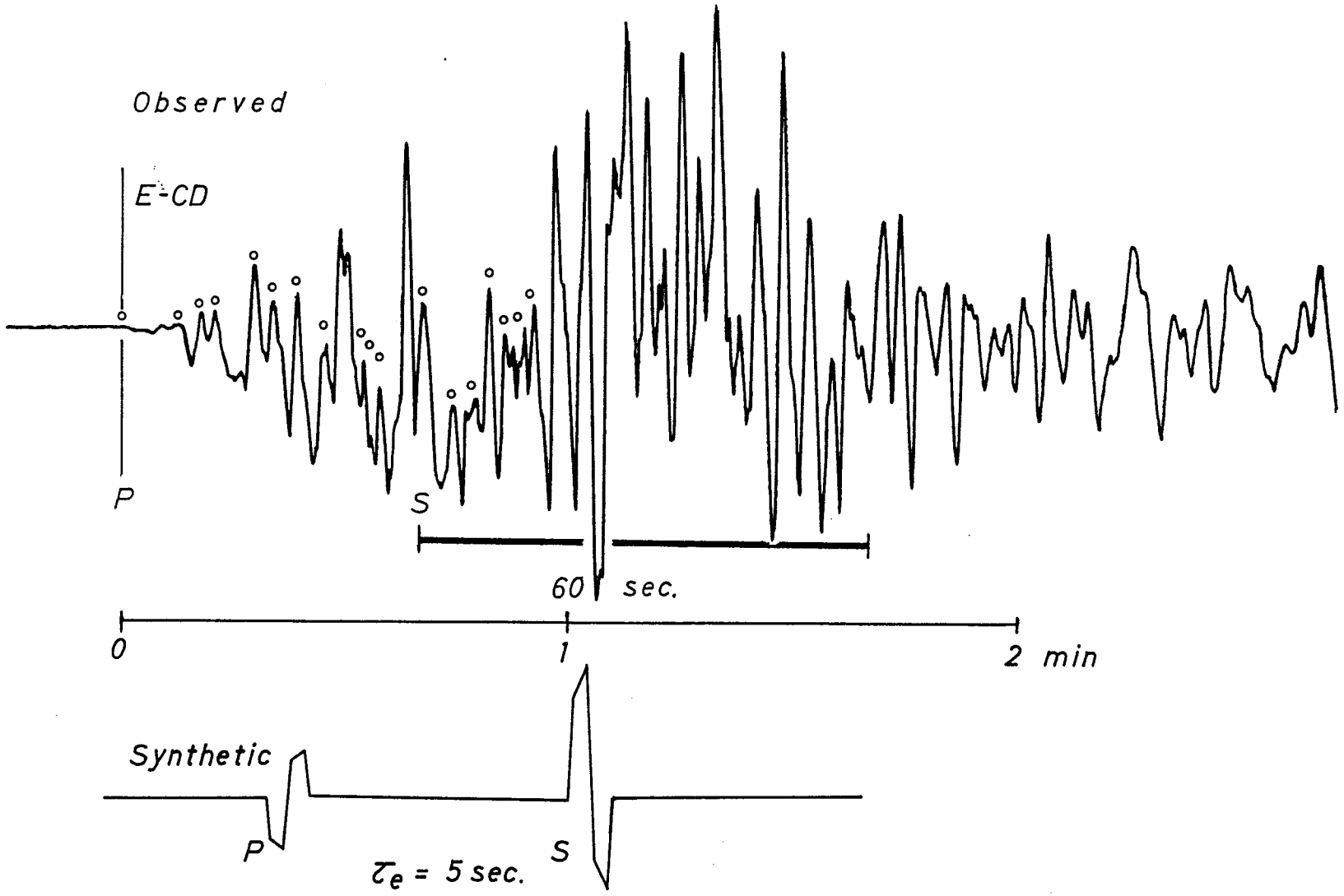

Fig.44

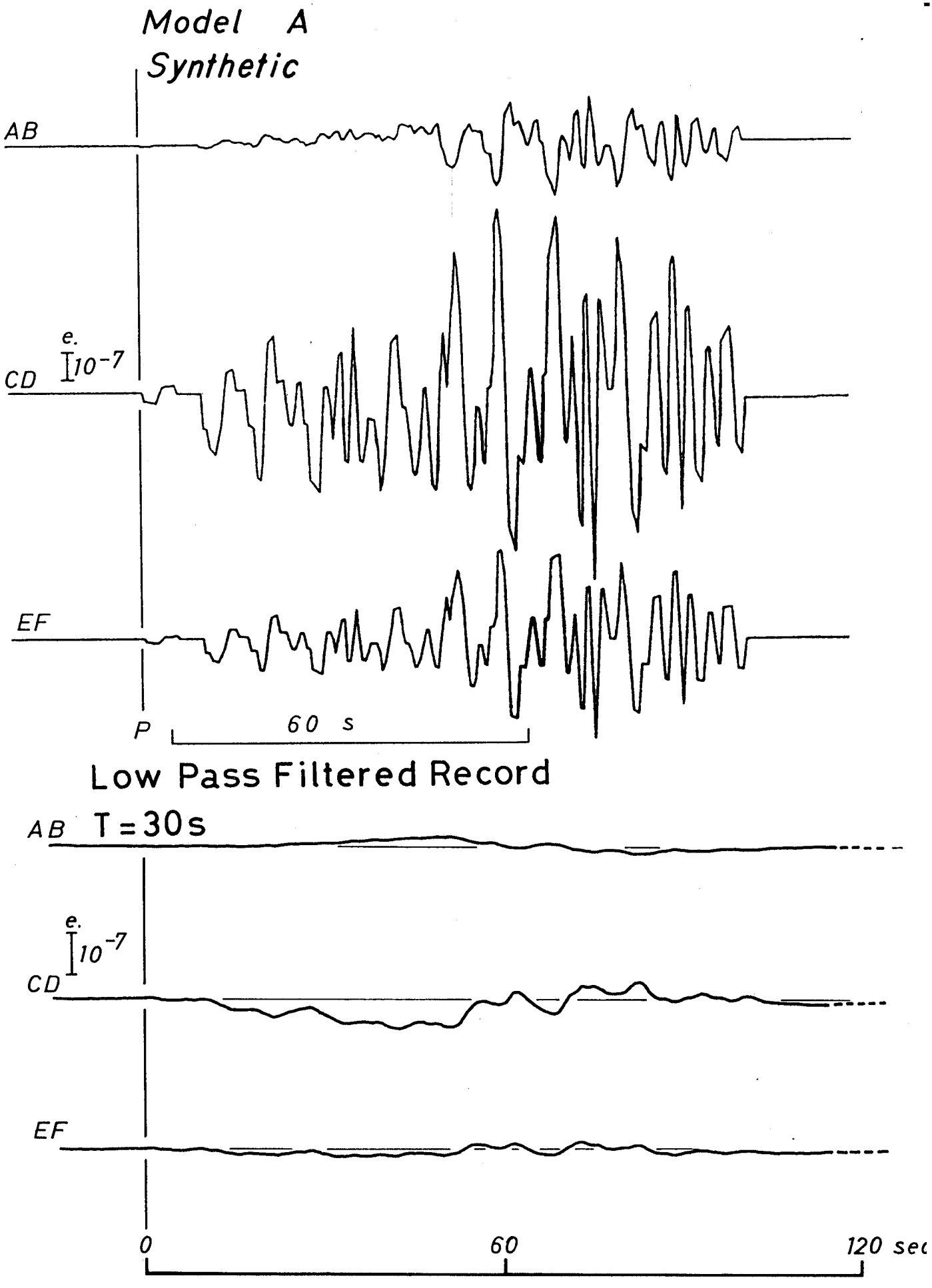
Model A
Synthetic
AB
e.
10-7
CD
EF
P
60 s
Low Pass Filtered Record
AB T=30s
e.
10-7
CD
EF
0
60
120 sec

Fig.45

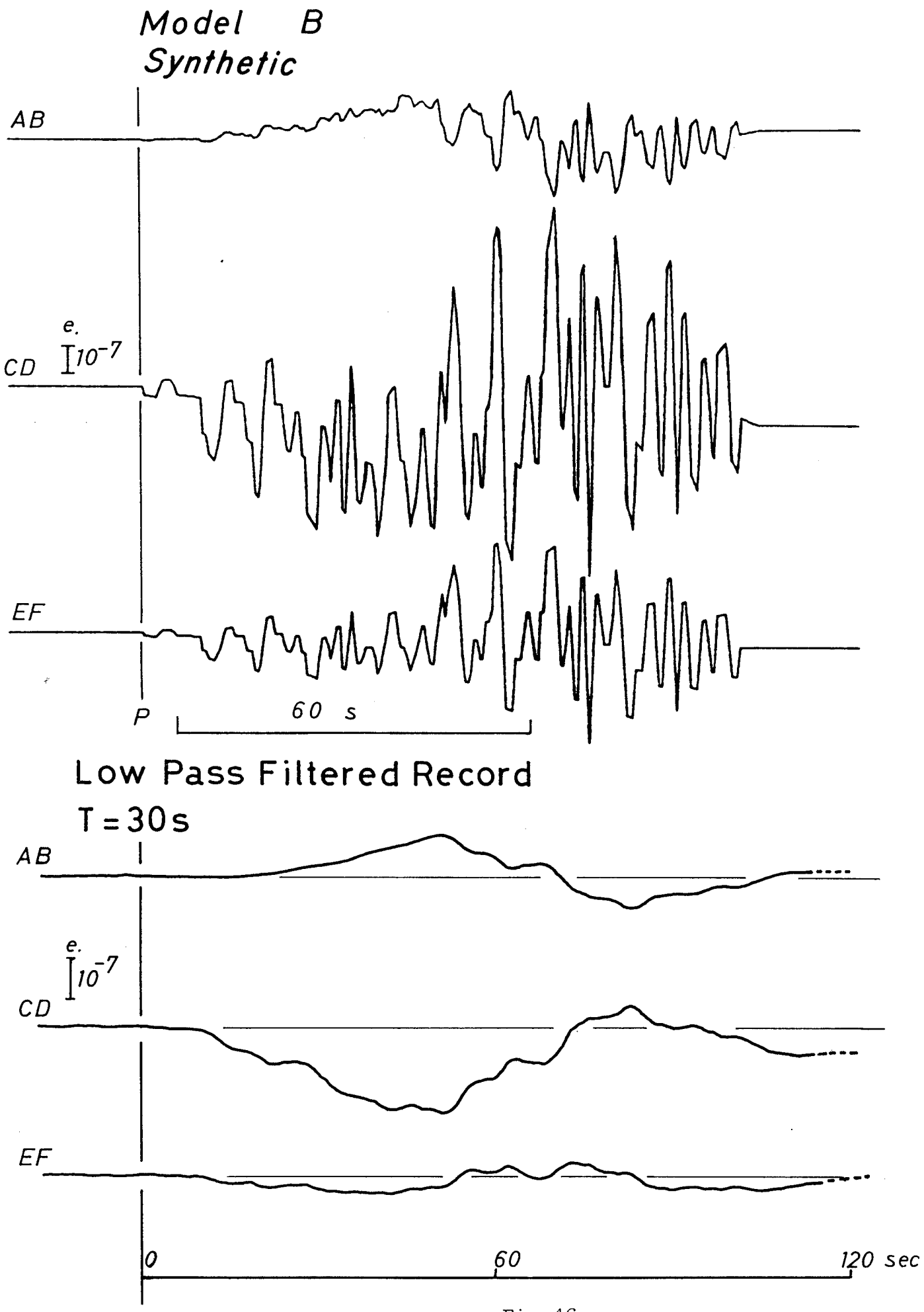
Model B
Synthetic
AB
e.
10^-7
CD
EF
P
60 s
Low Pass Filtered Record
T=30s
AB
e.
10^-7
CD
EF
0
60
120 sec

Fig.46

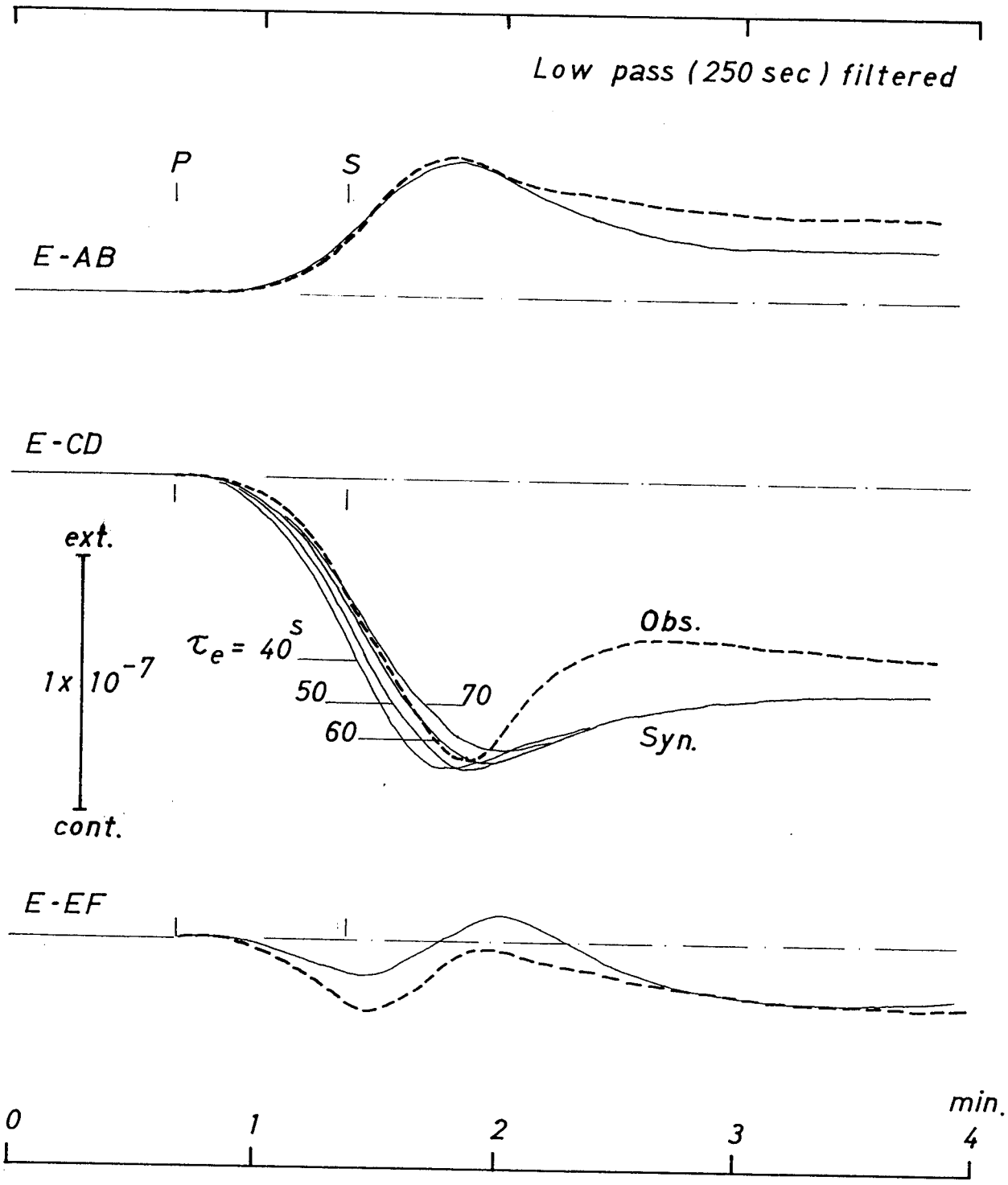
Low pass (250 sec) filtered
P
S
E-AB
E-CD
ext.
1x 10^-7
cont.
τe = 40 s
50
60
70
Obs.
Syn.
E-EF
0
1
2
3
4
min.

Fig.47

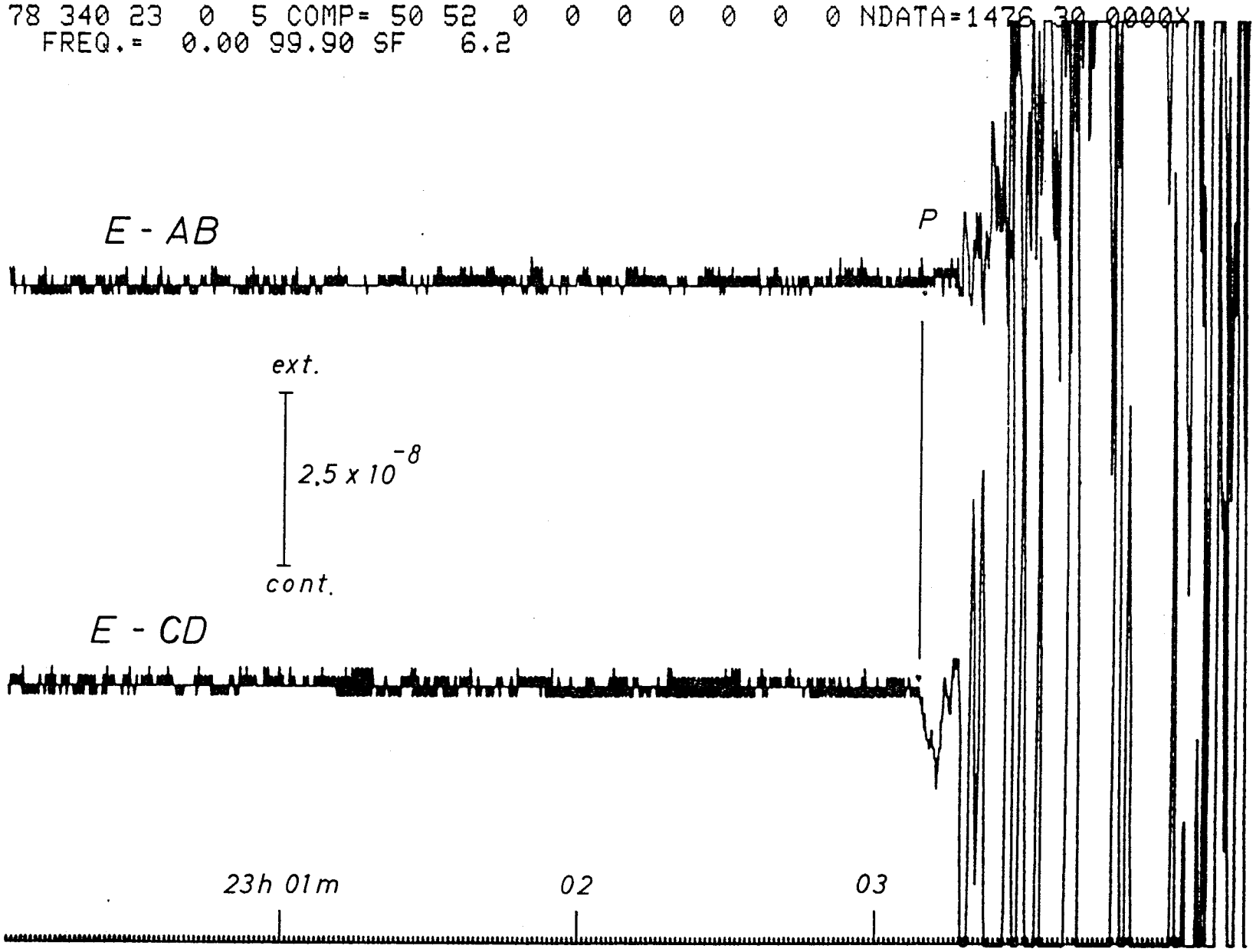
78 340 23 0 5 COMP= 50 52 0 0 0 0 0 0 0 NDATA=1476 30 0000X
FREQ.= 0.00 99.90 SF 6.2
E - AB
P
ext.
2.5 x 10^-8
cont.
E - CD
23h 01m
02
03

Fig.48

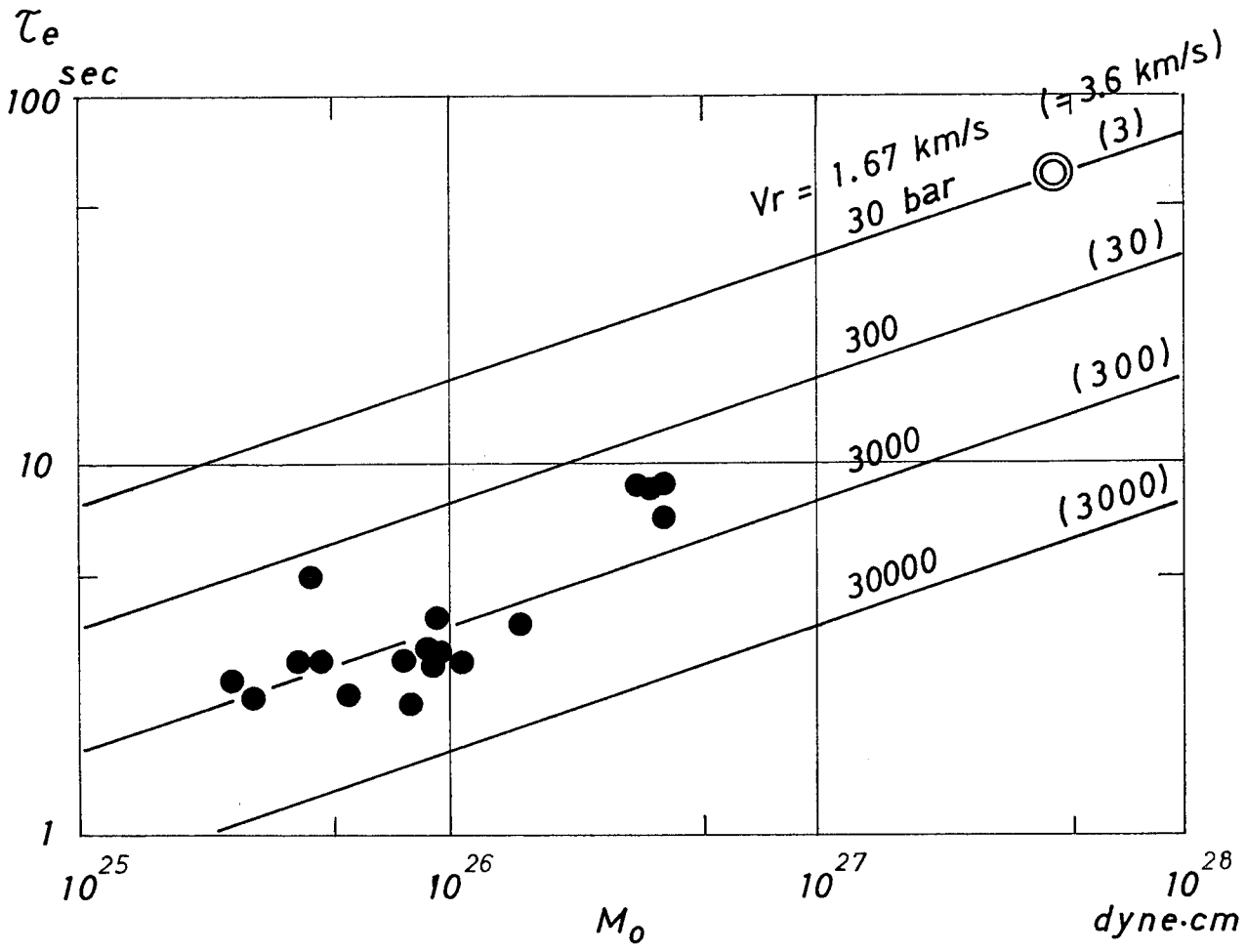
τe
sec
100
10
1
Vr = 1.67 km/s
30 bar
(= 3.6 km/s)
(3)
(30)
300
(300)
3000
(3000)
30000
10^25
10^26
10^27
10^28
M0
dyne·cm

Fig.49